GENETIC AND PHARMACOLOGIC INHIBITION OF CELLULAR INHIBITOR OF APOPTOSIS 1 (cIAP1) PROTEIN EXPRESSION PROTECTS AGAINST DENERVATION-INDUCED SKELETAL MUSCLE ATROPHY *IN VIVO*

Rim Lejmi Mrad

Thesis submitted to the
Faculty of Graduate and Postdoctoral Studies
in partial fulfillment of the requirements for the
Doctorate in Philosophy (PhD) degree
in Cellular and Molecular Medicine

Department of Cellular and Molecular Medicine
Faculty of Medicine
University of Ottawa

Abstract

Skeletal muscle atrophy is a debilitating condition caused by pathological conditions including cancer cachexia, disuse and denervation. Disuse atrophy is characterized by reduction in fiber size, fiber-type change and induction of markers of atrophy such as MuRF1 and Fn14. Recent studies have focused on understanding the fundamental role of signalling pathways and the proteolytic system in response to muscle atrophy. Unfortunately the exact mechanisms behind atrophy remain poorly understood. I recently demonstrated that cIAP1 and/or cIAP2 proteins are critical regulators of NF-kB activation, which has been shown to be involved in skeletal muscle atrophy. Here, I used genetic and pharmacological means to investigate the role of cIAP1 in a denervation-induced skeletal muscle atrophy model. Interestingly, I found that upon denervation loss of cIAP1 rescues muscle fiber size, prevents fiber-type changing and inhibits the expression of MuRF1 and Fn14. Moreover, treatment of mice with Smac mimetic compounds (SMC), a novel class of small molecule IAP antagonists, showed successful knockdown of cIAP1 in muscle and protects against denervation-induced muscle atrophy. Taken together, these data reveal that cIAP1 is both a novel mediator of skeletal muscle atrophy and an important therapeutic target.

Acknowledgments

I would like to take this opportunity to express my heartfelt gratitude to all those who helped me to make my thesis work a success. First and foremost, I would like to express my sincere gratitude to my supervisor, Dr. Robert Korneluk, for his support, guidance and providing me with an excellent environment to conduct my research. Your enthusiasm and determination to better lives through science is truly inspirational.

Many thanks to all members of the Korneluk lab., I have shared so many great memories and laughs with each and every one. In particular, Drs. Doug Mahoney and Herman Cheung who were my mentors when I started, Dr. Emeka Enwere, Martine St-Jean, Nathalie Earl, Lynn Kelly for all of their support during these years and tremendous assistance in my work. A special thank you to John Lunde (from Dr. Bernard Jasmin's Laboratory) for his genuine technical assistance. A special Thank you to my committee members: Drs. Nadine Wiper-Bergeron and Bernard Jasmin, for all their valued guidance, support and advice along the way.

Great appreciation goes to the following funding programs: the Ontario Graduate Scholarships in Science and Technology (OGSST), the Canadian Institutes of Health Research (CIHR), the Ottawa Regional Cancer Foundation, the Children's Hospital of Eastern Ontario Foundation and the Muscular Dystrophy Association.

A special thank you to Novartis pharmaceuticals and the Ontario Institute for Cancer Research (OICR) Medicinal Chemistry group for the design, synthesis, and provision of LCL161 and OICR720A respectively.

I am especially grateful to the leadership cadre at Health Canada who believed in me, brought the best of me and offered me a permanent employment opportunity as a Scientific Evaluator where I contribute to improving the safety of Canadians.

Most importantly, I wish to express my gratitude and indebtedness to my beloved parents Moncef Lejmi & Rachida Hadidane, my sister Chiraz and my brother Ahmed for their endless love, inspiration, encouragement and support in all my endeavours. I extend my affectionate appreciation to my husband Nezih Mrad for his consistent motivation, support and encouragement and last but not least a huge thank you to my two wonderful, and precious sons Rami and Rayan who give me strength and courage to bring forward the best in myself with their endless care and love. I certainly could not have done this without their support.

Dedication

This PhD thesis is dedicated to my

beloved parents “Moncef Lejmi & Rachida Hadidane” and family

for their endless love, support, and faith in me.

Table of Contents

Table of Figures

List of Abbreviations

APAF-1	Apoptosis protease activating factor-1
ATCC	American type culture collection
AVPI	Alanine-valine-proline-isoleucine (tetrapeptide)
bFGF	Basic fibroblast growth factor
bHLH	Basic helix-loop-helix
BIR	Baculoviral IAP repeat
BSA	Bovine serum albumin
BMP	Bone morphogenic protein
CARD	Caspase recruitment domain
Caspase	Cysteinyl, aspartate-specific protease
cFLIP	Cellular FLICE-like inhibitory proteins
CHEO	Children's Hospital of Eastern Ontario
cIAP1/2	Cellular inhibitor of apoptosis 1
cIAP2	Cellular inhibitor of apoptosis 2
CIHR	Canadian Institutes of Health Research
CSA	Cross-sectional area
DD	Death domain
DED	Death effector domain
DEN	Denervated
NDN	Nondenervated
°C	Degree Celsius

DD	Death domain
DIABLO	Direct IAP binding protein with low pH
DISC	Death-inducing signalling complex
DMD	Duchenne muscular dystrophy
DMEM	Dulbecco's modified Eagle medium
DMSO	Dimethyl sulfoxide
DNA	Deoxyribonucleic acid
DR4	Death receptor 4 (TRAILR1)
DR5	Death receptor 5 (TRAILR2)
ECL	Enhanced chemiluminescence
EDL	Extensor digitorum longus
FADD	Fas-associated death domain
FasL	Fas ligand
FCS	Fetal calf serum
FBS	Fetal bovine serum
FLICE	Fas-associated death domain-like interleukin-1beta-converting enzyme
GAPDH	Glyceraldehyde phosphate dehydrogenase
GFP	Green fluorescent protein
H&E	Haematoxylin and eosin
HGF	Hepatocyte growth factor
IAP	Inhibitor of apoptosis
IBM	IAP-binding motif
IkB α	Inhibitor of kB (IkB) α

IKKα	Inhibitor of IkB kinase-α
IKKβ	Inhibitor of IkB kinase-β
IMM	Inner mitochondrial membrane
IMS	Inner mitochondrial space
K48	Lysine48-linked ubiquitin
K63	Lysine63-linked ubiquitin
kDa	Kilodalton
LCL161	Designation for Novartisce c
LUBAC	Linear ubiquitination assembly complex
MAFbx	Muscle atrophy F-box
MEF	Mouse embryonic fibroblsts
MHC	Myosin heavy chain
MIKK	Muscle specific expression of activated IKKβ
Min	Minute
mM	Millimolar
Mm	Millimetre
MOMP	Mitochondrial outer membrane permeabilization
MuRF1	Muscle-specific ring finger1
NEMO	NF-kB essential modulator
NF-kB	Nuclear factor-kappa B
NIK	NF-kB interacting protein
NLS	Nuclear localization signal
OGSST	Ontario Graduate Scholarships in Science and Technology

OICR	Ontario Institute for Cancer Research
OICR720	Designation for bivalent SMC produced by OICR
OMM	Outer mitochondrial membrane
PARP	Poly (ADP-ribose) polymerase
PBS	Phosphate buffered saline
PCR	Polymerase chain reaction
PGC-1α	Peroxisome proliferator-activated receptor-gamma (PPAR-γ) coactivator-1α
PBS	Phosphate-buffered saline
qRT-PCR	Quantitative reverse real-time transcription polymerase chain reaction
RHD	Rel Homology Domain
RING	Really interesting new gene
RIAP1	Rabbit anti-rat IAP1
RIAP3	Rabbit anti-rat XIAP
RIP1	Receptor-interacting protein-1
RNA	Ribonucleic acid
RZF	RING zinc finger
SD	Standard deviation
siRNA	Small interfering RNA
SEM	Standard Error of the mean
SDS	Sodium dodecyl sulphate
SDS-PAGE	Sodium dodecyl sulphate polyacrylamide gel electrophoresis
Smac	Second mitochondrial-derived activator of caspases

SMC	Smac-mimetic compound
SMP	Skim milk powder (SMP)
TA	Tibialis anterior
TAD	Transcriptional activation domain
TAK1	Transforming growth factor-β TGFβ-activated kinase 1 (TAK1)
TAB2/3	TAK1-binding protein 2/3 (TAB2/3)
TNFα	Tumor necrosis factor-α
TNFR1	Tumor necrosis factor receptor 1
TRADD	TNFR1-associated death domain
TRAIL	TNF-related apoptosis-inducing ligand
TWEAK	TNF-related weak inducer of apoptosis
µl	Microlitre
Ub	Ubiquitin
UBA	Ubiquitin-associated
UPS	Ubiquitin Proteasome System
WT	Wild type
XAF1	XIAP-associated factor-1
XIAP	X-linked inhibitor of apoptosis

Chapter 1: Introduction

Skeletal muscle atrophy is a common and often debilitating complication of diverse conditions, including muscle disuse, fasting, aging, and many chronic illnesses. Although our understanding of how muscle atrophy occurs has improved measurably over the past two decades, the molecular basis of skeletal muscle atrophy is not completely understood. This introductory chapter examines evidence for the atypical role of regulators of apoptosis, in particular the cellular inhibitor of apoptosis protein 1, in the development of skeletal muscle atrophy. The thesis herein identifies important molecular mediators of muscle atrophy that could be used as potential therapeutic targets. This significantly advances our understanding of how muscle atrophy occurs and it opens up new avenues of investigation into the causes and treatment of muscle atrophy.

Overall significance

Skeletal muscle atrophy is an enormous societal and clinical problem that affects millions of people, both young and old. Despite its prevalence and severity, we lack an effective pharmacological therapy, largely because the molecular basis of skeletal muscle atrophy is not completely understood. However, as we have learned about other seemingly inevitable conditions, skeletal muscle atrophy is a regulated cellular process. This provides hope that an effective treatment can be developed if we gain a better understanding of the molecular mechanisms involved in skeletal muscle atrophy.

Therefore, this thesis aims to improve our current understanding of skeletal muscle atrophy and identify important molecular mediators of muscle atrophy that could

be used as potential therapeutic targets.

1.1 Apoptosis

Apoptosis, or programmed cell death, is a highly controlled process essential to the development and maintenance of tissue homeostasis, immune system modulation, and to embryonic and lymphocyte development (Straub, 2011; Plati et al., 2011). This cell suicide program involves the programmed elimination of harmful cells (Plati et al., 2011), and defects in apoptotic signaling contribute to numerous disease pathologies (Straub, 2011). Unlike other forms of cell death in which groups of cells are eliminated, apoptosis is characterized by the targeted death of a single cell (Wyllie et al., 1980). Typically, an apoptotic cell will display a distinct set of morphological changes that include plasma membrane blebbing, nuclear breakdown, and the packaging of cellular contents into membrane bound vesicles (Kerr et al., 1972).

While the mechanisms that initiate apoptosis are varied, a superfamily of evolutionarily conserved cysteine proteases, known as caspases (or cysteine-dependent aspartate specific proteases), execute the actual cellular degradation.

Caspases are synthesized as inactive proteins or zymogens, but once they dimerize or are cleaved by another protease, usually another caspase in the caspase activation cascade, they become active enzymes (Thornberry et al., 1998**)**. There are two classes of mammalian caspases involved in apoptosis: the initiator or upstream caspases, caspase-2, -8, -9 and -10, and the effector or downstream caspases, caspase-3, -6 and -7 (Flygare et al., 2010). Initiator caspases are recruited to oligomeric complexes by activating adaptor proteins in response to an apoptosis-inducing signal, resulting in their

subsequent activation as a result of dimerization of two caspase monomers that occurs as a consequence of their proximity (Pop et al., 2009). Once activated, initiator caspases activate downstream effector caspases by proteolytic cleavage of the linker region separating the two subunits of the catalytic domain of these caspases (Plati et al., 2011), leading to the ultimate dismantlement of the cell by cleaving numerous cellular proteins (Plati et al., 2011; Kumar, 1999).

1.2 Apoptotic pathways – the extrinsic and intrinsic pathways

Although various apoptotic stimuli can induce apoptosis, most signals activate one of two apoptotic pathways: the extrinsic pathway (or death receptor) and the intrinsic (or mitochondrial) pathway.

The extrinsic pathway is activated by the specific binding of death ligands, namely TNFα, FasL, and TRAIL, with their respective cell surface death receptors, including tumor necrosis factor receptor 1 (TNFR1), Fas/CD95/Apo1, DR4/TRAILR1, or DR5/Apo2 /TRAILR2 (Ashkenazi and Dixit 1998; Peter and Krammer 1998, Flygare et al., 2010). These death receptors belong to the TNFR family and can activate caspases within seconds of ligand binding causing cell death within hours (Ashkenazi and Dixit 1998). They contain cysteine-rich extracellular domains, a transmembrane domain, and a cytoplasmic death domain (DD) (Nagata 1997). Binding of ligands to their corresponding receptors induces receptor trimerization and recruitment of adaptor proteins. The interaction of receptors and adaptor proteins is mediated through their DDs. Adaptor proteins also carry a death effector domain (DED) which, in turn, binds to the DED of inactive procaspase 8 (Hsu *et al.* 1995). To activate procaspase 8, a complex must form

comprised of initiator caspase 8, RIP1 (Receptor Interacting Protein 1) and FADD (Fas-Associated protein with Death Domain) to form the Death Inducing Signaling Complex 'DISC' (Ashkenazi and Dixit 1999). Active caspase 8, as part of the death inducing signaling complex, then acts to bind and activate downstream effector caspases, such as caspases-3 and -7, to propagate the death signal (Flygare et al., 2010).

The intrinsic activation of the cellular death pathway involves mitochondrial outer membrane permeabilization which results from various stress stimuli including DNA damage, chemotherapeutic agents and radiation, growth-factor deprivation and disruption of cell-cell interactions (Plati et al., 2011; Flygare et al., 2010). The intrinsic pathway involves the disruption of mitochondria to mediate its death signal. Mitochondria are involved in the production of ATP *via* oxidative phosphorylation. Mitochondria possess an inner membrane (IMM), which encompasses the matrix, and an outer membrane (OMM), which surrounds and separates the inner mitochondrial space (IMS) from the cytoplasm (Fadeel et al.1999). The IMM contains molecules, such as cytochrome c. When apoptotic stress is transduced to mitochondria, Bcl-2 homology 3 (BH3)-only proteins, such as Bid and Bim induce oligomerization of the pro-apoptotic multi-BH domain protein, such as Bax and Bak to insert into the OMM, resulting in creation of the proteolipid pore responsible for cytochrome c release. Ultimate mitochondrial outer membrane permeabilization (MOMP) releases proteins which are typically stored in the IMS, such as cytochrome c, into the cytoplasm (Green and Reed 1998). Once released, cytochrome c induces formation of the apoptosome by binding to and inducing oligomerization of apoptosis protease activating factor-1 (APAF-1) and procaspase 9 (Wu et al., 2007). Procaspase 9 activates initiator caspase 9, and ultimately leads to

activation of downstream effector caspases 3 and 7 to potentiate cell death (Flygare, et al., 2010).

At the end of the apoptotic signaling cascade, the extrinsic and the intrinsic pathway converge at the activation of effector caspases-3 and -7, sharing a common signaling pathway.

1.3 The inhibitor of apoptosis proteins

The Inhibitor of APoptosis (IAP) proteins constitute a group of evolutionarily conserved proteins (Miller, 1999). The IAP proteins were originally identified on the basis of their ability to prevent apoptosis by binding to and inhibiting caspases (Liston et al., 1996). However, it is now clear that some members of the IAP family of proteins function as an E3 ubiquitin ligases mediating signaling events including the activation of the NF-kB (nuclear factor kappa-light-chain-enhancer of activated B Cells) pathway (Silke et al., 2013).

The IAP family members are characterized by the presence of at least one N-terminal Baculovirus IAP Repeat (BIR) domain, a zinc-binding fold of approximately 80 amino acids that binds to and inhibits activated caspase-3, -7 and -9, as well as other proteins, such as TNF-receptor-associated factor 2 (TRAF2) (Deveraux et al., 1999; Flygare et al., 2010). In addition, several IAPs contain a zinc finger C-terminal RING (Really Interesting New Gene) domain with ubiquitin E3 ligase activity which is required for signaling and targeting proteins for degradation (Deveraux et al., 1999; Hunter et al., 2007).

There are eight IAP proteins in humans (Figure 1): neuronal apoptosis inhibitory protein (also known as BIRC1), cellular IAP1 (cIAP1; also known as BIRC2), cellular IAP2 (cIAP2; also known as BIRC3), X chromosome-linked IAP (XIAP; also known as BIRC4), survivin (also known as BIRC5), ubiquitin-conjugating BIR domain enzyme apollon (also known as BIRC6), melanoma IAP (ML-IAP; also known as BIRC7), and IAP-like protein 2 (ILP2; also known as BIRC8). Among this family of IAPs, XIAP is the best characterized, and is recognized as the most potent anti-apoptotic member of this family of proteins (Plati et al., 2011; Flygare et al., 2010). XIAP is the only IAP capable of direct inhibition of the proteolytic activity of caspase 3, caspase 7 and caspase 9 (Eckelman et al., 2006). The linker region between the first BIR domain (BIR1) and the second BIR domain (BIR2), along with BIR2 of XIAP, binds to and inhibits both caspase-3 and -7 by obstructing their substrate-binding grooves (Flygare et al., 2010; Plati et al., 2011; Mace et al., 2010).In addition, the BIR3 domain of XIAP acts as a specific inhibitor of caspase-9, by mediating interactions with this caspase to ensure it remains in an inactive monomeric state (Plati et al., 2011; Mace et al., 2010).

Of particular interest within these IAP proteins are cIAP1and cIAP2, characterized by their three structurally similar BIR domains (Figure 2) (Eckelman et al., 2006). Both cIAP1 and cIAP2 also contain a caspase recruitment domain (CARD), which was reported to regulate its E3 ubiquitin ligase activity by mediating intramolecular inhibition (Lopez et al., 2011; Vandenabeele et al., 2012).

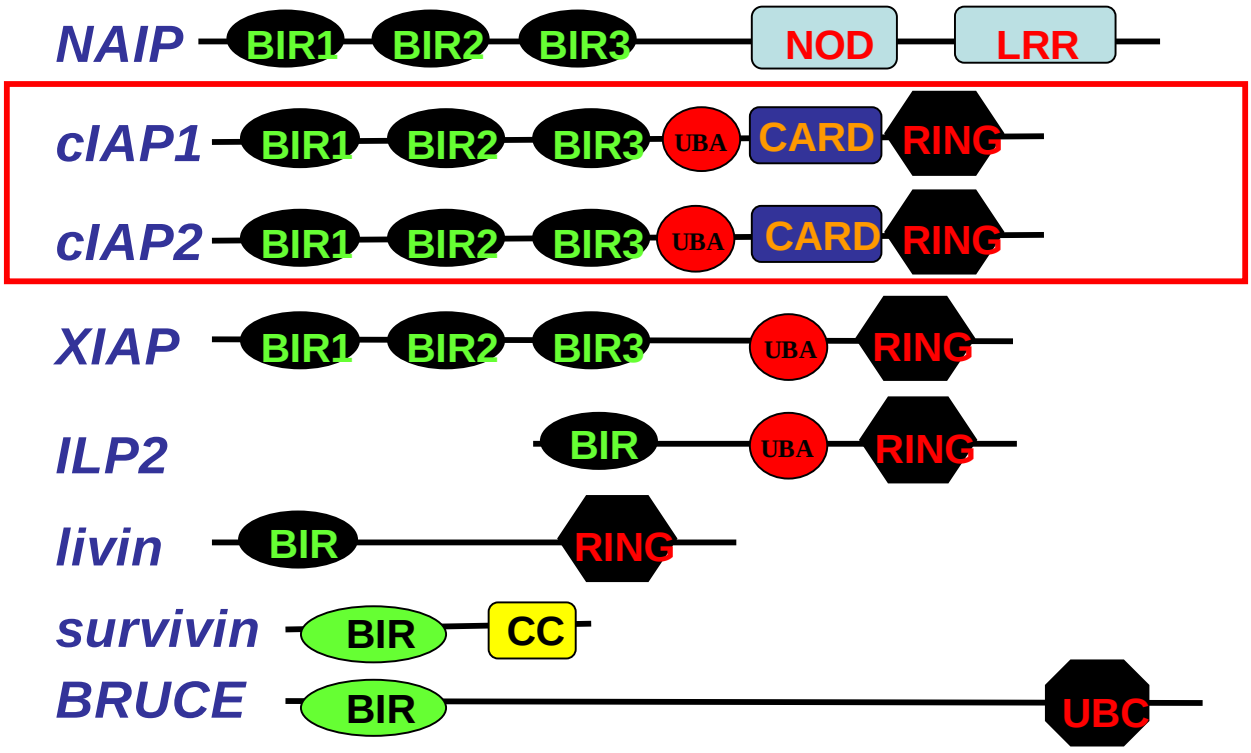

Figure 1. Domain structure of the eight mammalian IAP proteins

Members of the mammalian IAP gene family are characterized by a baculovirus IAP repeat (BIR) domain. cIAP1, cIAP2 and XIAP contain a RING E3 ubiquitin ligase and/or caspase recruitment (CARD) domains as well as an ubiquitin-binding, UBA, domain. The two IAPs most studied in this thesis are boxed in red.

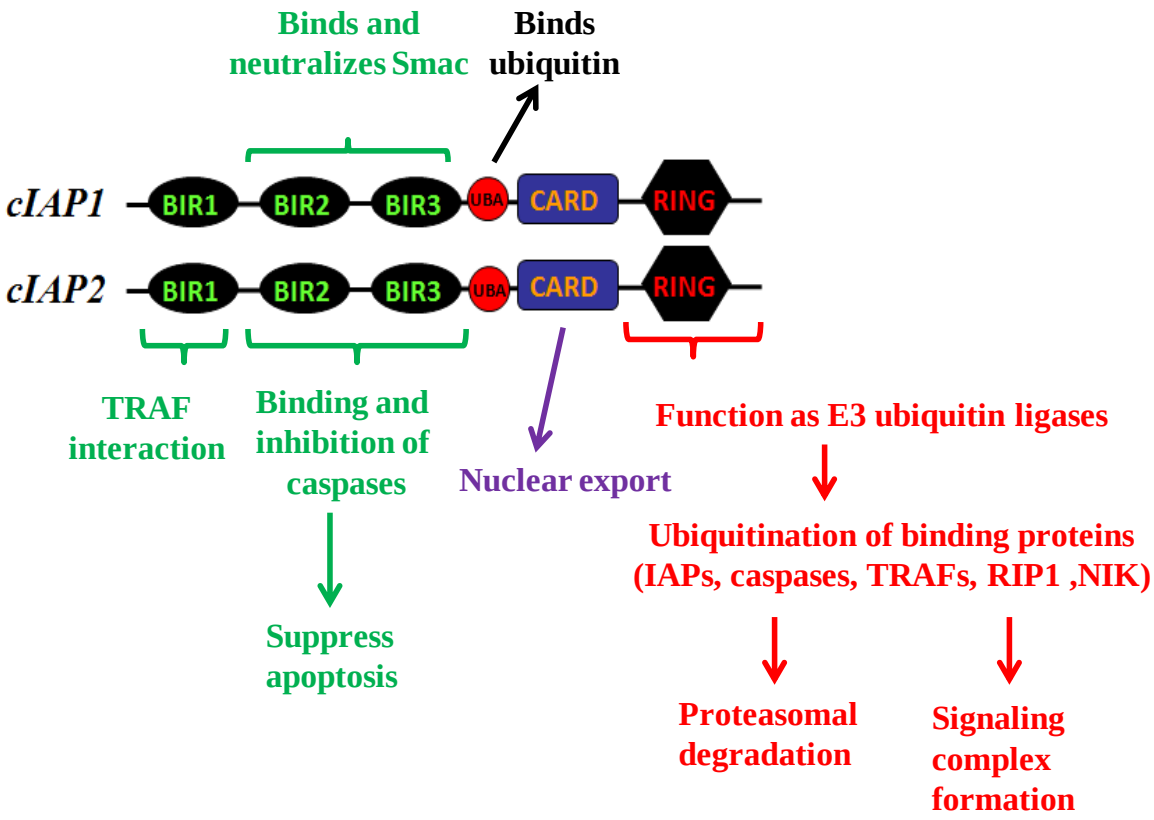

Figure 2. The cellular inhibitor of apoptosis 1 and 2 (cIAP1 and 2): structure and function

Both cIAPs are members of the mammalian IAP gene family, characterized by a baculovirus IAP repeat (BIR) domain. cIAP1/2 contain a RING E3 ubiquitin ligase and caspase recruitment (CARD) domains as well as an ubiquitin-binding, UBA, domain.

Various functional domains of cIAP1/2 allow for interaction with other signaling proteins, modulation of activity (neutralization of Smac) and caspase interaction. In particular, ubiquitination of various substrates is facilitated by the E3 ligase activity garnered by the RING domain. In addition, degradation of other substrates is mediated by the E3 ligase in an ubiquitin-independent manner.

Moreover, the cIAPs possess an Ub-associated (UBA) domain through which they interact with ubiquitinated proteins (Blankenship et al., 2009; Gyrd-Hansen et al., 2010), and a RING zinc finger (RZF) domain at the C-terminal that functions as an E3 ubiquitin ligase (Vaux et al., 2005; Hunter et al., 2007). Unlike XIAP, cIAP1 and cIAP2 possess the ability to bind caspases but are unable to directly inhibit caspases due to a lack of essential elements required for such inhibition (Eckelman et al., 2006). However, the anti-apoptotic potential of cIAP1 and cIAP2 was shown to depend on their E3 ubiquitin ligase activities (Bertrand et al., 2008; Varfolomeev et al., 2007; Vince et al., 2007; Choi et al., 2009). Both cIAP1 and cIAP2 have been shown to regulate TNFα-mediated classical (canonical) NF-kB activation by ubiquitinating RIP1 and forming a signaling complex (Mahoney et al., 2008). The cIAPs also control alternative (non-canonical) NF-kB signaling by ubiquitinating the NF-kB-inducing kinase (NIK) and causing its subsequent proteasomal degradation (Zarnegar et al., 2008), (Flygare et al., 2010; LaCasse et al., 2008).

1.4 Regulation of NF-kB signaling by cIAPs

Nuclear factor kappa B (NF-kB) belongs to a family of transcription factors which regulate a variety of biological processes, including innate and adaptive immunity, apoptosis, as well as tissue development and disease (Mourkioti et al., 2008; Hayden and Ghosh, 2008). NF-kB family consists of five closely related proteins, RelA (p65), RelB, c-Rel, p105/p50, and p100/p52. Both p105 and p100 proteins are synthesized as large precursors and can be cleaved into p50 and p52, respectively. These family members are characterized by the presence of a highly conserved N-terminal Rel Homology Domain

(RHD) which is responsible for homo- or heterodimerization of NF-kB subunits (the most common forms are the p65/p50 and p65/p52 dimers), binding to promoter and enhancer regions containing kB sites, and to specific inhibitors of NF-kB, such as the inhibitor of kB (IkB) α protein (Hacker and Karin 2006). RelA (p65), RelB, and c-Rel possess additional transcriptional activation domains (TAD) in their carboxyl ends allowing for positive regulation of gene expression. The absence of TAD domains in p50 and p52 subunits generates p50 and p52 homodimers that are considered to function as transcriptional repressor complexes (Tong et al., 2004; Peterson et al., 2011).

In most cells, NF-kB dimers are inactive due to their interaction with inhibitor of kB (IkB) proteins, which mask their nuclear localization signal (NLS). NF-kB pathway can be activated in response to a number of various stimuli, including viral and bacterial infection, exposure to pro-inflammatory cytokines (e.g. TNFα), growth factors, mitogens, and oxidative and biochemical stress (Li et al., 2008). Depending on the stimuli presented, a cascade of events is initiated that culminates in activation of IkB kinase (IKK) complex. The IKK complex is made up of two catalytic subunits (IKK-α and IKK-β), and a regulatory subunit (IKK-γ/NEMO) (Li et al., 2008). Depending on which IKK subunits is engaged, NF-kB is activated through either the classical (canonical) or alternative (non-canonical) pathway and is then translocated into the nucleus (Bonizzi and Karin, 2004). Depending on the pathway activated, each pathway regulates its own specific sets of target genes (Li et al., 2008).

Both cIAP1and cIAP2 have been determined to be functionally redundant critical regulators of both classical and alternative NF-kB signaling pathways (LaCasse et al., 2008; Gyrd-Hansen et al., 2010). While the classical NF-kB pathway depends on IKKβ

and IKKγ, and requires degradation of IkB proteins, the alternative NF-kB pathway is IKK-α and NIK-dependent and involves the processing of the p100 precursor protein (Hayden et al., 2008) (Figure 3).

Activation of the classical (canonical) NF-kB signaling pathway occurs when tumor necrosis factor-alpha (TNFα) a proinflammatory cytokine, stimulates its receptor TNFR1 (Dynek et al. 2013; Plati et al., 2011).Binding of TNFα triggers the recruitment of signaling adaptor proteins, including TNFR-associated death domain (TRADD) and TNFR-associated factor 2 (TRAF2), to TNFR1; these recruit c-IAP proteins and RIP1 to form the membrane-bound complex I (Park et al., 2000; Micheau et al., 2003; Vucic et al., 2011). Within this complex, cIAP1 and cIAP2 mediate ubiquitination of RIP1, themselves and other binding partners (Bertrand et al., 2008; Dynek et al., 2010; Varfolomeev, et al., 2008; Mahoney et al., 2008; Ikeda et al., 2010; Vucic et al., 2011; Varfolomeev et al., 2012). RIP1 ubiquitination allows the binding of the IKK (IKKα/β/ɣ also known as IKK1/IKK2 and NEMO) complex, the transforming growth factor-β TGFβ-activated kinase 1 (TAK1) - TAK1-binding protein 2/3 (TAB2/3), and linear ubiquitination assembly complex (LUBAC). Interestingly, ubiquitinated RIP1 does not activate the IKK complex but brings LUBAC and NEMO in proximity, allowing the ubiquitination and activation of the IKKβ kinase activity by LUBAC (Schmukle & Walczak, 2012; Silke, 2011; de Almagro and Vucic, 2012). Activated IKKβ phosphorylates IkB, leading to its ubiquitination and proteasomal degradation. This liberates NF-kB dimers and allows it to enter the nucleus to promote the expression of specific genes.

In the classical NF-kB pathway, the best characterized role of cIAP1 and cIAP2 is as an essential positive regulator of TNFα-mediated NF-kB activation (Bertrand et al., 2008; Mahoney et al., 2008). In this case, either cIAP1 or cIAP2 catalyzes the K63-ubiquitination of RIP1 (Bertrand et al., 2008), which assembles a signaling complex that is required for the activation of NF-kB. In the absence of both cIAP1 and cIAP2, TNFα-mediated NF-kB signaling is severely attenuated, and instead, RIP1 binds to caspase-8 and triggers apoptosis (Mahoney et al., 2008; Bertrand et al., 2008; Varfolomeev et al., 2008; Geserick et al., 2009). Consequently, the loss of both cIAP1 and cIAP2 sensitizes cells to TNFα-mediated apoptosis.

While cIAP proteins are required for the activation of TNF family-induced classical NF-kB signaling, they are negative regulators of the alternative NF-kB pathway (Bertrand et al., 2008; Blackwell et al., 2013; Mahoney et al., 2008; Varfolomeev et al., 2008; Vince et al., 2008).

Both cIAP1 and cIAP2 can promote K48-ubiquitination of NF-kB-inducing kinase (NIK), a key regulator of the alternative NF-kB signaling, to target it for proteasomal degradation, thus preventing the activation of the NF-kB pathway (He et al., 2007; Vallabhapurapu et al., 2008).

In the absence of cIAP1 and cIAP2, NIK accumulates and phosphorylates IKKα, thus promoting the processing of p100 into its functional p52 subunit, which then forms a heterodimer with RelB and translocates into the nucleus to target the transcription of specific genes (Bonizzi, et al., 2004; Zarnegar et al., 2008; Smale et al., 2012).

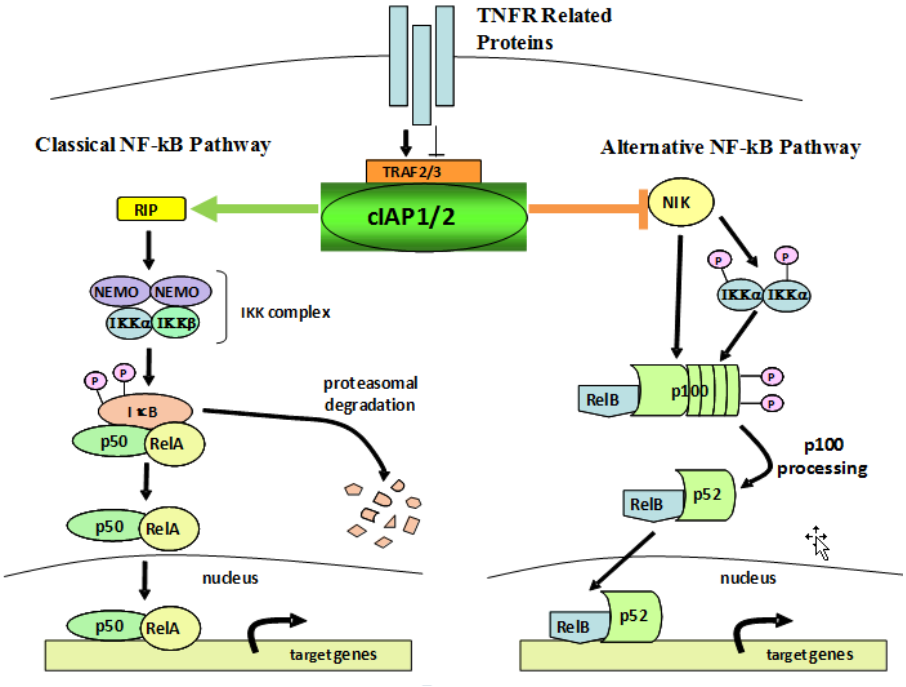

Figure 3. cIAP1 and cIAP2 positively regulate the classical NF-kB pathway and negatively regulate the alternative NF-kB

In the classical NF-kB pathway, NF-kB dimers (p50/RelA) are retained in the cytoplasm by interaction with IκB. In response to the binding of a ligand to a tumor necrosis factor receptor (TNFR) related protein, TRAF proteins are recruited to the receptor, and bring the cIAPs with them. Either cIAP1 or cIAP2 ubiquitinates RIP1 kinase, and then the IKK complex containing IKKa, IKKß and NEMO (IKKγ) is recruited and activated. The activated IKK complex in turn phosphorylates the inhibitor of κB (IκB), leading to its degradation, thereby releasing p50/RelA to translocate into the nucleus for transcriptional activation of targeted genes. By contrast, cIAP1/2 represses the alternative NF-kB pathway by promoting ubiquitination and degradation of NIK, which is required for phosphorylation of p100 in the p100/RelB complex. Phosphorylated p100 is processed into p52, and the p52/RelB dimer translocates into the nucleus for transcriptional activation of targeted genes.

Recent studies have demonstrated that both classical and alternative pathways are activated in skeletal muscle and aberrant activation of either of these two NF-kB pathways can lead to skeletal muscle atrophy (Cai et al., 2004; Hunter et al., 2004; Hunter et al., 2002; Mourkioti et al., 2006; Li et al., 2008).

1.5 The IAP antagonist Smac and its mimetic compounds

The endogenous antagonist of the IAPs, known as the second mitochondrial activator of caspases (Smac) in humans and direct IAP binding protein with low pI (DIABLO) in mice, is a mitochondrial protein that is proteolytically processed and released during apoptosis along with cytochrome c (Du et al., 2000; Verhagen et al., 2000). Smac contains an N-terminal sequence that localizes it to the mitochondria. Upon apoptotic stimulus, Smac is released from the mitochondria into the cytosol when this N-terminal sequence is proteolytically cleaved to expose its Ala-Val-Pro-Ile (AVPI) tetrapeptide motif that binds to XIAP, cIAP1 and cIAP2 (Wu et al., 2000; Chai et al., 2000; Kulathila et al., 2009). This cleaved Smac is able to bind to BIR2 and/ or BIR3 of these IAPs via its AVPI binding motif (Chai et al., 2000). Smac binds to BIR2 and BIR3 domains of XIAP and interferes with the interaction of XIAP with caspases to disrupt caspase inhibition (Liu et al., 2000; Wu et al., 2000). Smac also binds to BIR3 domain of cIAP1 and cIAP2 to promote their autoubiquitination and degradation (Yang & Du, 2004). Although Smac functions as an effective cellular antagonist of XIAP, cIAP1 and cIAP2 proteins, it can promote autoubiquitination and degradation of both cIAPs, but not XIAP (Yang & Du, 2004).

In recent years, our knowledge of the function of the N-terminal motif has contributed to the design and production of various small molecules, called Smac mimetic compounds (SMCs), that have recently emerged as promising anti-cancer therapeutics. SMCs mimic the binding of Smac protein to XIAP, cIAP1 and cIAP2. In the last decade, a large number of small-molecule SMAC mimetics have been designed and developed and several of them are currently in intense clinical development for cancer treatment (Fulda & Vucic, 2012). Their mechanism of action involves the suppression of the canonical NF-kB survival pathway by binding to cIAP1 and cIAP2 and stimulating cIAP1/cIAP2-dependent auto- or trans-ubiquitination (Flygare & Fairbrother, 2010). Induction of cIAP1/cIAP2 E3 ubiquitin ligase activity results in rapid auto-ubiquitination and subsequent proteasomal degradation of cIAP1 and cIAP2 (LaCasse et al., 2008; Cheung et al., 2009; Fulda, 2008) leaving RIP1 free to associate with FADD and to activate caspase-8. As the non-canonical NF-kB pathway is also regulated by the cIAP proteins through NIK ubiquitination, loss of cIAP1 and cIAP2 stabilizes NIK, therefore resulting in non-canonical NF-kB pathway activation, thereby leading to the induction of NF-kB target genes, including TNF-α which in turn facilitates cell death through an autocrine signaling loop (Straub, 2011; Flygare & Fairbrother, 2010).

SMCs have been developed in both monovalent and bivalent forms. Monovalent SMCs, such as LCL161 (Novartis) were designed to mimic the single AVPI binding motif which can interact with BIR domains of the IAP proteins. By contrast, the bivalent SMCs, such as OICR00720A compound, contain two AVPI binding motifs and therefore bind to IAP proteins with extremely high affinity (Mannhold et al., 2010; Straub, 2011).

Importantly, bivalent compounds demonstrate increased potency when compared to their corresponding monovalent versions. This increased potency is thought to arise from the dimers ability to bind the various IAPs together. In fact, bivalent antagonists can simultaneously bind the BIR2 and BIR3 domains of XIAP leading to enhanced activation of caspases and enhanced cell killing (Gao et al., 2007; Li et al., 2004; Varfolomeev et al., 2009, 2007; Silke & Vucic, 2014).

To date, four monovalent and two bivalent SMCs have reached phase I/II clinical trial and have been tested for their safety, pharmacokinetics, pharmacodynamics, and initial efficacy in patients with advanced solid tumors and hematological malignancies (Bai & Wang, 2014; Bai et al., 2014).

1.6 Skeletal muscle atrophy

1.6.1 Skeletal muscle

Skeletal muscle is the most abundant tissue in the human body and accounts for up to 50% of total body weight (Angione et al., 2011). Skeletal muscle mediates a variety of essential functions such as locomotion and respiration, as well as serving as a reservoir for energy storage.

Skeletal muscle is made up of multiple muscle fibers held together by connective tissue. Muscle fibers are long, cylindrical and multinucleated cells formed from the fusion of terminally differentiated myocytes, and myogenic precursor cells known as myoblasts (Scott et al., 2001).

Muscle fibers consist of myofibrillar proteins arranged in a repeating unit called a sarcomere. Sarcomeres are the basic functional unit of the muscle responsible for

contraction, and are important for muscle power, muscle growth, and protein turnover (Schiaffino and Reggiani, 2011; Tskhovrebova and Trinick, 2012). There are many myofibrillar/sarcomeric proteins; the predominant ones being, actin and myosin. Myosin is composed of heavy and light chains. One portion of myosin known as the myosin heavy chain (MHC) has multiple isoforms and is the prime determinant of the shortening velocity of muscle and the rate of force development (Bottinelli et al. 1996; Harridge et al. 1996). MHC isoforms are subdivided into two main categories: MHC type I (slow) and MHC type II (fast). MHC type I is more efficient at utilizing oxygen as a fuel source (aerobic, oxidative) and is suited for slower, prolonged contractions and is fatigue resistant. These fibers have been also referred to as "red" fibers, due to the presence of myoglobin (the primary oxygen-carrying molecule of muscle), which imparts a red color to the fiber. MHC type II (sometimes referred to as "white" fibers) is more efficient under anaerobic conditions (glycolytic) and is better suited for short bursts of intense activity (fatigable) (Pette and Staron 2000; Pette and Staron 2001). MHC type II is further divided into subtypes including MHC IIA, MHC IIX and MHC IIB (fastest). The various MHC isoforms create a spectrum of muscle phenotypes, the progression from slowest to fastest being: MHC I → MHC IIA → MHC IIX → MHC IIB. Most muscles contain a mixed population of fiber types although there are some exceptions such as the soleus muscle, which is comprised primarily of slow fibers (Falempin et al. 1990; Steffen et al. 1990; Thomason et al. 1987).

1.6.2 Skeletal muscle atrophy

Skeletal muscle atrophy is both a physiologic phenomenon that occurs as a natural consequence of muscle disuse, ageing and fasting and a pathophysiologic response to a multitude of insults including acute and chronic illnesses such as cancer, diabetes mellitus, chronic renal insufficiency, chronic obstructive pulmonary disease and denervation injury (Liu et al., 2000; Hornberger et al., 2001; Johansen et al., 2003; Pereira et al., 2005; Rhoads et al., 2010; Testelmans et al., 2010; Cooper et al., 2012). These conditions can cause muscle mass and protein content to fall below the threshold required to maintain respiratory muscles, resulting in death. Despite decades of research, no treatments have been developed to prevent loss of muscle mass. Muscle atrophy can occur locally, such as in the decreased innervation of specific muscles or can be systemic, such as during prolonged glucocorticoid treatment (Goldberg, 1969). Regardless of the initiating factors, skeletal muscle atrophy results predominantly from a loss of sarcomeric proteins due to an imbalance between myocyte protein synthesis and protein degradation (Bodine et al., 2001; Cao et al., 2005; Glass, 2010; Hansen et al., 2006; Kandarian and Jackman, 2006). This net increase in protein degradation results in smaller muscle fibers and decreased muscle mass which is associated with diminished force generating capacity.

1.6.3 Disuse skeletal muscle

Disuse muscle atrophy is mainly characterized by two significant changes in the affected muscle. The first is a decrease in overall cross-sectional area of muscle fibers (Bloomfield 1997; Edgerton et al. 2002; Kasper et al. 2002). The decrease in cross-

sectional area results primarily from an increase in protein degradation (primarily those proteins related to the contractile machinery of the muscle). This process includes activation of lysosomal (primarily cathepsins), cytosolic calcium dependent (primarily calpains), caspase and ubiquitin-proteosome pathways (Kandarian and Stevenson 2002; Ventadour and Attaix 2006). The second alteration in skeletal muscle as a result of disuse is the conversion of type I fibers to type IIX and type IIA (Bloomfield 1997; Bodine et al. 2001; Edgerton et al. 2002; Kasper et al. 2002; Pette and Staron 2000).

All muscles that are subjected to disuse conditions demonstrate the two hallmarks of atrophy; although not all muscles are affected to the same degree and at the same rate (Boonyarom and Inui 2006). In general, atrophied muscle will be weaker, have faster contractile characteristics and fatigue more rapidly. Disuse muscle atrophy affects more severely muscle that is enriched with slow fiber types, such as soleus muscle, than those with predominantly fast fiber types, such as the tibialis anterior (TA) (Bloomfield 1997; Grossman et al., 1998; Edgerton et al. 2002).Muscles enriched with slow fiber types, such as the soleus muscle, atrophy to a greater extent than those with predominantly fast fiber-types (Grossman et al., 1998). During disuse muscle atrophy, slow fiber-type I isoforms are lost, while faster type II isoforms are increased (Grossman et al., 1998). Therefore, upon disuse atrophy, muscles containing mostly type I fibers tend to shift toward a fast-twitch phenotype (Bigard et al., 1998; Stevenson et al., 2003; Lynch et al., 2007). Although the mechanisms accountable for these phenotypic changes are currently not known, it is thought to be likely due to both neuronal and myogenic factors (Lynch et al., 2007).

Disuse models of atrophy involve inducing the state of atrophy by physical means such as hind-limb suspension, bed-rest, spaceflight or denervation. Denervation is defined as a loss of nerve supply due to physical injury or motorneurone or chemical death. Denervation has been used extensively as a robust model for studying skeletal muscle atrophy. Denervation causes a breakdown of myofibrillar proteins, which is the primary cause of muscle mass loss (Goldberg, 1969) that is dependent upon the activation of the ubiquitin proteasomal pathway (Solomon and Goldberg, 1969). The ubiquitin proteasomal pathway is primarily defined by the rigorous action of three distinct enzymes which link the polypeptide cofactor ubiquitin to protein substrates to target them for degradation (Glickman and Ciechanover, 2002). Although these three enzymes work together to carry out this process, the most important is perhaps the E3 ubiquitin-ligating enzyme as it is responsible for determining which proteins are to be degraded by the proteasome and for pairing the activated ubiquitin with the protein substrates. Among the E3s of relevance to the process of muscle atrophy are the Muscle-specific Ring Finger protein 1 (MuRF1) and muscle atrophy F-box (MAFbx), whose levels were substantially elevated in disuse atrophy (Bodine et al., 2001).

Interestingly, MAFbx and MURF1 knock-out animals were considerably less sensitive to muscle atrophy than their wildtype littermates (Bodine et al., 2001). These studies fit well with many previous observations that the ubiquitin proteasome system plays a critical role during skeletal muscle atrophy (Jagoe et Goldberg, 2001).

1.7 The ubiquitin-proteasome system and its role in skeletal muscle atrophy

There are multiple proteolytic pathways in mammalian cells that participate in the development of skeletal muscle atrophy, including the lysosome/autophagy, calcium dependent calpain, and the ubiquitin proteasome system (UPS) (Zhao et al., 2007; Goll et al., 2007). Although, proteins may be degraded by calcium dependant proteases and lysosomal proteases, inhibition of these pathways is not sufficient to reverse the protein loss which occurs during skeletal muscle atrophy (Ventadour et al., 2006). However, inhibition of the proteasome can inhibit the increase of protein degradation in atrophying skeletal muscle (Price et al., 1996). Therefore, the UPS is considered the predominant proteolytic pathway responsible for the development of skeletal muscle atrophy (Wing et al., 1995; Annabelle et al., 2011).

Ubiquitination is a reversible post-translational modification that involves the covalent attachment of ubiquitin onto target proteins (Ciechnover, 1994). Ubiquitin is an 8.5 kDa protein that is ubiquitously expressed in all cell types. Ubiquitin exerts its effect by binding to a protein substrate (Glickman et al., 2002). Ubiquitin contains seven lysines (K6, K11, K27, K29, K33, K48, and K63), and ubiquitin molecules can be linked through any one of these seven lysines (Kravtsova-Ivantsiv et al., 2012; Bodine et al., 2014). Ubiquitin can be added to a protein as a single entity (monoubiquitin) or as a chain of variable length (polyubiquitin). In general, when polyubiquitin chains form on the K48 linkage, the substrate is recognized and degraded by the 26S proteasome (Hershko et al., 1998). Alternatively, the polyubiquitin chains that are formed on K63 linkage lead to proteasome independent functions, including roles in DNA repair, translation, protein trafficking, kinase activation and endocytosis (Mukhopadhyay et al., 2007).

The ubiquitination of proteins is a multistep process which is controlled by three distinct enzymes: ubiquitin-activating enzyme (E1), ubiquitin-conjugating enzyme (E2) and ubiquitin-ligase (E3) (Metzger et al., 2012). Ubiquitin is first activated by its ATP-dependent binding to E1. The activated ubiquitin is then transferred to E2. The final step takes place when E3 ligase transfers the activated ubiquitin from the E2 to a specific target protein (Navon et al., 2009; Passmore et al., 2004). During the polyubiquitination process, these three steps are repeated until a chain of four or more ubiquitin molecules is formed. The polyubiquitin-labeled protein, in case of K48 linkage, is then targeted for proteasomal degradation (Figure 4). It is important to mention that among the three enzymes involved in this process, it is the E3 ubiquitin ligase that plays a critical role in determining which protein is targeted for degradation thereby conferring specificity to the system (Chopard et al., 2009).

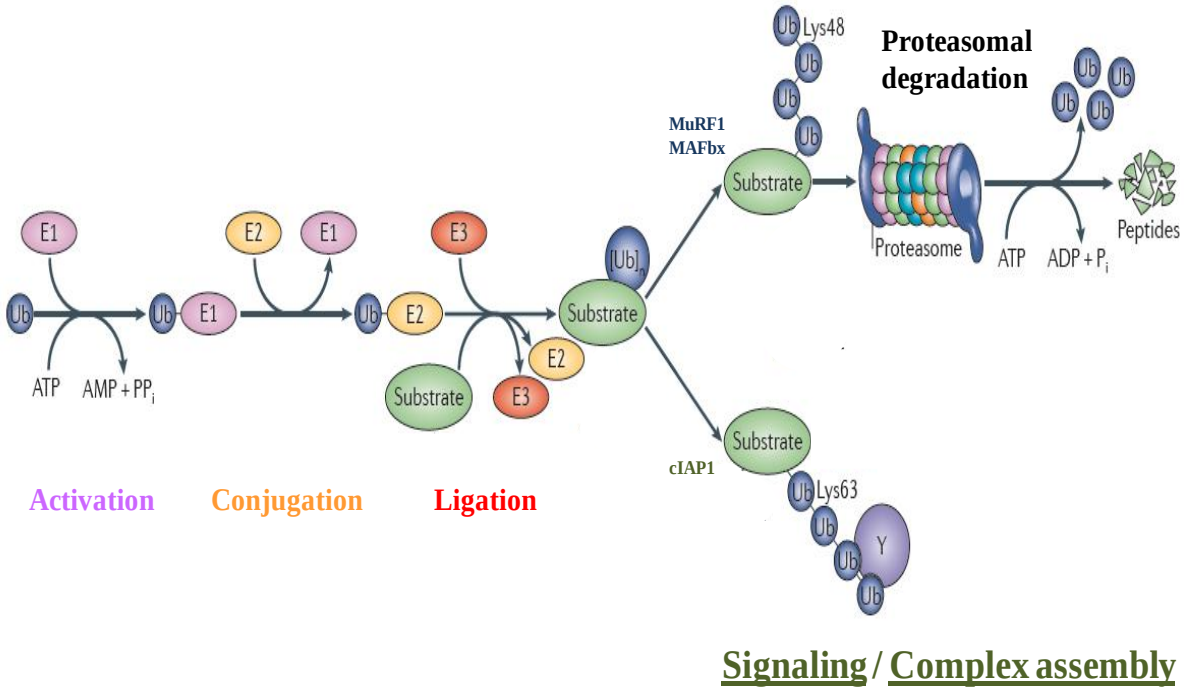

Figure 4. The ubiquitin–proteasome system

The ubiquitination and degradation of substrate proteins is achieved by a series of reactions mediated by the enzymes of the ubiquitin–proteasome system. In the activation reaction, ubiquitin is transferred to an E1 enzyme. The activated ubiquitin is subsequently transferred to an E2 enzyme in the conjugating reaction. The E2 enzyme then carries the ubiquitin to the E3 enzyme, which is also known as a ubiquitin ligase. The E3 enzyme ligates ubiquitin to Lys residues on the substrate protein, and thus mediates substrate specificity. This process of ubiquitin ligation may be repeated leading to the formation of a polyubiquitin chain on the target protein. Ligation of polyubiquitin has diverse biological consequences. Lys48-linked polyubiquitin chains target substrate proteins for proteasomal degradation, whereas Lys63-linked chains promote the assembly of signaling complexes. (Adapted from Vucic et al., 2011).

In 2001, two specific E3 ligases, muscle ring finger 1 (MuRF1) and muscle atrophy F-box (MAFbx) (also called atrogin 1) were found to play a critical role in the induction of skeletal muscle atrophy (Bodine et al., 2001; Gomes et al., 2001). Under several atrophy-inducing conditions, MuRF1 and MAFbx mRNA expression has been reported to be elevated and thus the two genes have become recognized as key markers of muscle atrophy (Bodine et al., 2014; Zhang et al., 2007). Mice lacking either the MuRF1 or MAFbx gene are phenotypically normal. However, under atrophy conditions mice lacking either of these two E3 ubiquitin ligase expression, MuRF1 or MAFbx, showed protection against skeletal muscle atrophy induced by denervation (Bodine et al., 2001).

MuRF1contains a RING finger E3 ligase domain, a MuRF1 family conserved domain, a B-box domain, coiled-coil domains, and an acidic tail region (Foletta et al., 2011; Bodine et al., 2014). MuRF1 has been shown to exert its ubiquitin-ligase activity via the RING domain (Bodine et al., 2001). It was reported that MuRF1 bind to many muscle structural proteins, including titin (Centner et al., 2001; McElhinny et al., 2002), troponin I (Kedar et al., 2004), and more importantly to the most abundant protein in the skeletal muscle: myosin heavy chain (MHC) (Clarke et al., 2007; Fielitz et al., 2007), as well as myosin binding protein C and myosin light chain (Cohen et al., 2009). Unlike titin and troponin I, which also bind MuRF1, myosin heavy chain as well as myosin binding protein C and myosin light chain can be directly ubiquitinated by MuRF1 (Clarke et al., 2007; Cohen et al., 2009; Egerman et al., 2014).

MAFbx contains 2 nuclear localization signals, a leucine-zipper domain, a leucine charged residue-rich domain, an F-box domain, and a PDZ domain (Foletta et al., 2011). Among these domains, the F-box is responsible for targeting specific protein to

proteasomal degradation (Zhan et al., 2007). Both MyoD, a key muscle transcription factor involved in the myogenic program as well as protein synthesis, and eIF3f, an important activator of protein synthesis, have been shown to be targeted for degradation by MAFbx (Csibi et al., 2010; Tintignac et al., 2005).

1.8 NF-kB involvement in skeletal muscle atrophy

Nuclear factor-kappa B (NF-kB) is a nuclear transcription factor complex expressed in several tissues including skeletal muscle (Mourkioti et al., 2008). The NF-kB pathway has long been known to be a robust inducer of atrophy (Li et al., 1998; Jackman et al., 2004, Minetti et al., 2011), and several studies indicate that MuRF1 is an NF-kB transcriptional target (Cai et al., 2004; Mourkioti et al., 2006; Li et al., 2008; Mittal et al., 2010). NF-kB signaling plays an important role in the development of skeletal muscle atrophy due to cancer cachexia (Cai et al, 2004), sepsis (Penner et al., 2001), disuse (Hunter et al., 2002; Hunter and Kandarian, 2004), and muscle denervation (Cai et al., 2004; Mourkioti et al., 2006).The role of NF-kB in denervation-induced skeletal muscle atrophy was elucidated by two independent studies using transgenicc mice (Cai et al., 2004; Mourkioti et al., 2006).

Cai and his team studied the in vivo role of NF-kB in denervation-induced skeletal muscle atrophy using muscle specific expression of either constitutively active IkB kinase β (IKKβ) in skeletal muscle of mice referred to as MIKK (muscle specific expression of activated IKKβ), or a dominant inhibitory form of IkBα in the skeletal muscle of mice, referred to as MISR (muscle specific overexpression of IkBα super-repressor) (Cai et al., 2004). In this study, the group demonstrated that selective

activation of NF-kB pathway in MIKK mice resulted in the development of severe skeletal muscle atrophy; whereas, as expected, blockage of NF-kB pathway in MISR mice did not affect muscle mass. Furthermore, inhibition of the NF-kB pathway in MISR mice which were subjected to denervation-induced atrophy significantly blunted denervation-induced loss of skeletal muscle mass and fiber size (Cai et al., 2004), suggesting that the classical NF-kB plays a critical role in denervation-induced skeletal muscle atrophy.

This demonstrates that constitutive activation of NF-kB by IKKβ is sufficient to promote skeletal muscle atrophy. This concept is supported by another study which demonstrated that targeted deletion of IKKβ in mice ameliorated denervation atrophy (Mourkioti et al., 2006).

Similar to these studies, the Kandarian group studied the in vivo role of NF-kB using unloading-induced atrophy model and reported that overexpression of the IkBα super-repressor in muscle inhibited atrophy (Judge et al., 2007). Furthermore, overexpression of either IKKβ or IKKα super-repressor in muscle blunted unloading-induced atrophy (Van Gammeren et al., 2009). During immobilization, overexpression of IKKβ super-repressor also inhibited atrophy (Reed et al., 2011). Therefore, both kinases of the IKK complex, IKKα and IKKβ are necessary and required for disuse-induced skeletal muscle atrophy (Jackman et al., 2013**)**.

Moreover, it has been reported that unloading resulted in significant increase of the nuclear levels of p50 (NF-kB family member) and Bcl-3 ((B cell lymphoma 3), an unusual member of the IkB family which is known to activate p50 homodimer-induced gene expression but not p65 (Hunter et al., 2002). This evidence suggested that

unloading-induced muscle atrophy is associated with the activation of an alternative NF-kB pathway that involves p50 and Bcl-3, but not p65. Using NF-kB1 (encodes p50) and Bcl-3 knockout mice, the Kandarian group showed that muscle atrophy induced by unloading was blocked in NF-kB1-null as well as Bcl-3-null mice (Hunter and Kandarian, 2004), indicating that p50 and Bcl-3 are both required for unloading atrophy. More recently, this group demonstrated that atrophy was not blocked in c-Rel-null mice (Judge et al., 2007), suggesting that unlike p50 and Bcl-3, c-Rel is not required for unloading-induced atrophy.

Although it is well established that constitutive NF-kB activity promotes muscle atrophy (Cai et al., 2004; Hunter and Kandarian 2004), the upstream initiating and downstream regulatory events involved in NF-kB in muscle in muscle are still poorly understood.

1.9 TWEAK/Fn14 system and its involvement in skeletal muscle atrophy

Tumour necrosis factor (TNF)-like weak inducer of apoptosis (TWEAK) is a multifunctional cytokine that belongs to the TNF family members (Chicheportiche et al., 1997; Winkles, 2008). Although, as its name suggests, TWEAK was originally found to be a weak activator of apoptosis for certain tumor cell lines (Chicheportiche et al., 1997), subsequent studies revealed its involvement in many other cellular responses including proliferation, differentiation, survival, migration, angiogenesis and inflammation (Burkly et al., 2011; Winkles, 2008).

TWEAK is broadly expressed in various tissues including heart, brain, pancreas, intestine, ovary, vasculature, liver, kidney and skeletal muscle (Chicheportiche et al., 1997; Marsters et al., 1998).

TWEAK is synthesized as a type II class transmembrane protein comprising a C-terminal extracellular domain, a transmembrane domain and an N-terminal intracellular domain. While TWEAK can be cleaved at its C-terminal domain to function as a soluble form (Wajant 2013; Winkles, 2008), full length TWEAK can function as a membrane-bound form (Winkles, 2008). In both cases, TWEAK trimerizes and signals as homotrimer molecule (Winkles, 2008).

TWEAK binds to its receptor, called fibroblast growth factor-inducible 14 (Fn14), which is the smallest TNF receptor super family member with a molecular weight of about 14 kDa (Wiley et al., 2001). Fn14 is expressed at low levels in healthy tissues except in progenitor cells (Sato et al., 2014). By contrast, the expression of Fn14 is upregulated after tissue injury and in various disease conditions, such as cancer, inflammatory liver diseases, rheumatoid arthritis, multiple sclerosis, cardiac dysfunction and failure, systemic lupus erythematosus, and skeletal muscle atrophy (Burkly et al., 2011; Winkles 2008; Sato et al., 2014). Fn14 was initially identified as a transcriptional target of fibroblast growth factor-1 in NIH 3T3 fibroblasts (Meighan-Mantha *et al*., 1999), however it was later recognized as a TNF receptor family member able to transduce TWEAK signals (Wiley *et al*., 2001; Wajant, 2013). Fn14 is a transmembrane type I receptor comprising an N-terminal extracellular domain, a transmembrane domain and a C-terminal intracellular domain. The extracellular domain contains a cystein-rich domain necessary for TWEAK binding (Brown et al., 2003; He et al., 2009). The

intracellular domain contains a TNFR-associated factor (TRAF) binding site which allows recruitment of various TRAFs including TRAF1, TRAF2, TRAF3 and TRAF5 (Brown et al., 2003; Winkles 2008) but, unlike other members of TNFRSF, does not contain a death domain (Brown et al., 2003). This intracellular domain has a short cytoplasmic tail, yet it can activate various signaling pathways including MAPK, PI3K/Akt and both the classical and alternative NF-kB signaling in various cell type including skeletal muscle (Srivastava et al., 2007; Han et al., 2003; Polek et al., 2003; Dogra et al., 2007; Burkly 2011; Bhatnagar et al., 2012). TWEAK binding to Fn14 can activate the classical NF-kB pathway characterized by the phosphorylation and subsequent degradation of IκBα, allowing the p50/p65 heterodimer to translocate into the nucleus, bind to DNA and regulate gene expression of various genes (Roos et al., 2010; Saitoh et al., 2003). FN14 also has the capability for long-lasting NF-kB signaling, which requires p100 processing into p52. This results in the formation of the p52 – RelB complex that translocates to the nucleus and initiates the transcription of target genes (Saitoh et al., 2003; Razani et al., 2011).

In cultured myotubes, addition of soluble TWEAK causes severe atrophy resulting in reduced myotube size and decreased protein content including the reduction of myosin heavy chain (MHC) levels (Dogra et al., 2007; Bhatnagar et al., 2012). It has been shown that the primary system that induces the degradation of selective muscle proteins is the ubiquitin-proteasomal system (UPS) (Bodine et al., 2001; Foletta et al., 2011). In cultured myotubes, TWEAK increases the expression of both MuRF1 and MAFbx, which are two key enzymes of the UPS involved in the breakdown of structural proteins including MHC leading to myotube atrophy (Bhatnagar et al., 2012; Dogra et al.,

2007; Sato el al., 2014). More specifically, it has been reported that MuRF1 causes degradation of MHC and atrophy in cultured myotubes through sustained activation of NF-kB pathway (Clarke et al., 2007; Dogra et al., 2007; Cohen et al., 2009; Yamaki et al., 2012). In addition to ubiquitin-proteasome system, the autophagy-lysosomal system and caspases play important roles in muscle proteolysis in TWEAK-induced myotube atrophy (Bhatnagar et al., 2012).

Consistent with studies *in vitro*, TWEAK also induces atrophy *in vivo.* Treatment of mice with TWEAK leads to significant reduction in body weight, muscle weight as well as cross-sectional area when compared to wild type mice (Dogra et al., 2007). Muscle-specific TWEAK transgenic (mTWEAK-Tg) mice or systemic and chronic administration of TWEAK in mice causes NF-kB activation, increased expression of MuRF1 and degradation of muscle proteins including MHC (Dogra et al., 2007; Mittal et al., 2010). Interestingly, although expression of MAFbx was induced in TWEAK-treated myotubes, no significant difference was observed in skeletal muscle of mTWEAK-Tg and wild type mice (Dogra et al., 2007; Bhatnagar et al., 2012).

The role of TWEAK was further investigated in disuse atrophy including denervation-induced skeletal muscle atrophy. Upon denervation, the loss of muscle mass, fiber cross-sectional area and muscle atrophy significantly increased in mTWEAK-Tg mice compared to wild type mice (Mittal et al., 2010). Conversely, skeletal muscle mass and affected functions were spared in denervated fibres from TWEAK-null mice compared to wild type mice (Mittal et al., 2010). Additionally, overexpression of TWEAK in skeletal muscle stimulated NF-kB activation and induced MuRF1 expression in denervated skeletal muscle of mTWEAK-Tg mice compared with corresponding

control mice, whereas depletion of TWEAK expression blunted NF-kB activation and MuRF1 expression in denervated muscle of the TWEAK-null mice (Dogra et al., 2007; Mittal et al., 2010). Interestingly, expression of Fn14, but not TWEAK, was dramatically increased in skeletal muscle upon denervation (Mittal et al., 2010). Taken together, these studies provide evidence that TWEAK/Fn14 system mediates skeletal muscle atrophy in response to denervation.

1.10 Hypotheses and objectives of the thesis

The overall hypothesis of my PhD thesis was to test whether cIAP1is a critical regulator of skeletal muscle atrophy.

For this, I first tested whether cIAP1 positively regulate NF-kB signaling pathway. The objective of this study was to investigate the role of cIAP1 in TNFα-mediated NF-kB signaling in myoblasts by using combined genetic knockout and siRNA-mediated knockdown strategies.

The second hypothesis of my thesis was that cIAP1 is a critical regulator of skeletal muscle atrophy. To test this, I elucidated the role of cIAP1 in a denervation-induced model of skeletal muscle atrophy. To this end, I used novel genetic and pharmacological means to inhibit cIAP1 expression.

Furthermore, I investigated the molecular mechanism(s) by which the absence of cIAP1 confers protection against denervation-induced muscle atrophy. Hence, I first asked whether loss of cIAP1 affects the expression of two muscle-specific E3 ligases in response to denervation. Additionally, I determined the expression of both TWEAK and Fn14 in the absence of cIAP1 in denervated muscles. Moreover, since no direct correlate

exists for testing denervation-induced atrophy *in vitro*, I tested the effects of cIAP1-deficiency in culture models of TWEAK-induced atrophy to further dissect the protection.

Chapter 2: Materials and Methods

2.1 Cell culture

Murine C2C12 myoblasts and human HeLa cervical carcinoma cells were purchased from American Type Culture Collection (ATCC), maintained at 37°C and 5% CO_2, and cultured in complete media: Dulbecco's modified Eagle medium (DMEM) (Invitrogen) supplemented with 10% heat-inactivated fetal calf serum (FCS) (Invitrogen), penicillin, and streptomycin (Invitrogen). C2C12 cells stably expressing an NF-kB luciferase reporter were purchased from Panomics Laboratories and cultured in complete medium. Wild type (WT) and cIAP1-null mouse embryonic fibroblsts (MEFs) were kindly provided by T. W. Mak (Campbell Family Institute for Breast Cancer Research, Toronto, Canada) and cultured in complete media supplemented with nonessential amino acids.

2.2 siRNA transfection and TNFα treatment

Chemically synthesized siRNA duplexes were purchased from Invitrogen, and the following sequences were used for all experiments: *non-targeting*: GGA UCC UUG ACA AUA CCA A[dT][dT] and UUG GUA UUG UCA AGG AUC C[dT][dT]; *cIAP1*: GCA AGU GCU GGA UUC UAU U[dT][dT] and AAU AGA AUC CAG CAC UUG C[dT][dT]; *cIAP2*: GCA CAA GUC CCU ACC ACU U[dT][dT] and AAG UGG UAG GGA CUU GUG C[dT][dT]; *XIAP*: GGA CAU CCU CAG UUA ACA A[dT][dT] and UUG UUA ACU GAG GAU GUC C[dT][dT]. For siRNA transfection, cells transfected with a total of 500 ng of siRNA using 5 μl of Lipofectamine RNAi MAX (Invitrogen).

For TNFα treatment**,** cells were incubated in the presence of recombinant mouse TNFα (R&D Systems) at a concentration of 10 ng/ml (non toxic dose).

2.3 Adenovirus rescue experiment

For adenovirus rescue experiments, C2C12 myoblasts were seeded at 5 X 10^4 per 35-mm well and treated with siRNA targeting cIAP1 the next morning. Four hours later the media were replaced, and adenovirus expressing LacZ, XIAP, or cIAP1 was added at an MOI of 100. Twenty hours later, the media were replaced and experiments were conducted.

2.4 Protein extraction and western blotting

Cells were washed with phosphate-buffered saline (PBS) and harvested by adding total cell lysis buffer (50 mM Tris-HCl; 150 mM NaCl; 1% Triton X-100; 1% SDS) directly to the culture wells. Cell lysates were then ‘‘sheared’’ using a 28-g insulin syringe. Protein content was determined using the Lowry assay (Bio-Rad Laboratories). Total cell lysates were prepared in SDS sample buffer, and 5–50 µg of total protein was separated by SDS-PAGE on 10% Bis-Tris gels and transferred to nitrocellulose membranes. For experiments performed to study the role of cIAPs in TNFα-induced NF-kB signaling, membranes were probed with primary antibodies diluted in 5% skim milk powder (SMP) overnight at 4°C, followed by HRP-conjugated secondary antibodies diluted in 5% SMP for 1 h at room temperature. Membranes were then treated with enhanced chemiluminescence (ECL) reagent, exposed to x-ray film and developed (Kodak X-Omat 2000A). The following primary antibodies were used: GAPDH

(Advanced ImmunoChemical), phopsho-IκBα (Ser32) (Cell Signaling Technology), IκBα (Cell Signaling Technology), phospho-p65 (Ser536) (Cell Signaling Technology), p65 (Cell Signaling Technology), c-FLIP (Alexis Biochemicals), PARP (Cell Signaling Technology), caspase 3 (Cell Signaling Technology), caspase 8 (Cell Signaling Technology), and myc-tag (Stressgen Biotechnologies).

For *in vivo* (denervation-induced atrophy) and *in vitro* (TWEAK-induced atrophy) experiments, protein content of lysates was determined using the Bio-Rad (Mississauga, ON, Canada) protein assay using bovine serum albumin (BSA) as a standard. Samples were solubilised with sample buffer (62.5 mM Tris-HCl, pH 6.8 containing 2% SDS, 1% *β*-mercaptoethanol and 5% glycerol). Equal amounts of samples, 20 - 100µg, were separated on a 10 - 15% Sodium Dodecyl Sulphate PolyAcrylamide Gel Electrophoresis (SDS-PAGE) then transferred to a nitrocellulose membrane. Following protein transfer, the membrane was blocked with Odyssey blocking buffer (LI-COR, Biosciences) for 1 hour at room temperature. Individual proteins were detected by using the following primary antibodies: anti-Fn14 (1:500; Cell Signaling Technology), anti- MuRF1 (1:200; R&D Systems), anti-MHC (1:500; Development Studies Hybridoma Bank, MF20), anti-Gapdh (1:10000; Advanced ImmunoChemical, clone 6C5). Our rabbit anti-rat IAP1 (RIAP1) (1: 5000) and anti-rat IAP3 (RIAP3) (1: 10000) polyclonal antibody was used to detect mouse cIAP1/2 and XIAP respectively (Mahoney et al., 2008). Membranes were washed with Tris- Phosphate Buffered Saline with Tween (TBT-T) 3 times for 15 minutes each. Bound primary antibodies were reacted with secondary antibodies conjugated to AlexaFluor680 (Invitrogen) or IRDye800 (Rockland, Gilbertsville, PA, USA). Membranes were then washed 4 times for 15 minutes with TBT-T and the infrared

fluorescent signals were detected using the Odyssey Infrared Imaging System (LI-COR, Biosciences).

2.5 Viability assays

Cell viability was assessed using the WST-1 viability assay, as outlined in the manufacturer's instructions (Promega). WST-1 produces a specific dye (formazan) upon metabolically active cells, allowing a colorimetric measurement of cell viability.

2.6 NF-kB luciferase activity analyses

To measure luciferase activity, cells were lysed directly on plates in lysis buffer (25 mM Gly-Gly; 15 mM MgSO4; 1% Triton X-100; 1 mM DTT). 10 µl of cell lysates was added to 90 µl of assay buffer (80 mM Gly-Gly; 12 mM MgSO4; 16 mM KPO4; 2 mM ATP; 2 mM DTT) and 100 µl of Luciferin Reagent (0.1 mM Luciferin; 90 mM Gly-Gly; 15 mM MgSO4) and read, in triplicate, on a luminometer.

2.7 Animal models and experimental design

2.7.1 Mouse lines and genotyping

C57BL/6 and cIAP1-null mice were housed in a clean, temperature-controlled (20-22°C) room at the Animal Care Facility of the University of Ottawa, Faculty of Medicine, on a twelve-hour light/dark cycle, and had ad libitum access to standard diet. cIAP1-null mice were obtained from Dr Tak W. Mak (Toronto, ON., Canada) (Conze et al., 2005) (Mahoney et al., 2008). Because cIAP1-null mice were in the C57BL/6 background, C57BL/6 mice were chosen to be used as control. These mice were

purchased from Charles River Laboratories (St Constant, PQ, Canada). To obtain wild type sibling control animals, cIAP1-null were backcrossed to a C57BL/6 background for several generations to produce cIAP1-null and wild type littermates. Their genotype was determined by Polymerase Chain Reaction (PCR) analysis from ear or tail DNA and was confirmed by western blotting analysis of cIAP1 protein level in brain and spleen. To induce muscle atrophy by disuse, four to six-week-old cIAP1-null and/or C57BL/6 mice were subjected to sciatic denervation of the left hind limb. The contralateral limb was used as control. Mice were sacrificed and tissues were collected at day 7, 14 or 28 post-denervation. To study the effect of cIAP1 inhibition using SMC on denervation-induced muscle loss, four to six-week-old C57BL/6 mice were treated with SMC or vehicle, then four days later were subjected to denervation. Mice were sacrificed and tissues were collected at different time points. See below for more details.

All animal procedures, including surgical and drug treatment procedures, were approved by the Institutional Animal Care and Use Committee at the University of Ottawa.

2.7.2 Denervation of hind limb muscles

Disuse atrophy was modeled in mice by denervation of the sciatic nerve. Four to six-week-old C57BL/6 and/or cIAP1-null mice were anesthetised, left hind quarters were shaved, and a one-centimeter incision was made in the mid-lateral side of the thigh. Muscles were then separated, the sciatic nerve was lifted out using a surgical forceps, and a five to ten millimeter piece was removed from the sciatic nerve that innervates the entire hindlimb. The incision was then closed with surgical sutures. The contralateral leg served as an internal control. Mice were sacrificed after 7, 14, or 28 days of denervation

and skeletal muscles such as gastrocnemius, TA and soleus were carefully excised from both the denervated and nondenervated limbs of the mice. Brain and spleen were also collected to analyze the level of cIAP1 protein.

2.7.3 Smac mimetic compound (SMC) formulation and administration *in vivo*

The monovalent Smac mimetic LCL161 was kindly provided by Novartis Pharmaceuticals and was used in this *in vivo* study. SMC was initially dissolved in 0.1 N HCl and then diluted in 100 mM of sodium acetate buffer pH 4.63 to produce a final solution with pH 4.3 – 4.6. To inhibit cIAP1 *in vivo*, age-matched C57BL/6 mice were randomly assigned to control (vehicle) or SMC-treatment. SMC, LCL161, was delivered once a week via oral gavage, at a dose of 100 mg/kg (unless otherwise specified). At various time points following SMC treatment, mice were sacrificed and tissues were collected to examine levels of cIAP1 protein using Western blotting.

To study the effect of SMC-induced cIAP1 degradation on denervation-induced skeletal muscle loss, age-matched C57BL/6 mice were randomly assigned to control (vehicle) or SMC-treatment (once a week, as just described), four days later these mice were either denervated (as described previously) or not. Fourteen days post-denervation, mice were sacrificed and skeletal muscles were collected for histological experiments or protein extraction and western blotting.

2.8 Tissue preparation

Gastrocnemius, tibialis anterior (TA) and soleus muscles were carefully collected individually from both the denervated (DEN) and nondenervated (NDN) limbs, using

standard dissection methods. Brain and spleen were also collected to confirm the genotype. Following excision, tissues were either 1) flash-frozen in liquid nitrogen for RNA and protein extraction or 2) embedded in OCT compound (Thermo Shandon, Pittsburgh, PA, USA), frozen in melting isopentane precooled with liquid nitrogen, and stored in -80oC until further processing.

2.9 Muscle histology and fiber cross-sectional area (CSA) analysis

2.9.1 Muscle sectioning

Denervated and nondenervated OCT-embedded muscles were cut into ten microns trans-sections using a cryostat and stored at (-80°C) until later use.

2.9.2 Haematoxylin and eosin staining

To assess muscle morphology, muscle transverse sections were stained with haematoxylin and eosin (H&E) using standard technique. Briefly, sections were prepared for staining by air-drying at room temperature for 15 minutes, incubated in Mayer's haematoxylin for 3 minutes, rinsed in distilled water, counterstained in eosin solution for 1 minute, rinsed again, dehydrated in 95% ethanol then in absolute alcohol twice for 2 minutes each. Muscle sections were then equilibrated by incubating the slides in two changes of xylene for 5 minutes each, and then mounted using xylene based mounting solution and allowed to dry for 1 hour before analysis.

2.9.3 Measurement of fiber cross-sectional area, fiber size distribution and data analysis

The stained sections were photographed using Zeiss Axiophot microscope equipped with a digital camera and Northern Eclipse image analysis software (Empix Imaging, Mississauga, Ontario). Fiber cross-sectional areas (CSA) of both nondenervated and denervated C57BL/6 and cIAP1-null, were traced and measured in μm^2 using ImageJ software. Data was transferred into a Microsoft Excel sheet. Mean fiber CSA was calculated using standard formula and the results were reported as means ± standard errors.

Frequency distribution of fiber size of nondenervated and denervated sections from C57BL/6 and cIAP1-null mice were calculated by determining the number of measurements that fell within the given area ranges.

2.10 Immunohistochemical and fibre type composition analysis

2.10.1 Immunofluorescent staining

For immunohistochemistry study, denervated and nondenervated frozen transverse soleus sections from C57BL/6 and cIAP1-null mice were air dried at room temperature for fifteen minutes, washed twice in phosphate-buffered saline (PBS) for five minutes each, and incubated, overnight at 4°C under humidified conditions, with primary antibodies diluted in PBS containing 0.3% Triton X-100 (Sigma) and 10% of blocking serum. The primary antibodies were rabbit anti-laminin (Sigma) and mouse anti–MHC type I (Sigma). The next day, sections were washed three times in PBS for five minutes each at room temperature, and incubated with the appropriate secondary antibody, Alexa

Fluor 546–conjugated secondary and FITC antibodies (Invitrogen) diluted in PBS with the nuclear counterstain Hoechst (Sigma), for one hour at room temperature in a humidified chamber protected from light. Sections were then washed three times in PBS in the dark for five minutes each. The slides were mounted using fluorescence medium (Vector Laboratories) and covered with cover slips and allowed to dry in the dark prior to analysis. Fluorescence-stained sections were visualized under a fluorescent microscope at room temperature then stored in the dark at 4°C until later use.

2.10.2 Fibre type composition analysis

The Fluorescence-stained soleus sections from cIAP1-null and C57BL/6 mice were photographed using a Zeiss Axiophot microscope equipped with a digital camera and Northern Eclipse image analysis software (Empix Imaging, Mississauga, Ontario). Images were analyzed and MHC type I (red-stained) and MHC type II (unstained) fibers, from the whole section of each muscle, were counted using ImageJ software. Data was transferred into a Microsoft Excel sheet and the sums of each fiber type and the total number of fibers per section were calculated using standard formula. Each fiber type was presented as percentage of the total fibers ± standard errors.

2.11 RNA extraction

To measure relative mRNA expression levels, total RNA was extracted from pulverized soleus muscle samples using the Qiagen RNeasy Fibrous Tissue kit (Qiagen Inc., Missisauga, ON) according to the manufacturer's protocol. DEN and NDN soleus muscle, isolated from C57BL/6 and cIAP1-null mice were used. RNA was eluted into

25ul RNase-free water and kept on ice. RNA concentration was determined by measuring the absorbance at 260 nm (A_{260}) using a spectrophotometer (Eppendorf Biophotometer, Hamburg, Germany). Purified RNA was kept on ice or stored in (-80°C) to avoid RNA degradation until further use.

2.12 Quantitative reverse real-time transcription polymerase chain reaction (qRT-PCR)

To measure the mRNA levels of different genes one step quantitative reverse transcription-PCR was performed, using the QuantiTect SYBRGreen RT-PCR kit (Qiagen), on an Eppendorf Mastercycler ep realplex. The following validated gene-specific QuantiTect Primers (MuRF1: QT00291991; Fn14: QT00255038; TWEAK: QT01743252; Gapdh: QT01658692) were used according to the manufacturer's instructions. To quantify the MAFbx mRNA level, the following primer sets: MAFbx-5'-AGCGACCTCAGCAGTTACTGC-3' and 5'-CTTCTGGAATCCAGGATGGC-3', 18s-5'-CGCCGCTAGAGGTGAAATC-3' and 5'- CCAGTCGGCATCGTTTATGG-3' were used with the following thermal conditions: initial denaturation step at 95°C for 15 s, annealing at 60°C for 30 s, and extension at 72°C for 30s, and a final melting curve step at 95°C for 15 s, 60°C for 15 s, and 95°C for 15 s. To reduce variation, all reactions were performed in duplicate. No genomic DNA amplification was seen with controls that lack the reverse transcription step. Data normalization was accomplished using the endogenous control (glyceraldehyde-3-phosphate dehydrogenase (Gapdh) or 18s), and the normalized values were subjected to a $2^{-\Delta\Delta Ct}$ formula to calculate the fold change between the control and experimental groups.

2.13 Protein extraction from mouse tissue

Isolated tissues from denervated cIAP1-null and C57BL/6 mice were homogenized in buffer A (50 mM Tris, pH 7.4, 150 mM NaCl, 1% Triton X-100, 1% SDS, 0.1 mM PMSF, 10 ug/ml leupeptin, 10 ug/ml aprotinin, 5 ug/ml peptstain A) or RIPA buffer (Sigma-Aldrich) using a Polytron tissue homogenizer. Samples were incubated on ice for 45 minutes then centrifuged for 20 minutes at 4°C at 300 x g. The supernatant was collected and kept on ice or at (-80°C) until further processing.

2.14 Primary myoblast isolation

Satellite cells were isolated from hind limb muscles of 4-week-old C57BL/6 and cIAP1-null mice. Muscle samples were first cleaned from excess connective tissues and fat in sterile PBS, then cut longitudinally to about halfway down their length and transferred with collagenase (Invitrogen)/Dispase (Roche) solution in shaker at 37°C for 2 hours. The digested muscle was triturated until complete dissociation of the myofibers, filtered through a 0.2 µm membrane to remove undigested connective tissue, spun at 300 x g for 5 minutes, resuspended in plating media containing Dulbecco's modified Eagle medium (DMEM) (ATCC) with 10% equine serum and 5 ng/ml bFGF (basic Fibroblast Growth Factor) (Peprotech via Cedarlane). It is important to mention that primary culture derived from skeletal muscle contain mainly myoblasts and fibroblasts. In order to separate these two cell populations and purify the culture from unwanted fibroblasts, cells were enriched by pre-plating onto a standard (uncoated) 10 cm tissue culture plate for 1 h at 37°C and 5% CO_2. Non-adherent myoblasts were transferred to a 35-mm matrigel-coated plate (Growth factor-reduced Matrigel was obtained from BD Biosciences and

diluted 1:10 in ice-cold DMEM). After approximately 48 h in culture, the myoblasts were transferred to and maintained in growth media containing DMEM, 20% Fetal Bovine Serum (FBS), 10% equine serum, 10 ng/ml bFGF, and 2 ng/ml HGF (Hepatocyte Growth Factor) (Peprotech via Cedarlane).

2.15 Primary myoblast culture

Primary myoblasts were maintained in matrigel-coated plates and growth medium (DMEM, 20% FBS, 10% equine serum, 10 ng/ml bFGF, and 2 ng/ml HGF) was changed every day. Cells were split before they reach 80% confluence. Conversely, they should not be seeded at less than 20% confluence. Every 2-3 passages and before seeding primary myoblasts for an experiment, cells were pre-plated for 1 hour to purify the culture from fibroblasts.

2.16 Primary myoblast differentiation

Primary myoblasts were seeded overnight at equal densities on matrigel-coated plates. They were differentiated into myotubes by incubation in differentiation medium, DMEM supplemented with 10% equine serum, for 48 hours.

2.17 TWEAK-induced atrophy model

C57BL/6 and cIAP1-null primary myoblasts were differentiated into myotubes for 48 hours then treated with vehicle (PBS) or 100 ng/ml of mouse recombinant TWEAK (R&D systems) for 24 hours.

2.18 Pharmacologic inhibition of cIAP1using SMC in primary muscle cells

C57BL/6 primary myoblasts were differentiated in the presence of vehicle or 500 nM of SMC-OICR720A (gift from Ontario Institute of Cancer Research OICR (Toronto, Ontario, Canada) for 48 hours then treated with vehicle (DMSO) or 100 ng/ml of soluble TWEAK for another 24 hours. SMC was added daily to ensure a constant knockdown of cIAP1.

2.19 Primary myoblast transfection and rescue experiment

Primary myoblasts isolated from cIAP1-null mice were transfected, using jetPRIME DNA transfection reagent (Polyplus transfection) according to the manufacturer protocol, for 24 hours with expression vectors encoding Green Fluorescent Protein GFP or 6 myc-tagged cIAP1. Differentiation was induced by switching to low serum medium for 48 hours. Differentiated myotubes were then treated with vehicle or 100 ng/ml of TWEAK for 24 hours.

2.20 Protein extraction from primary muscle cells

To extract protein from C57BL/6 and cIAP1-null primary myotubes, lysis buffer A was added directly to the culture wells, and the lysates were sheared using an insulin syringe. Protein content was determined using the Bio-Rad (Mississauga, ON, Canada) Protein Assay using bovine serum albumin as a standard and kept on ice or in (-80°C) until further use.

2.21 Immunocytochemistry

For Immunocytochemistry assay, primary myoblasts were seeded on matrigel-coated cover slips, differentiated for 48 hours in the presence or not of SMC and treated with vehicle or TWEAK for 24 hours. Myotubes were then washed twice with PBS and fixed in cold 4% paraformaldehyde (PFA) in PBS for 5 minutes. Cells were then washed twice with PBS, permeabilized with 0.3% Triton X-100 (Sigma), blocked with 10% blocking serum and incubated overnight at 4°C with the desired primary antibody: anti-MHC (1:100; MF20) or anti-myc (1:200). After washing, myotubes were incubated with the secondary antibody and counterstained with Hoechst (Sigma) for 1 hour at room temperature. Stained cells were washed, mounted on glass slides and analyzed under a fluorescent microscope (Zeiss Axiophot). Pictures were captured using a Zeiss digital camera and Northern Eclipse image analysis software (Empix Imaging, Mississauga, Ontario).

2.22 Myotube diameter analysis

To measure C57BL/6 and cIAP1-null myotube diameter, ImageJ software was used and MHC and Hoechst staining images were merged. The average myotube diameter was calculated as the mean of five measurements taken along the length of the myotube (as described by Dogra et al., 2007_FASEB). For cIAP1-null myotubes, diameters were measured between myotube branch points for greatest consistency.

2.23 Statistical analysis

Results are presented as mean ± standard error of the mean (SEM). Statistical significance was determined using two-tailed *t* test. A value of $p < 0.05$ was considered statistically significant unless otherwise specified.

Chapter 3: Results

3.1 cIAP1 and cIAP2 regulate TNFα-induced NF-kB activation in skeletal myoblasts

3.1.1 Differential expression of cIAP2 in the absence of cIAP1

Although cIAPs have been implicated in NF-kB activation, the sole lack of cIAP1 in murine embryonic fibroblasts (MEFs), splenocytes and thymocytes did not impair NF-kB activation (Conze et al., 2005). Interestingly, these cells had markedly elevated levels of cIAP2 protein (Conze et al., 2005) suggesting that cIAP2 can functionally compensate for cIAP1. Before investigating this further, I asked whether cIAP2 induction occurs in other cIAP1-deficient tissues. For this, a line of cIAP1-null mice obtained from Dr. Tak Mak was used. These mice exhibit no obvious abnormalities (Conze et al., 2005). Tissues samples were extracted from either wild type (WT) or cIAP1-null mice, homogenized and protein lysates were immunoblotted. The cIAP levels were determined using our rat IAP1 (RIAP1) polyclonal antibody to simultaneously detect both cIAP1 and cIAP2 (Holcik et al., 2002). cIAP2 migrates only approximately 2 kDa larger than cIAP1, this distinction is not always visualized but can be seen for example in figure 5. When knocking down the other IAP, the small shift in migration between cIAP1 and cIAP2 protein is readily seen.

As previously published, cIAP2 expression was dramatically induced in cIAP1-deficient spleen (Figure 5B and 5C), presumably due to lack of cIAP1-mediated cIAP2 ubiquitination and degradation (Conze et al., 2005). Similar results were obtained using cIAP1-null MEFs which were included as control (Figure 5B). In contrast, cIAP2 was expressed to a much lesser extent in heart isolated from cIAP1-null mice (Figure 5B).

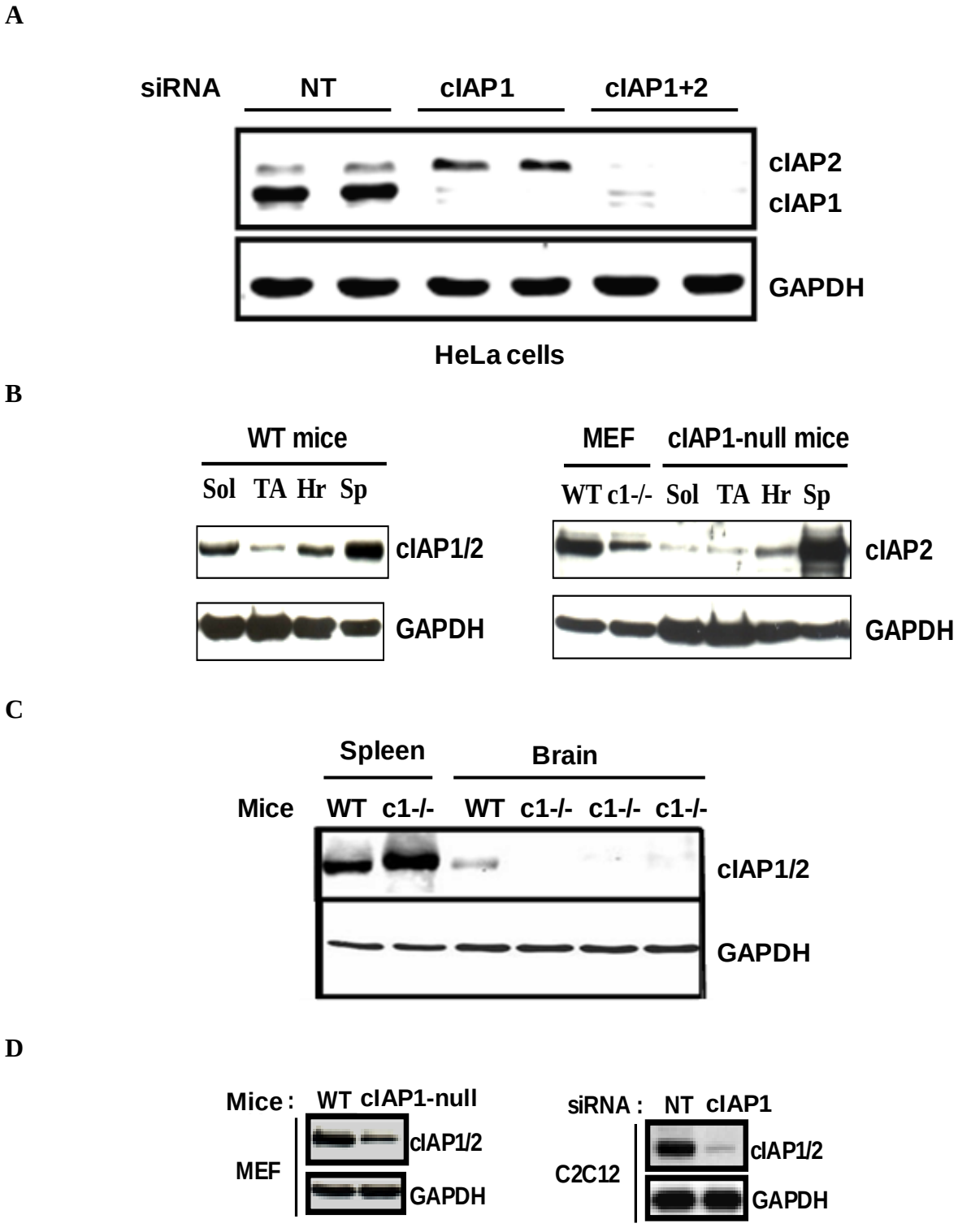

Figure 5. Differential upregulation of cIAP2 in tissues from cIAP1-null mice

(A) Characterization of the RIAP1 antibody. HeLa cells were cultured and treated with non-targeting (NT) or siRNA targeting either cIAP1 alone or cIAP1 and 2. Total protein lysates were immunoblotted using our rabbit anti-rat IAP1 (RIAP1) antibody. cIAP2 was clearly up-regulated when cIAP1 was knocked down. GAPDH was used as loading control. (**B**) Mice embryonic fibroblast (MEF) cells or tissues samples from either wild type (WT) or cIAP1-null mice were homogenized and protein lysates were immunoblotted for cIAP1 and 2 levels using our RIAP1 antibody. MEF cells were included as controls to illustrate cIAP2 induction in the absence of cIAP1. Tissues were soleus (Sol), tibialis anterior (TA), heart (Hr), and spleen (SP). (**C**) Spleen and brain samples from WT or cIAP1-null (c1-/-) mice were homogenized and immunoblotted for cIAP1 and 2. GAPDH was used as loading control. (**D**) Murine C2C12 myoblasts were cultured, treated with nontargeting (NT) or siRNA targeting cIAP1and immunoblotted for cIAP1 and 2. Mouse embryonic fibroblast (MEF) cells derived from wild type (WT) or cIAP1-null (cIAP1-/-) mice were used as control. GAPDH was used as loading control.

Surprisingly, cIAP2 expression was modestly detected in both soleus (contains mainly slow twitch) and tibialis anterior (TA) (containing mainly fast twitch) skeletal muscle from cIAP1-null mice (Figure 5B), and not detected in the brain (Figure 5C). Therefore these data suggest that cIAP1-null mice exhibit tissue-specific cIAP2 up-regulation. In agreement with these results from tissue, very little cIAP2 expression was detected in cultured murine C2C12 skeletal myoblasts treated with siRNA-targeting cIAP1 (siRNA was used to knockdown cIAP1) (Figure 5D). In contrast, cIAP2 was moderately expressed in cIAP1-null MEFs, which was again used as control (Figure 5D).

Taken together, these data demonstrate that the up-regulation of cIAP2 in the absence of cIAP1 is tissue specific and suggest that cIAP1 might be particularly critical in skeletal muscle biology.

3.1.2 Loss of cIAP1 attenuates TNFα–mediated NF-kB activation in C2C12 myoblasts

It has been reported that lack of cIAP1 in MEFs did not impair NF-kB activation, presumably due to cIAP2 compensation (Conze et al., 2005). Since skeletal muscle myoblasts express cIAP1 but not cIAP2 (Figure 5B), I asked whether TNFα-mediated NF-kB activation depends on cIAP1. To examine the role of cIAP1 in TNFα-mediated NF-kB signaling, I used siRNA to knockdown cIAP1 in the mouse myoblast line C2C12 prior to the treatment with a non-toxic level of TNFα (10 ng/ml). TNFα strongly activated NF-kB in C2C12 myoblasts treated with nontargeting siRNA, as evidenced by the rapidly and transient degradation of IkBα and phosphorylation of the NF-kB protein p65 (Figure 6A). In contrast, upon cIAP1 knockdown NF-kB activation was blunted as

demonstrated by the unaltered levels of IkBα expression and p65 phosphorylation (Figure 6A), indicating complete abrogation of NF-kB signaling in C2C12 cells treated with cIAP1-specific siRNA. In addition, I measured NF-kB activity using C2C12 myoblasts stably expressing an NF-kB luciferase reporter construct (Guttridge et al., 2000) and found that cIAP1 knockdown inhibited luciferase activation in response to TNFα (Figure 6B).

To further confirm that the lack of cIAP1 blunts TNFα-mediated NF-kB activation in C2C12 cells, I examined the level of cFLIP, a prosurvival protein that requires proper NF-kB activation to avoid being degraded in response TNFα (Chang et al., 2006). As expected, cFLIP expression was inhibited in response to TNFα in C2C12 treated with cIAP1-targeted siRNA (Figure 6C).

These striking results demonstrate that cIAP1 is crucial for NF-kB activation in response to TNFα in C2C12 skeletal myoblasts.

A

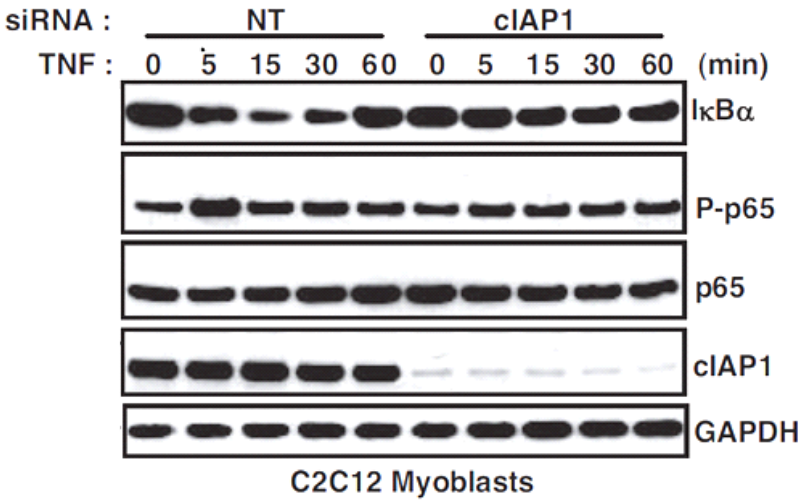

B

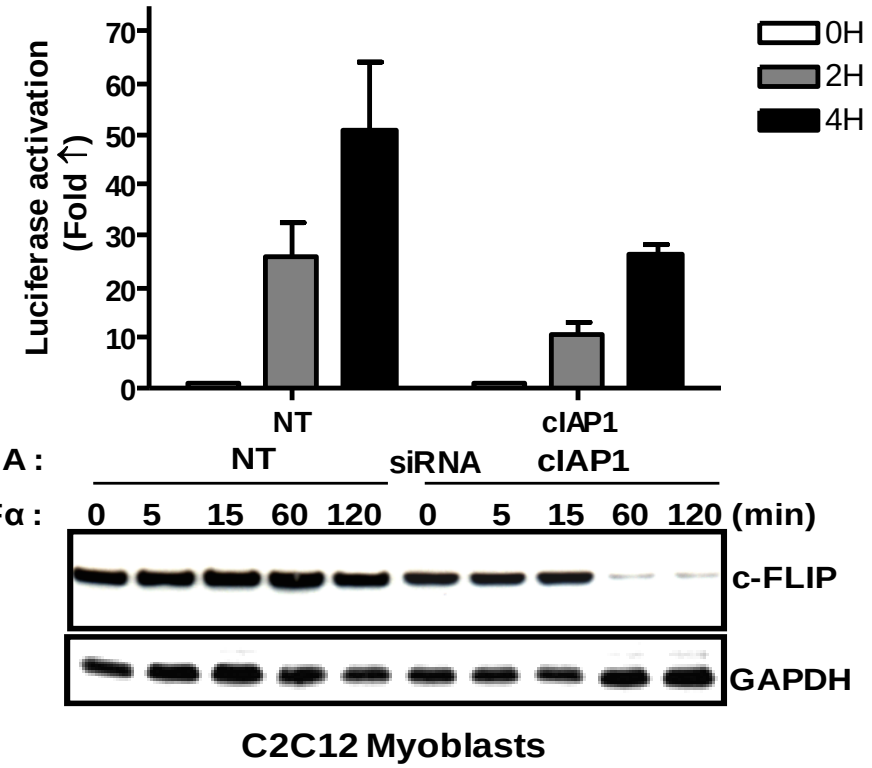

C

Figure 6. Knockdown of cIAP1 blunts TNFα-mediated NF-κB activation in C2C12 myoblasts

(A) C2C12 myoblasts were treated with nontargeting (NT) or cIAP1-targeting siRNA for 24 hours, treated with TNFα for the indicated times, and immunoblotted for members of

the NF-kB signaling pathways. GAPDH was used as loading control. (**B**) C2C12 myoblasts stably expressing an NF-kB luciferase reporter construct were treated with siRNA for 24 hours, followed by TNFα for the indicated amounts of time before luciferase activity was measured.

(**C**) C2C12 myoblasts were treated with siRNA for 24 hours, and then treated with TNFα. Protein lysates were extracted at the indicated time, and immunoblotted for cFLIP. GAPDH was used as loading control.

3.1.3 Loss of cIAP2 does not alter TNFα-mediated NF-κB activation in C2C12 myoblasts

To investigate the role of cIAP2 in TNFα-mediated NF-kB activation in muscle cells, I used siRNA to knockdown cIAP2, cIAP1 or both cIAP1 and cIAP2 in C2C12 myoblasts. TNFα induced strong NF-kB activation, which occurred in C2C12 cells treated with nontargeting siRNA or that treated with cIAP2 siRNA, as assessed by the rapid and transient phosphorylation of IKKβ and IkBα, and the degradation of IkBα (Figure 7A). In contrast, siRNA-mediated cIAP1 or dual siRNA-mediated knockdown of cIAP1 and cIAP2 blunted NF-kB activation (Figure 7A). These data demonstrate that cIAP2 is not necessary for TNFα-mediated NF-kB activation in C2C12 skeletal myoblasts.

3.1.4 Loss of XIAP does not alter TNFα-mediated NF-κB activation in C2C12 myoblasts

It has been reported that X-linked IAP is involved in the NF-kB signaling (Lu et al., 2007). To test the possibility that XIAP regulates TNFα-mediated NF-kB activation, I used siRNA-targeting XIAP in C2C12 cells. The absence of XIAP in C2C12 myoblasts did not affect NF-kB activation in response to TNFα, as evidenced by the rapid and transient IkBα degradation and p65 phosphorylation (Figure 7B). Taken together, these results show that, similar to the cIAP2 knockdown, siRNA-targeting XIAP did not alter TNFα-mediated NF-kB activation in C2C12 skeletal myoblasts.

A

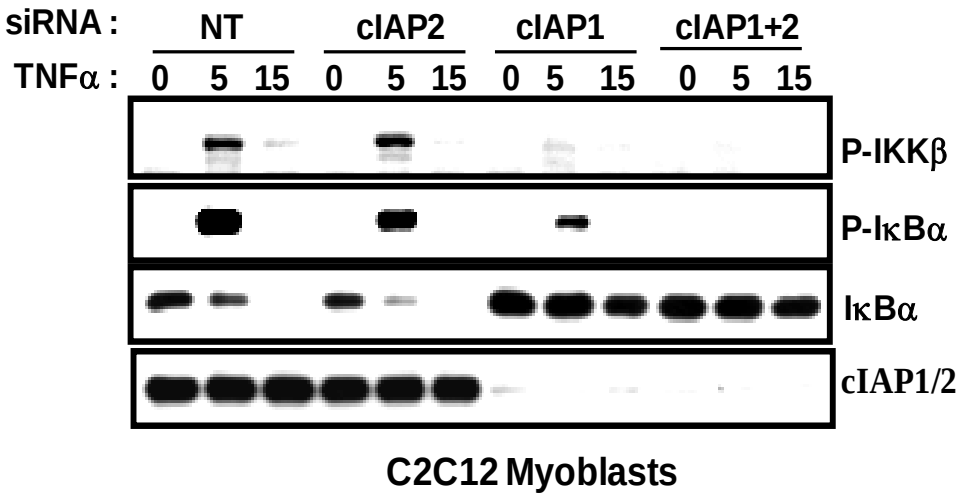

B

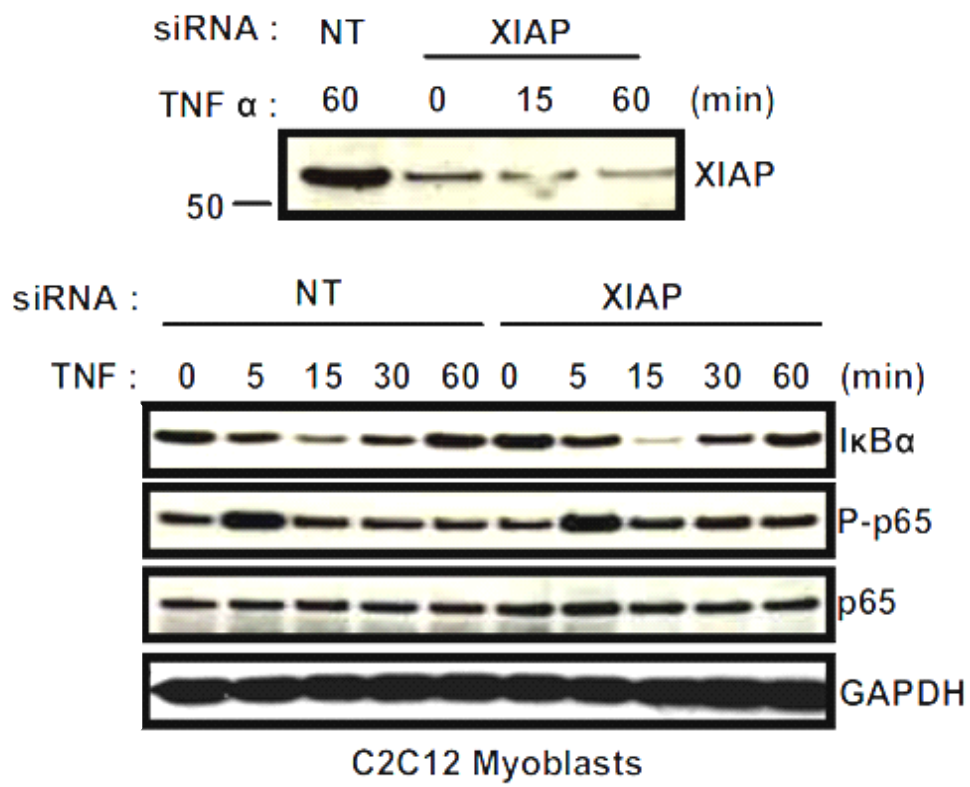

Figure 7. Knockdown of cIAP2 or XIAP does not alter TNFα-mediated NF-kB activation in C2C12 myoblasts

(**A**) C2C12 myoblasts were treated with nontargeting (NT), cIAP2, cIAP1 or both cIAP1 and cIAP2-targeting siRNA for 24 hours, treated with TNFα for the indicated times, and immunoblotted for members of the NF-kB signaling pathways. GAPDH was used as loading control. (**B**) C2C12 myoblasts were treated with nontargeting (NT) or XIAP-targeting siRNA for 24 hours, treated with TNFα for the indicated times, and immunoblotted for members of the NF-kB signaling pathways. GAPDH was used as loading control.

3.1.5 cIAP1 and cIAP2 redundantly regulate TNFα-mediated NF-κB activation in MEF cells

Unlike that found in C2C12 cells, the knockdown of cIAP1 in MEFs up-regulates the expression of cIAP2 (as seen in figure 8A). In addition, it has been reported that the absence of cIAP1 in MEFs did not blunt NF-kB activation, presumably due to cIAP2 compensation (Conze et al., 2005). To investigate this and examine the role of cIAP2 in TNFα-mediated NF-kB activation in MEFs, I used siRNA to knockdown cIAP2, cIAP1 or both cIAP1 and cIAP2. In WT MEFs treated with cIAP1 or cIAP2 siRNA, the other cIAP is expressed (note the small shift in migration between cIAP1 and cIAP2 protein, Figure 8A). NF-kB activation in response to TNFα is not altered in the absence of one or the other cIAP, as in the nontargeting condition (Figure 8A). In contrast, dual siRNA-mediated knockdown in WT MEFs blunted IkBα degradation and severely attenuated IKKβ and IκBα phosphorylation in response to TNFα treatment (Figure 8A). Similar data was observed in cIAP1-null MEFs when treated with siRNA-targeting cIAP2 (Figure 8B). To further investigate the observed functional redundancy between cIAP1 and cIAP2, I examined the effect of ectopic expression of cIAP2 (using adenovirus infection) on NF-kB signaling in C2C12 cells treated with siRNA-targeting cIAP1. Interestingly, ectopic expression of cIAP2 rescues the impairment of TNFα-mediated NF-κB activation in cIAP1-deficient C2C12 myoblasts (Figure 8C). Taken together, these data demonstrate that both cIAP1 and cIAP2 redundantly regulate NF-κB activation upon TNFα stimulation in certain cells such as MEFs.

A

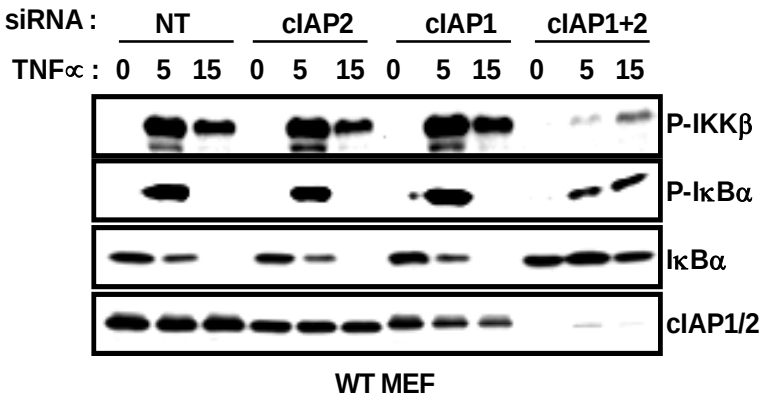

B

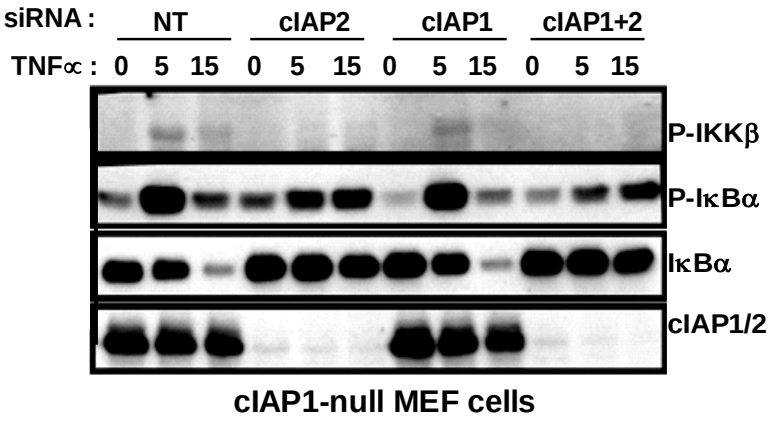

C

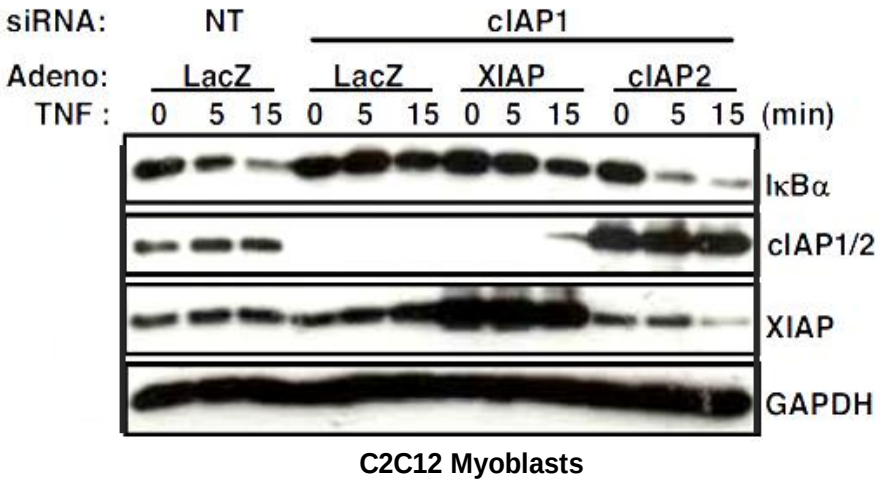

Figure 8. cIAP1 and cIAP2 redundantly regulate TNFα-mediated NF-κB activation in MEF cells

(**A**) WT MEFs were treated with non-targeting, cIAP1, cIAP2 or both cIAP1 and cIAP2 siRNA for 24 hours, and then treated with TNFα. Protein lysates were extracted at the indicated time points and analyzed by immunoblotting. (**B**) cIAP1-null MEFs treated with a non-targeting, cIAP2, cIAP1 or both cIAP1 and cIAP2 siRNA for 24 hours, then were subjected to TNFα treatment for the indicated times. Samples were collected and analyzed by immunoblotting.

(**C**) C2C12 myoblasts were treated with siRNA, and 4 hours later infected with adenovirus (Adeno). Twenty hours later, cells were treated with TNFα, protein lysates were then collected at the indicated time point, and immunoblots performed.

3.1.6 Knockdown of cIAP1 sensitizes C2C12 myoblasts to TNFα-induced apoptosis

NF-kB activation in response to TNFα stimulation induces the transcription of a number of survival genes such as cFLIP, which specifically inhibits caspase 8 activation (Thome and Tschopp, 2001). Thus, proper NF-kB activation might prevent TNFα-induced apoptosis. Given the crucial role of cIAP1 in TNFα-induced NF-kB activation and cFLIP upregulation (Figure 6C), I reasoned that the lack of cIAP1 might sensitize C2C12 to TNFα-mediated apoptosis. To test this, I transfected C2C12 myoblasts with nontargeting or cIAP1 siRNA, then treated them with TNFα. Loss of cIAP1 dramatically reduced cell viability in response to TNFα treatment (Figure 9A), and induced markers of apoptosis as assessed by caspase 3 as well as poly (ADP-ribose) polymerase (PARP) cleavage (Figure 9B). In contrast, as found with nontargeting siRNA, the loss of XIAP did not sensitize C2C12 muscle cells to TNFα-mediated apoptosis **(**Figure 9B). These data indicates that cIAP1 regulates sensitivity to TNFα-induced cell death in skeletal muscle cells.

A

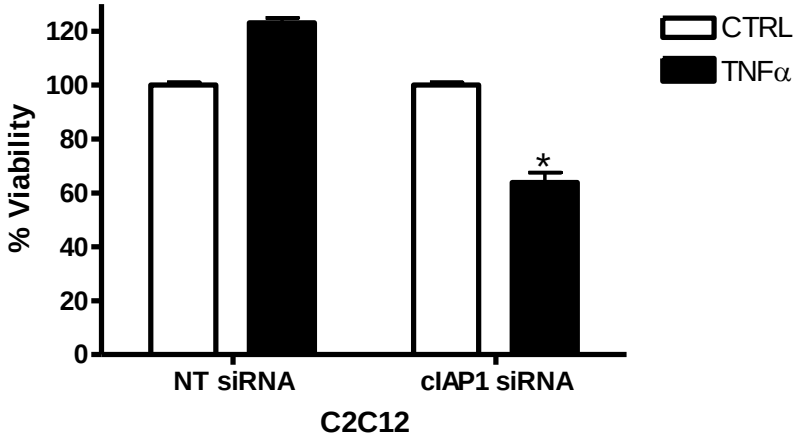

B

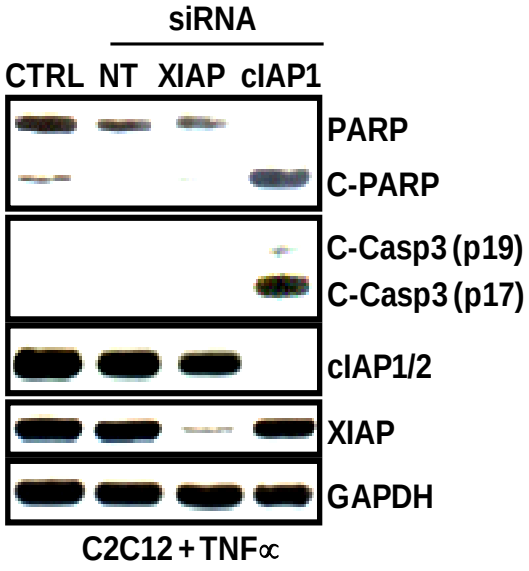

Figure 9. Knockdown of cIAP1 sensitizes C2C12 myoblasts to TNFα–mediated apoptosis

(**A**) C2C12 myoblasts were treated with siRNA for 24 h, followed by TNFα treatment for 24 h, and cell viability was assessed. Data are expressed as % viability ± SD relative to no TNF treatment controls (set at 100%), *n*=4 per condition. (**B**) C2C12 myoblasts treated with siRNA (24 h) followed by TNFα (24h) were immunoblotted for markers of caspase activation.

3.1.7 Either cIAP1 or cIAP2 is required to protect C2C12 or MEF cells against TNFα-mediated apoptosis

One of the important goals in this study was to overcome the potentially confounding effects of functional redundancy between the cIAPs and to elucidate their role in TNFα signaling. Given that cIAP2 is not expressed in C2C12 myoblasts (Figure 5D and 6A), I was interested to elucidate whether it could functionally rescue cIAP1 in response to TNFα. For this, I transfected C2C12 cells with nontargeting or cIAP1 siRNA, then infected them with adenovirus expressing LacZ, XIAP or cIAP2. Twenty four hours later, cells were treated with TNFα. Ectopic expression of cIAP2 in cIAP1-deficient C2C12 cells, completely rescued the phenotype, to the same extent as XIAP, and strongly inhibit apoptosis (Figure 10).

To investigate this further, I used MEF cells, and treated them with or without siRNA-mediated cIAP1 and/ or cIAP2 knockdown. Wild type MEFs treated with TNFα dose for 24 hours remained viable (Figure 11A) and caspase cleavage was not detected (Figure 11B). In cIAP1-null MEFs, and as seen above, cIAP2 was induced and these cells also remained viable when treated with TNFα (Figure 11A). In contrast, knockdown of cIAP2 in cIAP1-null MEFs (designated "double knockout") dramatically sensitized cells to TNFα, resulting in a loss of cell viability (Figure 11A) and induced cleavage of PARP, caspases 3, 8 and 9 (Figure 11B). It is also interesting to note that the mitochondrial pathway was strongly activated (as evidenced by caspase 9 cleavage) by crosstalk in dual knockout cells.

Collectively, these results indicate that cIAP1and cIAP2 are functionally redundant and necessary for the protection against TNFα-induced apoptosis.

A

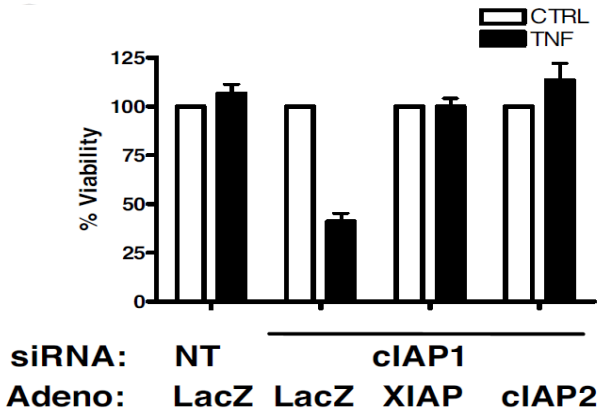

B

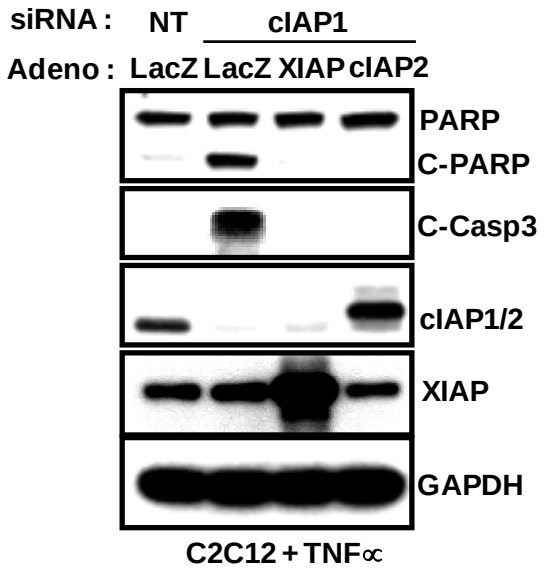

Figure 10. Ectopic expression of cIAP2 rescues the cIAP1 knockdown-mediated apoptosis in C2C12 myoblasts in response to TNFα

(**A**) C2C12 myoblasts were treated with siRNA and 4 hours later infected with adenovirus (Adeno). After 24 h of knockdown, cells were treated with TNFα for 24 h, and cell viability was assessed. Data are expressed as % viability ± SD relative to no TNF treatment controls (set at 100%), n=4 per condition. (**B**) C2C12 cells were treated as in A, and protein lysates were immunoblotted for the indicated proteins.

A

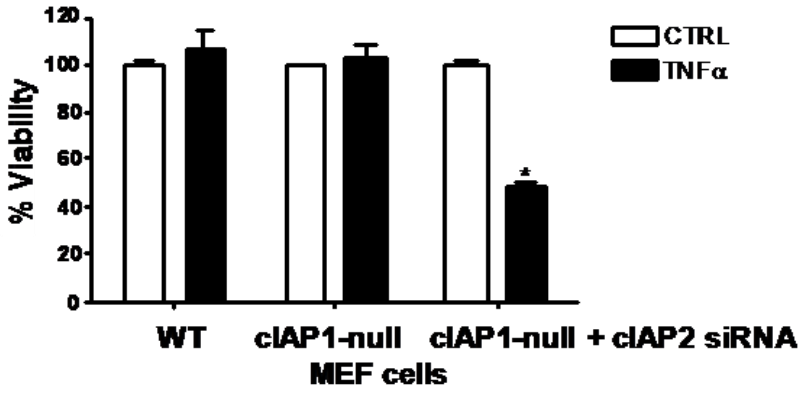

B

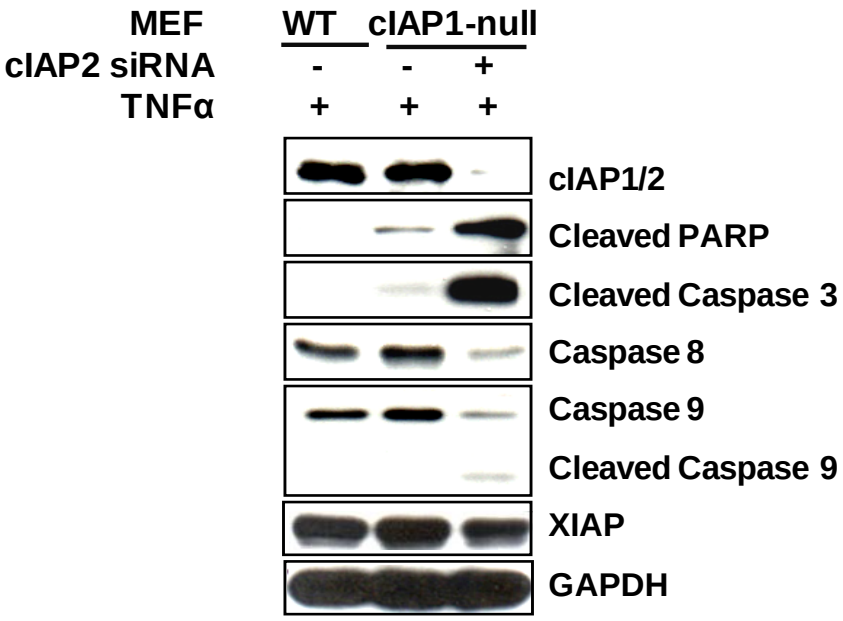

Figure 11. Either cIAP1 or cIAP2 is required to protects cells against TNFα–mediated apoptosis in MEF cells

(A) MEF cells were treated with siRNA for 24 hours, then treated with TNFα for another 24 hours, and cell viability was measured. Data are expressed as % viability ± SD relative to no TNF treatment controls (set at 100%), n=4 per condition. (**B**) MEF cells were treated as in A, and protein lysates were immunoblotted for various apoptotic proteins at the indicated proteins.

3.2 Genetic and pharmacologic inhibition of cIAP1 expression protects against denervation-induced skeletal muscle atrophy in mice

3.2.1 Genetic depletion of cIAP1 protects against denervation-induced skeletal muscle atrophy *In Vivo*

To investigate the role of cIAP1 in skeletal muscle atrophy, I used the denervation-induced skeletal muscle atrophy model in cIAP1-null and C57BL/6 control mice. Briefly, Hind-limbs of four to six-week-old C57BL/6 and cIAP1-null mice were denervated by removing a portion of the sciatic nerve in the mid-thigh region of the left hind limb. The contralateral limb was used as control. At day 7, 14 and 28 post-denervation, mice were sacrificed and skeletal muscles were collected. Skeletal muscles were sectioned, stained with haematoxylin and eosin (H&E) dyes and their fiber cross-sectional areas (CSA) were quantified in the denervated (DEN) and nondenervated (NDN) muscles of cIAP1-null and C57BL/6 mice.

3.2.1.1 Genetic ablation of cIAP1 attenuates skeletal muscle atrophy at 7 days post-denervation

To examine the role of cIAP1 in skeletal muscles after 7 days of denervation, I performed histological analysis in denervated and contralateral (nondenervated) TA muscles of cIAP1-null and C57BL/6 mice. As anticipated, H&E stained TA cross-sections delineated a significant decrease of muscle fiber CSA in C57BL/6 denervated TA compared to the contralateral nondenervated muscle (Figure 12A). By contrast, in the denervated TA of cIAP1-null mice the decrease of fiber CSA was smaller (Figure 12A), suggesting that at this time point, the absence of cIAP1 confers protection against

A

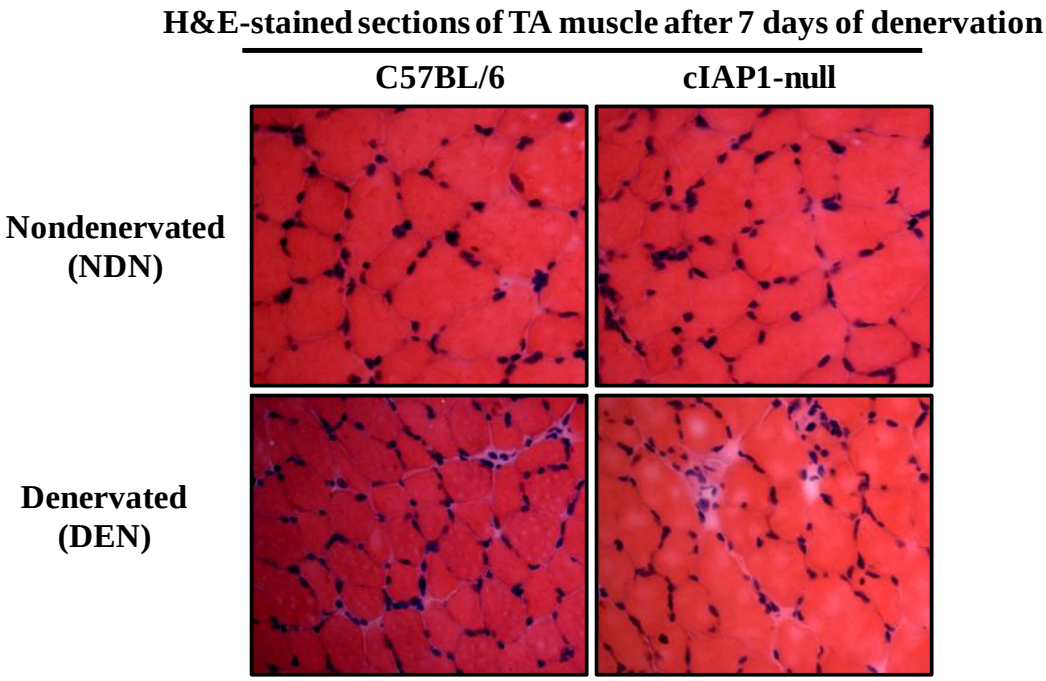

B

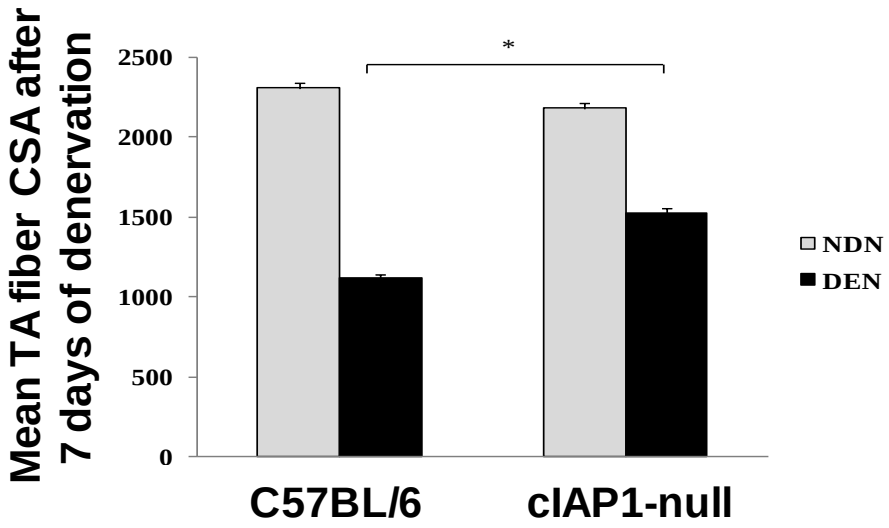

Figure 12. Loss of cIAP1 protects TA muscle from atrophy after 7 days of denervation

(**A**) Four to six-week-old C57BL/6 and cIAP1-null mice were denervated by transection of the sciatic nerve of the left hind limb. Denervated and nondenervated TA muscles

were isolated at day 7 post-denervation, sectioned using a cryostat microtome and stained with haematoxylin and eosin dyes. Images were taken using an Axioskop microscope and Northern Eclipse software.

(**B**) The H&E stained sections, of TA muscle collected from C57BL/6 and cIAP1-null mice at day 7 post-denervation, were photographed using Zeiss Axiophot microscope equipped with a digital camera and Northern Eclipse image analysis software. For each muscle, fiber cross-sectional areas (CSA) were traced and measured in μm^2 using ImageJ software. Data was transferred into a Microsoft Excel sheet, mean fiber CSA was calculated using standard formula and the results were reported as means ± standard errors. n=4 for each group. * indicates significant difference, with $p < 0.01$.

denervation-induced skeletal muscle atrophy.

To confirm this observation, I measured the CSA of the myofibers of each TA muscle from C57BL/6 and cIAP1-null mice, and calculated the average fiber CSA of denervated (DEN) and nondenervated (NDN) cIAP1-null and C57BL/6. By 7 days following nerve transection, the C57BL/6 denervated TA showed a significant reduction of 52% in the average of fiber CSA compare to only 30% decrease in the absence of cIAP1 (Figure 12B). In addition, I calculated the frequency distribution of fiber CSA in both denervated and nondenervated C57BL/6 and cIAP1-null TA muscles after 7 days of denervation. As expected, C57BL/6 TA muscles displayed a big shift of fiber CSA distribution towards smaller values in denervated compared to nondenervated muscles (Figure 13A). In contrast, denervated cIAP1-null TA muscles did not exhibit this shift in frequency distribution (Figure 13B). In fact, analysis of the frequency distribution of denervated TA muscles from C57BL/6 and IAP1-null mice reveals a clear difference between the maintained cIAP1-null fiber size and the atrophied C57BL/6 fibers (Figure 13C). To determine whether the protection seen in the absence of cIAP1 could also occur in soleus, a muscle known to be very sensitive to denervation-induced skeletal muscle atrophy, I performed similar analyses using C57BL/6 and cIAP1-null mice. The results from H&E stained sections at day 7 post-denervation revealed a protection against atrophy in cIAP1-null soleus, similar to that seen in TA, when compared to controls (Figure 14A). Furthermore, measurements of the average of fiber CSA of soleus muscles, showed a dramatic difference between the decrease in fiber size of C57BL/6 (55%) and cIAP1-null (35%) muscles (Figure 14B), and further confirmed the protection in cIAP1-null mice. Moreover, C57BL/6 soleus fibers underwent the expected dramatic shift

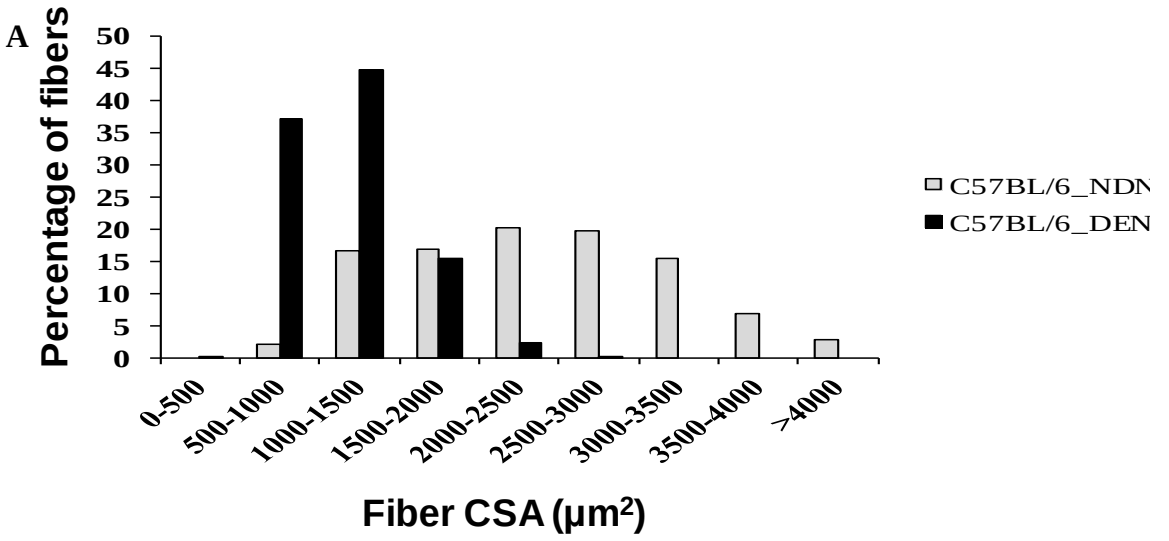
A
Percentage of fibers
50
45
40
35
30
25
20
15
10
5
0
0-500
500-1000
1000-1500
1500-2000
2000-2500
2500-3000
3000-3500
3500-4000
>4000
Fiber CSA (µm²)
C57BL/6_NDN
C57BL/6_DEN

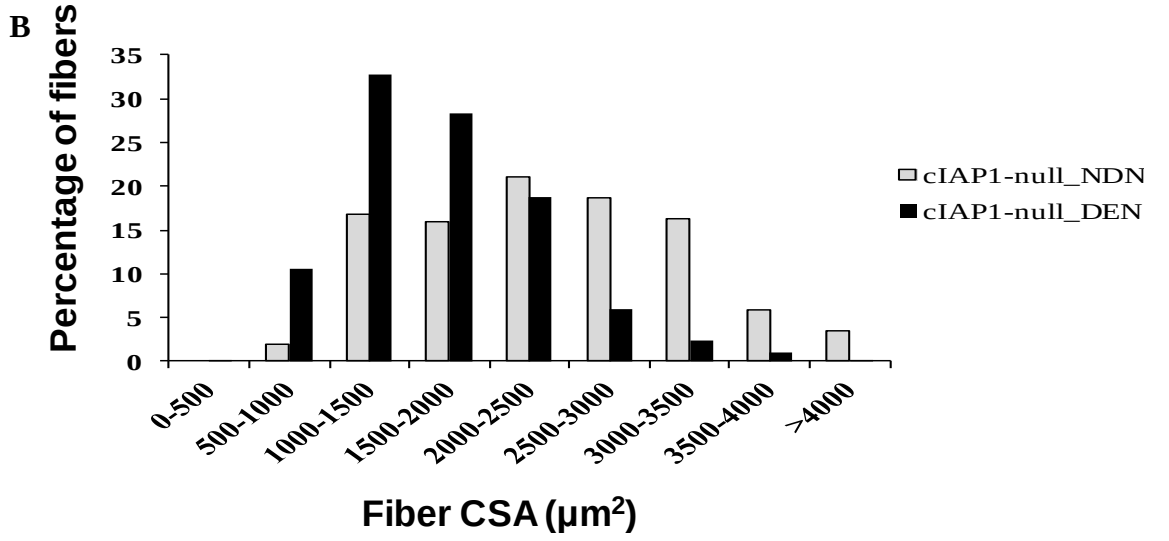
B
Percentage of fibers
35
30
25
20
15
10
5
0
0-500
500-1000
1000-1500
1500-2000
2000-2500
2500-3000
3000-3500
3500-4000
>4000
Fiber CSA (µm²)
cIAP1-null_NDN
cIAP1-null_DEN

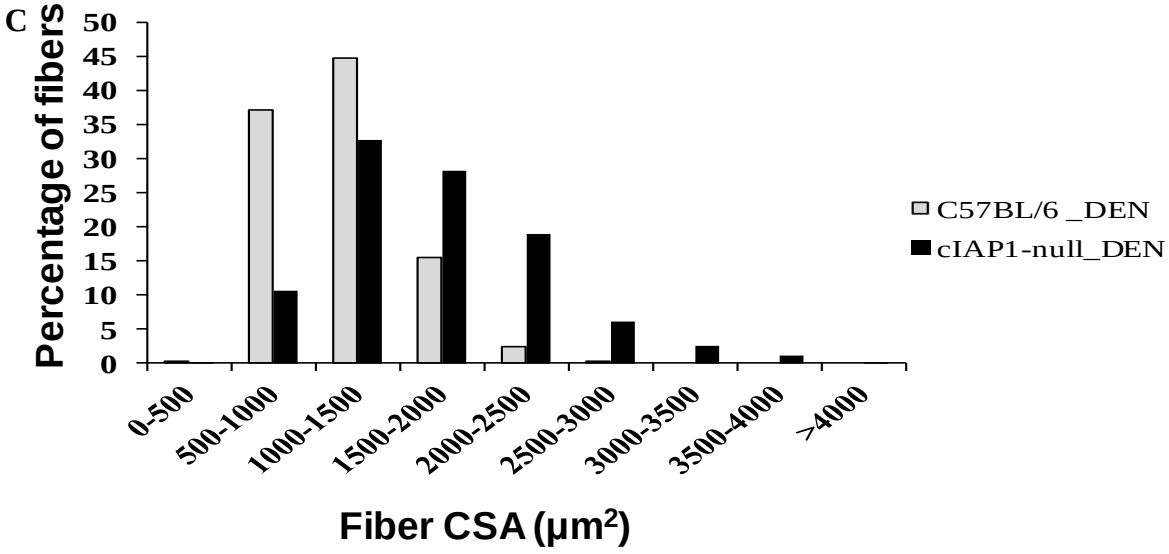
C
Percentage of fibers
50
45
40
35
30
25
20
15
10
5
0
0-500
500-1000
1000-1500
1500-2000
2000-2500
2500-3000
3000-3500
3500-4000
>4000
Fiber CSA (µm²)
C57BL/6 _DEN
cIAP1-null_DEN

Figure 13. Atrophic shift in TA fiber cross-sectional area to smaller size is minimal in the absence of cIAP1 after 7 days of denervation

(**A**) Frequency distribution of fiber CSA of C57BL/6 TA muscle after 7 days of denervation. (**B**) Frequency distribution of fiber CSA of cIAP1-null TA muscle after 7 days of denervation. (**C**) Frequency distribution of fiber CSA of denervated C57BL/6 and cIAP1-nll TA muscle after 7 days of denervation. The H&E stained sections, of TA muscle collected from C57BL/6 (n=4) and cIAP1-null (n=4) mice at day 7 post-denervation, were photographed using Zeiss Axiophot microscope equipped with a digital camera and Northern Eclipse image analysis software. For each muscle, fiber cross-sectional areas (CSA) were traced and measured in μm^2 using ImageJ software. Data was transferred into a Microsoft Excel sheet, and the frequency distribution of nondenervated and denervated sections from each animal in both C57BL/6 and cIAP1-null mice were calculated by determining the number of fibers that fell within the given area ranges.

A

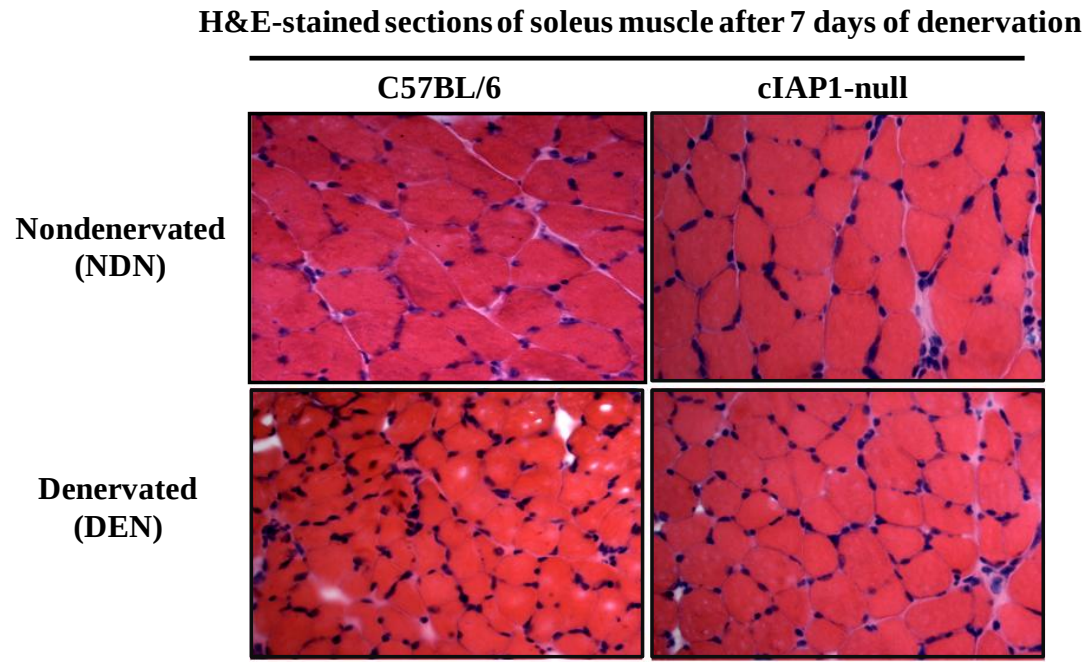

B

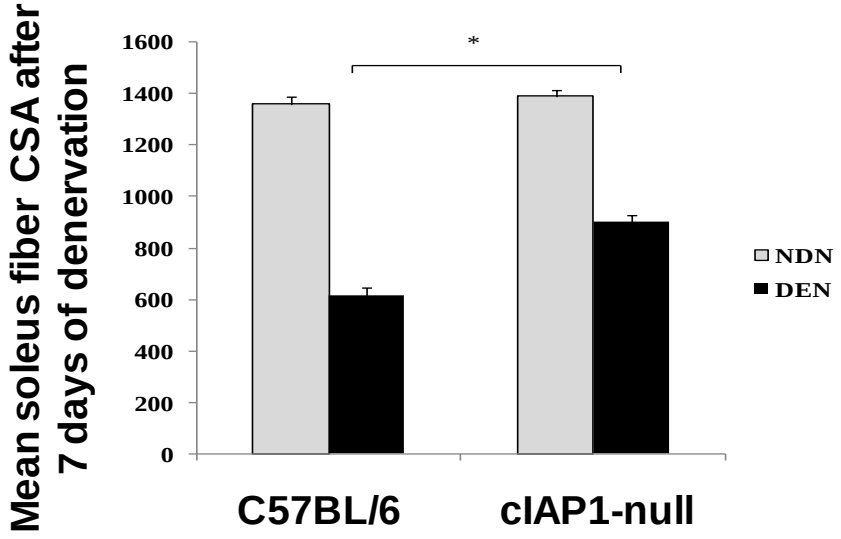

Figure 14. Loss of cIAP1 protects soleus muscle from atrophy after 7 days of denervation

(**A**) Four to six-week-old C57BL/6 and cIAP1-null mice were denervated by transection of the sciatic nerve of the left hind limb. Denervated and nondenervated soleus muscles were isolated at day 7 post-denervation, sectioned using a cryostat microtome and stained with haematoxylin and eosin dyes. Images were taken using an Axioskop microscope and Northern Eclipse software.

(**B**) The H&E stained sections, of soleus muscle collected from C57BL/6 and cIAP1-null mice at day 7 post-denervation, were photographed using Zeiss Axiophot microscope equipped with a digital camera and Northern Eclipse image analysis software. For each muscle, fiber cross-sectional areas (CSA) were traced and measured in μm^2 using ImageJ software. Data was transferred into a Microsoft Excel sheet, mean fiber CSA was calculated using standard formula and the results were reported as means ± standard errors. n=4 for each group. * indicates significant difference, with $p < 0.01$.

A

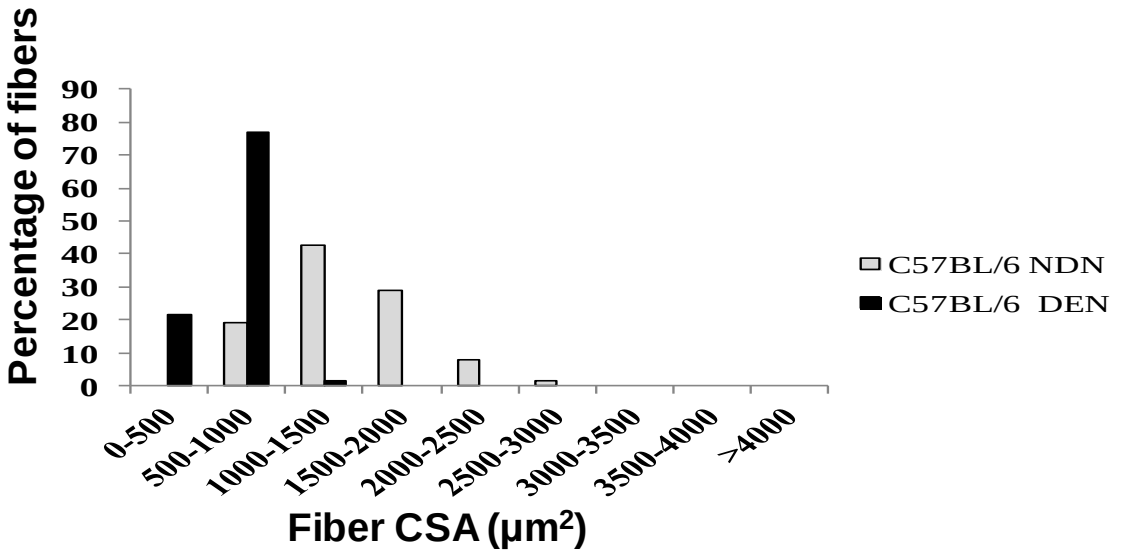
Percentage of fibers
90
80
70
60
50
40
30
20
10
0
0-500
500-1000
1000-1500
1500-2000
2000-2500
2500-3000
3000-3500
3500-4000
>4000
Fiber CSA (µm²)
C57BL/6 NDN
C57BL/6 DEN

B

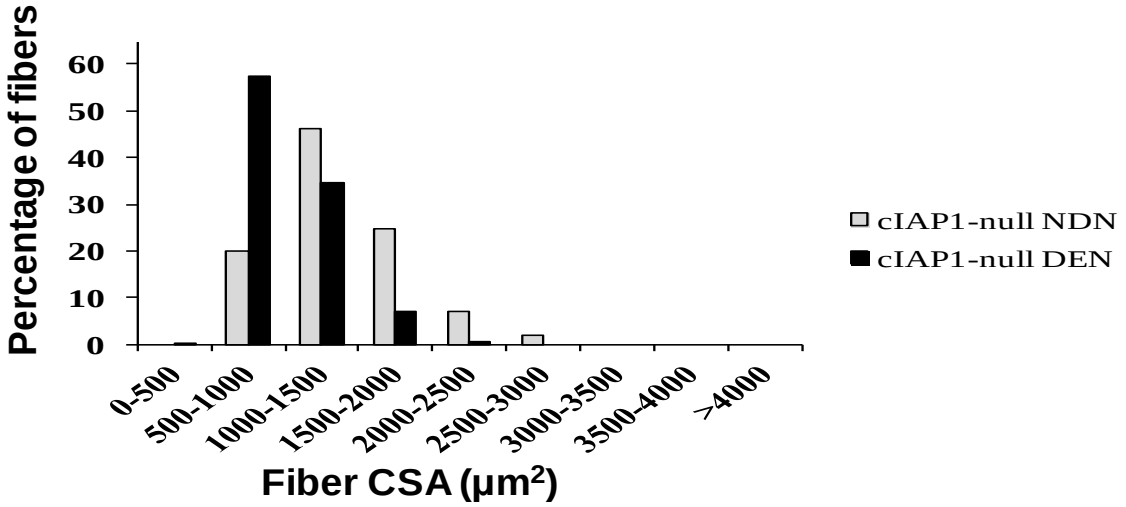
Percentage of fibers
60
50
40
30
20
10
0
0-500
500-1000
1000-1500
1500-2000
2000-2500
2500-3000
3000-3500
3500-4000
>4000
Fiber CSA (µm²)
cIAP1-null NDN
cIAP1-null DEN

C

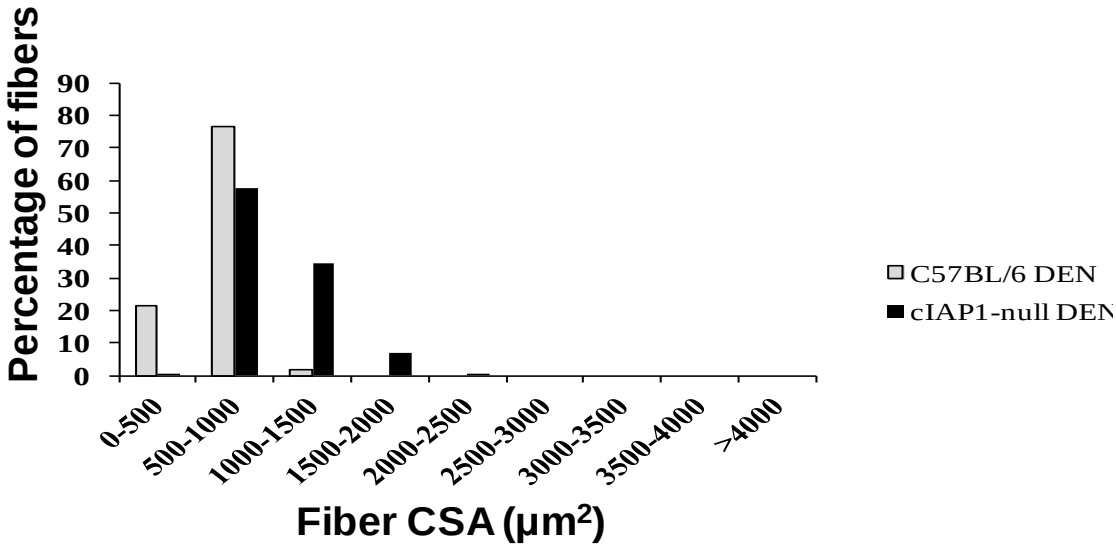
Percentage of fibers
90
80
70
60
50
40
30
20
10
0
0-500
500-1000
1000-1500
1500-2000
2000-2500
2500-3000
3000-3500
3500-4000
>4000
Fiber CSA (µm²)
C57BL/6 DEN
cIAP1-null DEN

Figure 15. Shift of soleus fiber cross-sectional area to smaller size in the absence of cIAP1 is minimal after 7 days of denervation

(**A**) Frequency distribution of fiber CSA of C57BL/6 soleus muscle after 7 days of denervation. (**B**) Frequency distribution of fiber CSA of cIAP1-null soleus muscle after 7 days of denervation. (**C**) Frequency distribution of fiber CSA of denervated C57BL/6 and cIAP1-nll soleus muscle after 7 days of denervation. The H&E stained sections, of soleus muscle collected from C57BL/6 (n=4) and cIAP1-null (n=4) mice at day 7 post-denervation, were photographed using Zeiss Axiophot microscope equipped with a digital camera and Northern Eclipse image analysis software. For each muscle, fiber cross-sectional areas (CSA) were traced and measured in μm^2 using ImageJ software. Data was transferred into a Microsoft Excel sheet, and the frequency distribution of nondenervated and denervated sections from each animal in both C57BL/6 and cIAP1-null mice were calculated by determining the number of fibers that fell within the given area ranges.

toward a smaller size (Figure 15A) whereas cIAP1-null fibers failed to exhibit this shift after 7 days of denervation (Figure 15B). Taken together, these results showed that genetic depletion of cIAP1 attenuated skeletal muscle atrophy after 7 days of denervation.

3.2.1.2 Genetic depletion of cIAP1 spares skeletal muscles from atrophy at 14 days post-denervation

To further study the role of cIAP1 in response to denervation-induced skeletal muscle atrophy, I analyzed the skeletal muscles of C57BL/6 and cIAP1-null mice at a longer time point, specifically at 14 days post-denervation. Analysis of H&E-stained TA sections revealed a significant decrease of muscle fiber CSA in C57BL/6 denervated TA compared to the contralateral muscle.

In contrast, in the denervated TA of cIAP1-null mice the decrease of fiber CSA was less evident (Figure 16A). Furthermore, the average CSA measurements clearly demonstrated that, at 14 days after denervation, the denervated TA of C57BL/6 mice displayed a dramatic decrease of about 58% in fiber CSA compared to the contralateral muscle, whereas in cIAP1-null mice this reduction was only about 34% (Figure 16B). Frequency distribution of TA fiber CSA data clearly demonstrated maintenance of the fiber size in the absence of cIAP1, whereas denervated C57BL/6 fibers displayed the expected dramatic shift toward smaller fiber size after 14 days of sciatic nerve transection (Figure 17C).

Comparable protection against atrophy at 14 days post-denervation was also observed in soleus muscle in the absence to cIAP1. Histological analysis of H&E-stained sections of

soleus muscle after 14 days of denervation delineated a significant decrease of muscle fiber CSA in C57BL/6 denervated soleus compared to the contralateral muscle, whereas the denervated soleus of cIAP1-null mice exhibited a smaller decrease (Figure 18A). Moreover, average fiber CSA quantification further confirmed the protection against neurogenic atrophy in the absence of cIAP1, as at 14 days post-denervation the fiber CSA of denervated C57BL/6 soleus displayed a significant decrease of 65% compared to only 34% in cIAP1-null (Figure 18B). Furthermore, a clear protection in the absence of cIAP1 was also seen in the fiber CSA frequency distribution graphs of soleus muscle (Figure 19) which showed an inhibition of the shift toward smaller fiber size (Figure 19B) that was evident in the atrophied C57BL/6 fibers of soleus muscle (Figure 19A). In conclusion, these data provide further strong evidence that genetic ablation of cIAP1 counteract skeletal muscle atrophy in response to denervation and demonstrate that the protection is significant, maintained and even more pronounced at 14 days post-denervation.

A

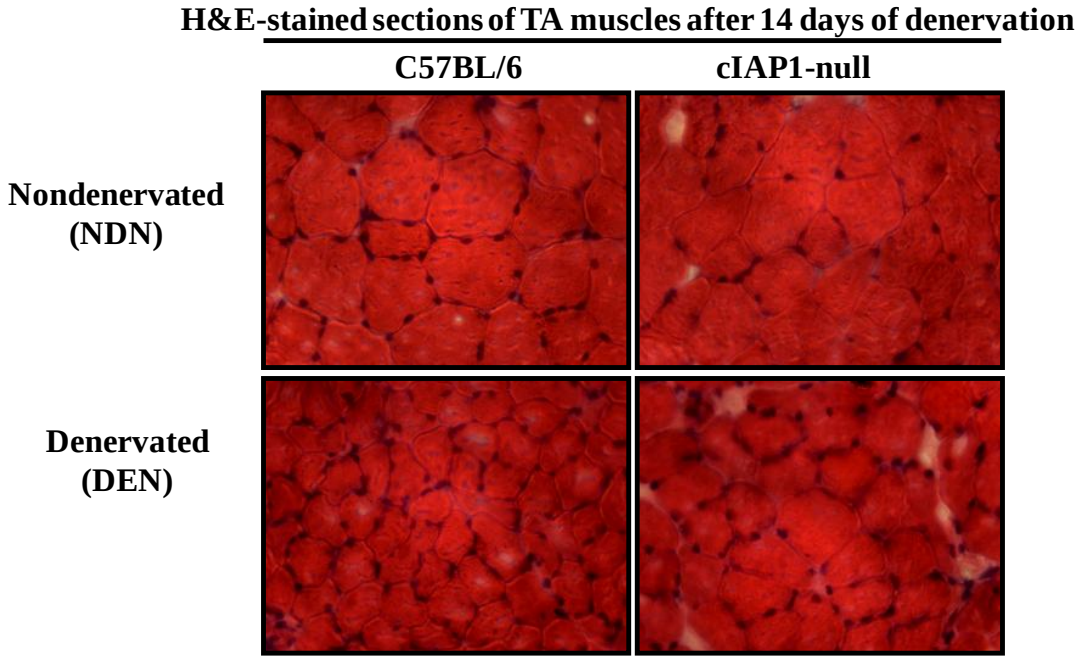

B

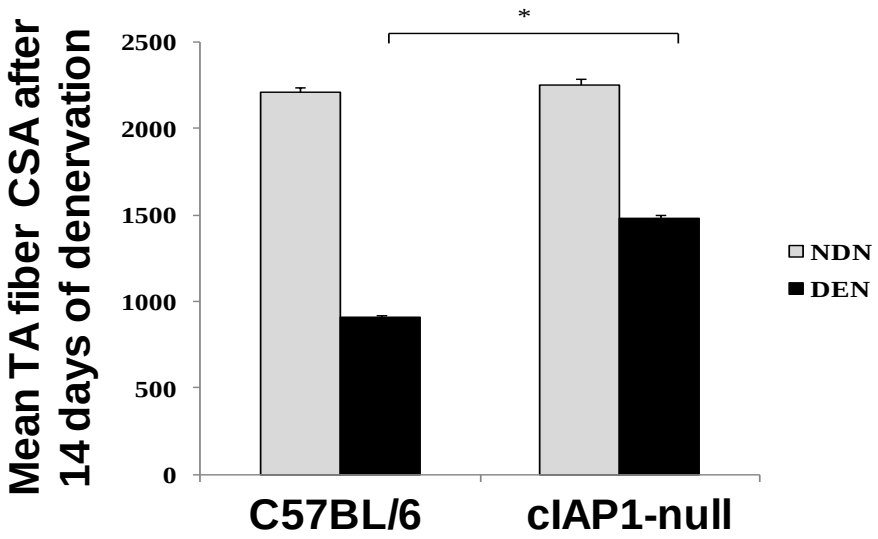

Figure 16. Loss of cIAP1 protects TA muscle from atrophy after 14 days of denervation

(**A**) Four to six-week-old C57BL/6 and cIAP1-null mice were denervated by transection of the sciatic nerve of the left hind limb. Denervated and nondenervated TA muscles

were isolated at day 14 post-denervation, sectioned using a cryostat microtome and stained with H&E. Images were taken using an Axioskop microscope and Northern Eclipse software. (**B**) The H&E stained sections, of TA muscle collected from C57BL/6 and cIAP1-null mice at day 14 post-denervation, were photographed using Zeiss Axiophot microscope equipped with a digital camera and Northern Eclipse image analysis software. For each muscle, fiber cross-sectional areas (CSA) were traced and measured in μm^2 using ImageJ software. Data was transferred into a Microsoft Excel sheet, mean fiber CSA was calculated using standard formula and the results were reported as means ± standard errors. n=4 for each group. * indicates significant difference, with $p < 0.01$.

A

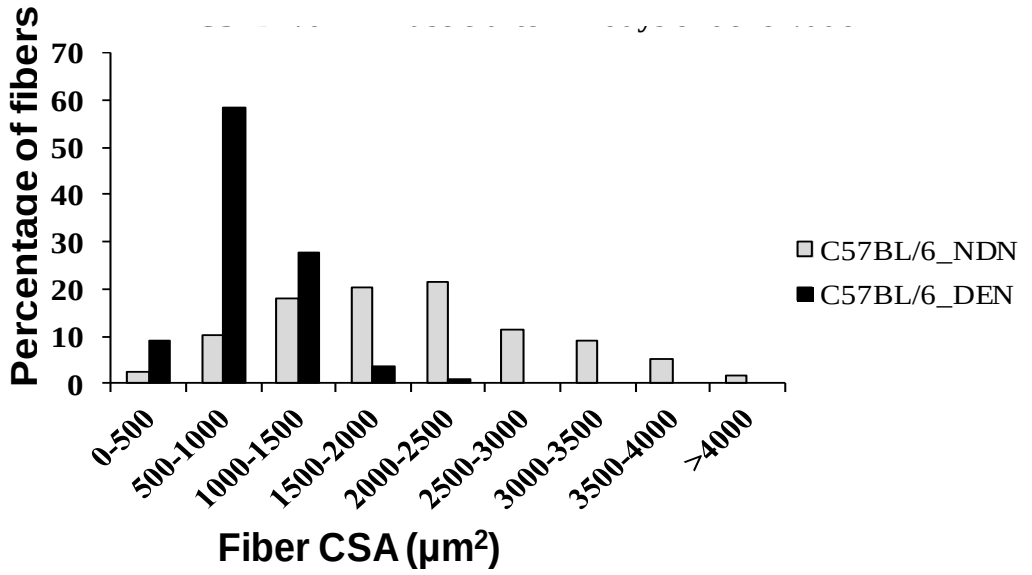
Percentage of fibers
70
60
50
40
30
20
10
0
0-500
500-1000
1000-1500
1500-2000
2000-2500
2500-3000
3000-3500
3500-4000
>4000
Fiber CSA (µm²)
C57BL/6_NDN
C57BL/6_DEN

B

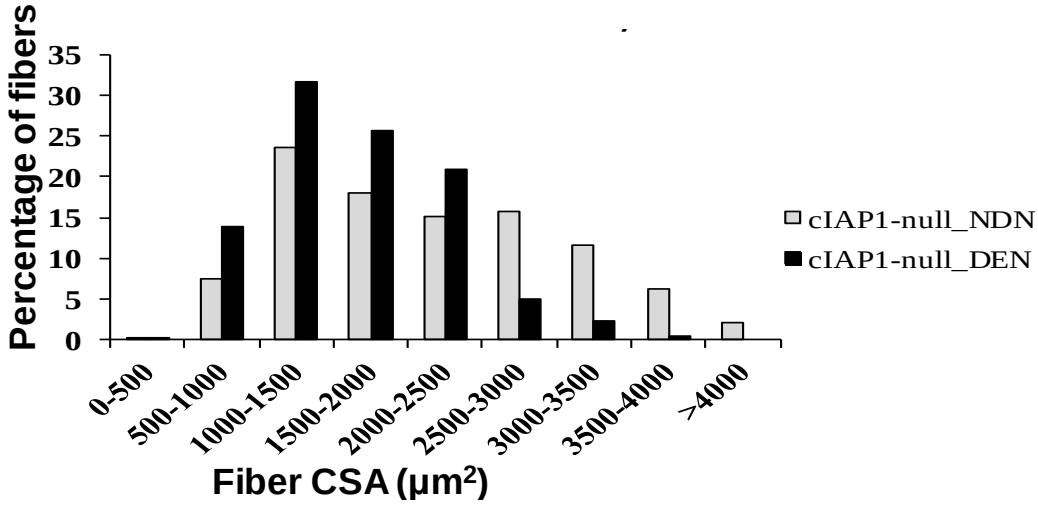
Percentage of fibers
35
30
25
20
15
10
5
0
0-500
500-1000
1000-1500
1500-2000
2000-2500
2500-3000
3000-3500
3500-4000
>4000
Fiber CSA (µm²)
cIAP1-null_NDN
cIAP1-null_DEN

C

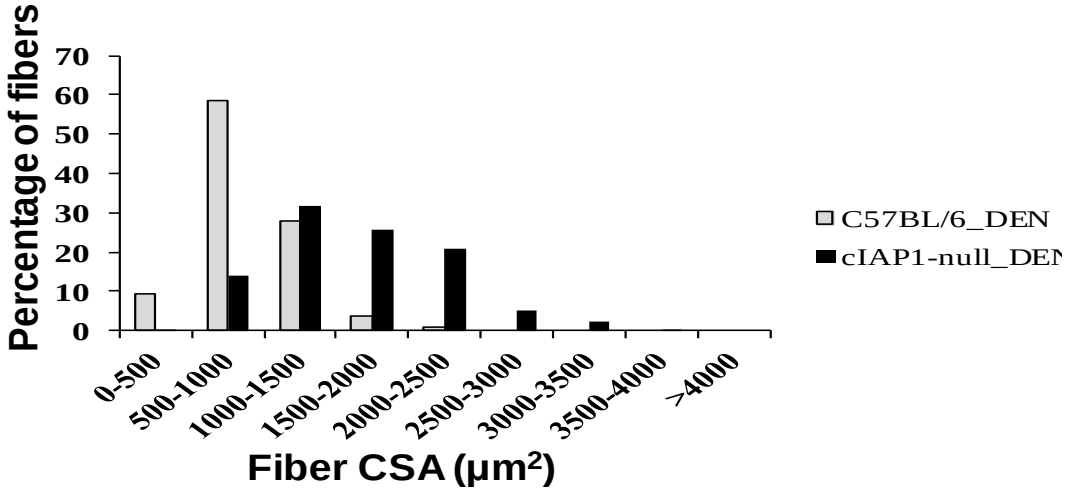
Percentage of fibers
70
60
50
40
30
20
10
0
0-500
500-1000
1000-1500
1500-2000
2000-2500
2500-3000
3000-3500
3500-4000
>4000
Fiber CSA (µm²)
C57BL/6_DEN
cIAP1-null_DEN

Figure 17. Atrophic shift of TA fiber cross-sectional area to smaller size is minimal in the absence of cIAP1 after 14 days of denervation

(**A**) Frequency distribution of fiber CSA of C57BL/6 TA muscle after 14 days of denervation. (**B**) Frequency distribution of fiber CSA of cIAP1-null TA muscle after 14 days of denervation. (**C**) Frequency distribution of fiber CSA of denervated C57BL/6 and cIAP1-nll TA muscle after 14 days of denervation. The H&E stained sections, of TA muscle collected from C57BL/6 (n=4) and cIAP1-null (n=4) mice at day 14 post-denervation, were photographed using Zeiss Axiophot microscope equipped with a digital camera and Northern Eclipse image analysis software. For each muscle, fiber cross-sectional areas (CSA) were traced and measured in μm^2 using ImageJ software. Data was transferred into a Microsoft Excel sheet, and the frequency distribution of nondenervated and denervated sections from each animal in both C57BL/6 and cIAP1-null mice were calculated by determining the number of fibers that fell within the given area ranges.

A

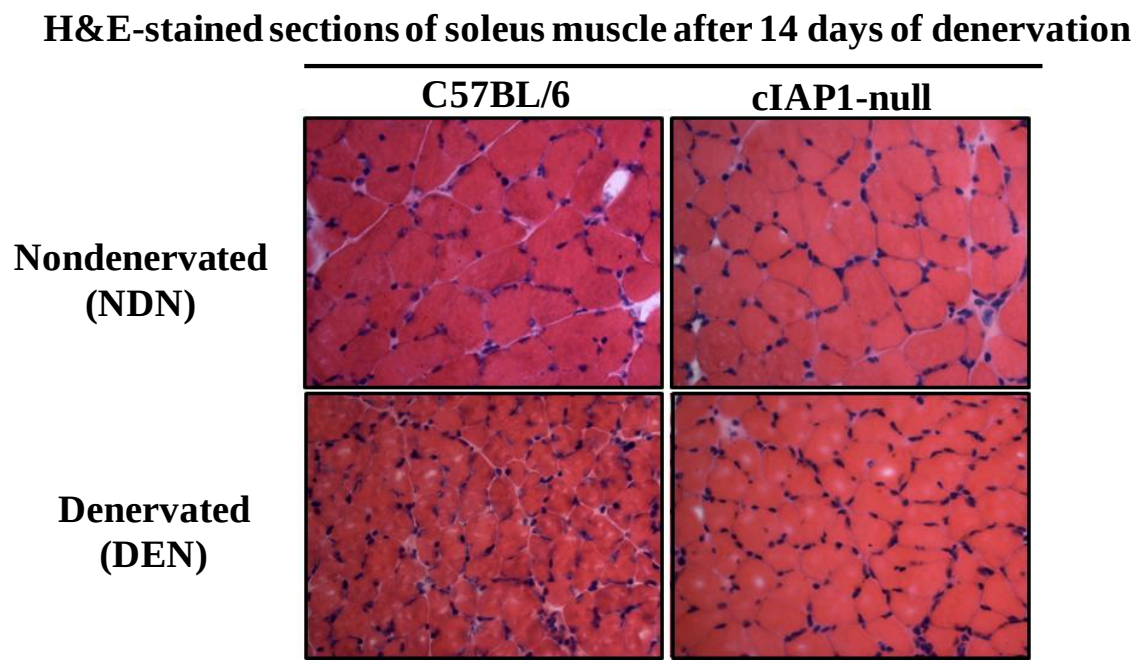

B

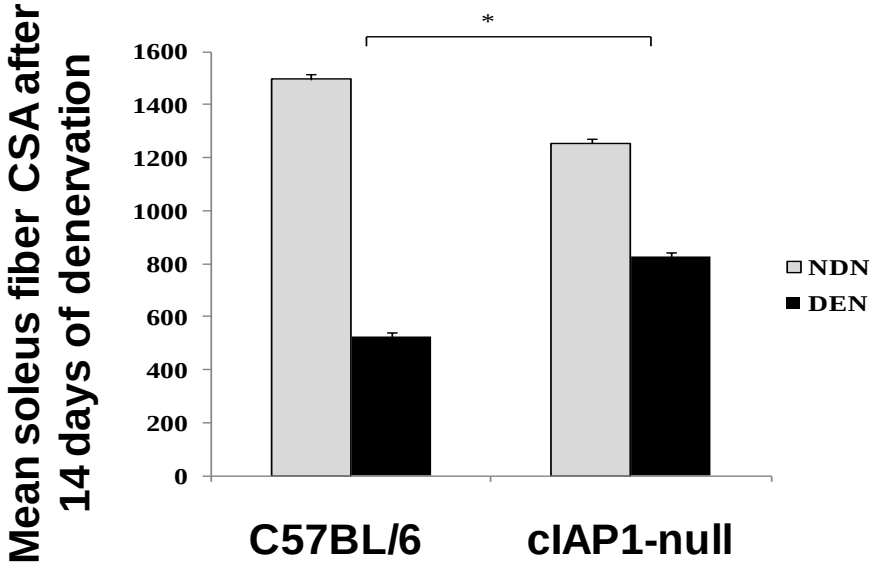

Figure 18. Loss of cIAP1 protects soleus muscle from atrophy after 14 days of denervation

(**A**) Four to six-week-old C57BL/6 and cIAP1-null mice were denervated by transection of the sciatic nerve of the left hind limb. Denervated and nondenervated soleus muscles were isolated at day 14 post-denervation, sectioned using a cryostat microtome and stained with haematoxylin and eosin dyes. Images were taken using an Axioskop microscope and Northern Eclipse software. (**B**) The H&E stained sections, of soleus muscle collected from C57BL/6 and cIAP1-null mice at day 14 post-denervation, were photographed using Zeiss Axiophot microscope equipped with a digital camera and Northern Eclipse image analysis software. For each muscle, fiber cross-sectional areas (CSA) were traced and measured in μm^2 using ImageJ software. Data was transferred into a Microsoft Excel sheet, mean fiber CSA was calculated using standard formula and the results were reported as means ± standard errors. n=4 for each group. * indicates significant difference, with $p < 0.01$.

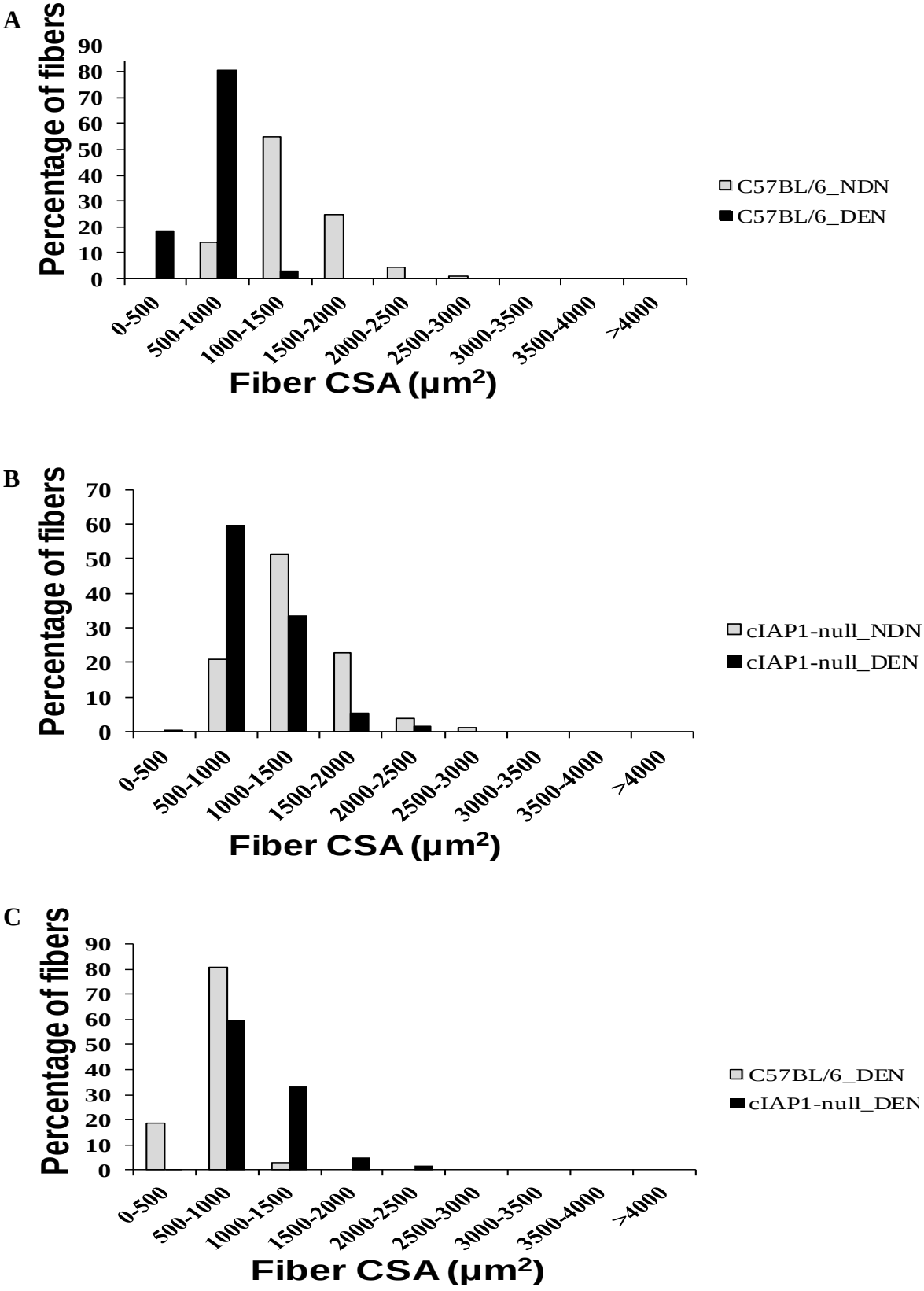
A
Percentage of fibers
90
80
70
60
50
40
30
20
10
0
0-500
500-1000
1000-1500
1500-2000
2000-2500
2500-3000
3000-3500
3500-4000
>4000
Fiber CSA (µm²)
C57BL/6_NDN
C57BL/6_DEN
B
Percentage of fibers
70
60
50
40
30
20
10
0
0-500
500-1000
1000-1500
1500-2000
2000-2500
2500-3000
3000-3500
3500-4000
>4000
Fiber CSA (µm²)
cIAP1-null_NDN
cIAP1-null_DEN
C
Percentage of fibers
90
80
70
60
50
40
30
20
10
0
0-500
500-1000
1000-1500
1500-2000
2000-2500
2500-3000
3000-3500
3500-4000
>4000
Fiber CSA (µm²)
C57BL/6_DEN
cIAP1-null_DEN

Figure 19. Atrophic shift of soleus fiber cross-sectional area to smaller size is minimal in the absence of cIAP1 after 14 days of denervation

(**A**) Frequency distribution of fiber CSA of C57BL/6 soleus muscle after 14 days of denervation. (**B**) Frequency distribution of fiber CSA of cIAP1-null soleus muscle after 14 days of denervation. (**C**) Frequency distribution of fiber CSA of denervated C57BL/6 and cIAP1-nll soleus muscle after 14 days of denervation. The H&E stained sections, of soleus muscle collected from C57BL/6 (n=4) and cIAP1-null (n=4) mice at day 14 post-denervation, were photographed using Zeiss Axiophot microscope equipped with a digital camera and Northern Eclipse image analysis software. For each muscle, fiber cross-sectional areas (CSA) were traced and measured in μm^2 using ImageJ software. Data was transferred into a Microsoft Excel sheet, and the frequency distribution of nondenervated and denervated sections from each animal in both C57BL/6 and cIAP1-null mice were calculated by determining the number of fibers that fell within the given area ranges.

3.2.1.3 Genetic Inhibition of cIAP1 Sustained Skeletal Muscle Protection at 28 Days Post-Denervation

Because the absence of cIAP1 protects against denervation-induced skeletal muscle atrophy at 7 and 14 days post-denervation, and that this protection is even more pronounced at 14 days following denervation, I next asked whether this protection would be maintained at an experimental time point extended to 28 days. In brief, section of the sciatic nerve was performed in C57BL/6 and cIAP1-null mice and skeletal muscles were collected 28 days later. H&E-stained sections of TA muscles were used to measure fiber cross-sectional areas (CSA) and analyse their frequency distribution in the denervated (DEN) and nondenervated (NDN) muscles of cIAP1-null and C57BL/6 mice. Remarkably, the protection against disuse-induced skeletal muscle atrophy persists for at least 28 days in the absence of cIAP1, as seen in H&E-stained TA sections (Figure 20A). Moreover, the mean fiber CSA quantification revealed a drastic decrease (69%) in fiber CSA of denervated C57BL/6 TA muscle compared to a smaller decrease (only 46%) in cIAP1-null mice, and highlighted that this decrease in fiber size was 23% higher in the absence of cIAP1 (Figure 20B). Fiber size distribution analysis demonstrated a protection against denervation-induced skeletal muscle atrophy, as a lack of shift toward smaller fiber size was noticed in cIAP1-null TA muscle compared to C57BL/6 controls after 28 days of denervation (Figure 21C).

These results clearly confirm genetic ablation of cIAP1 significantly decreases the magnitude of muscle atrophy and show that this protection is maintained up to 28 days following disuse atrophy.

A

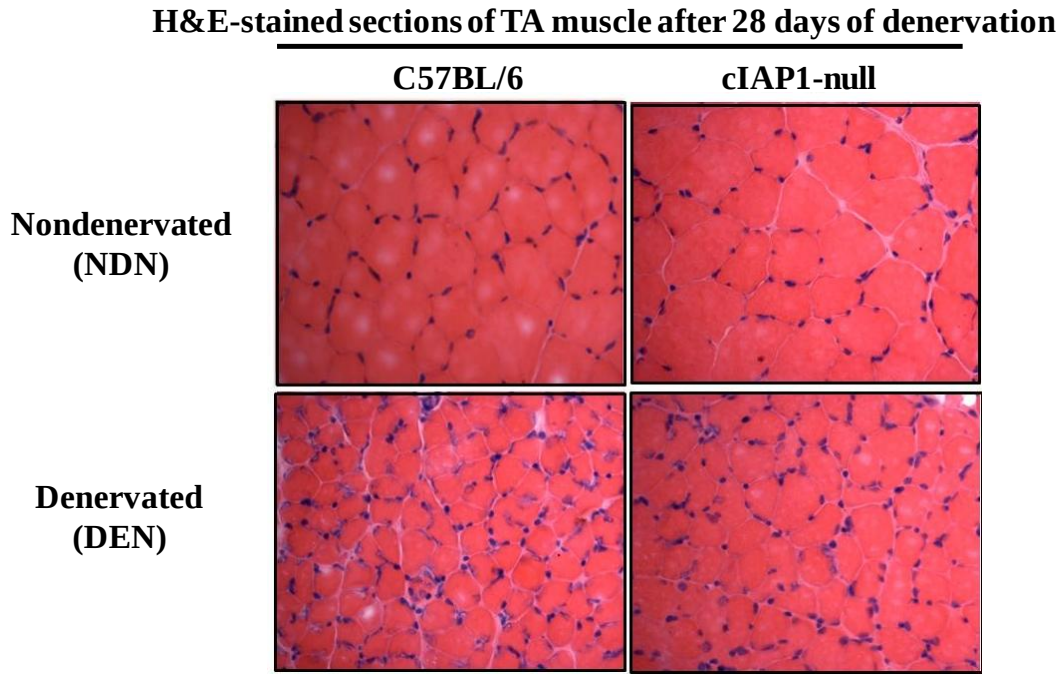

B

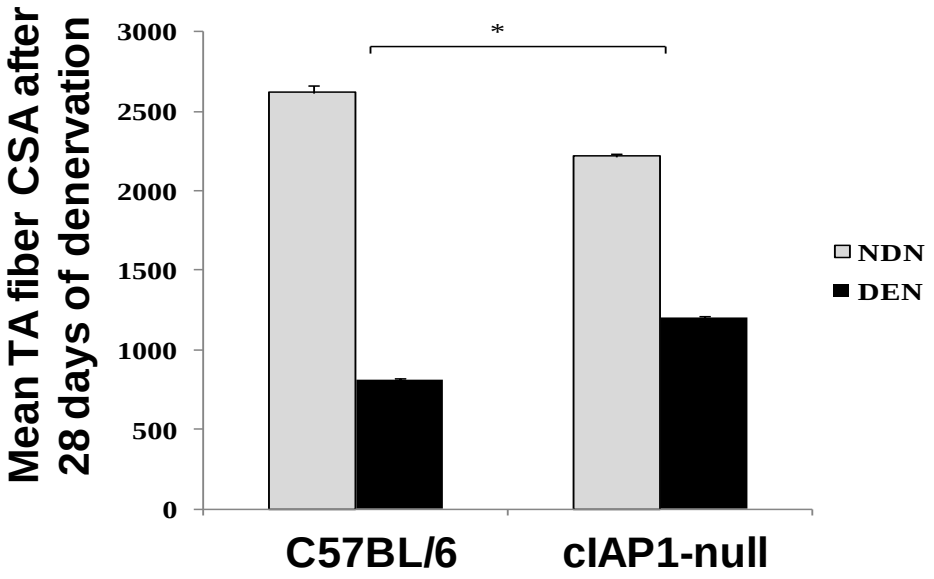

Figure 20. Loss of cIAP1 protects TA muscle from atrophy after 28 days of denervation

(**A**) Four to six-week-old C57BL/6 and cIAP1-null mice were denervated by transection of the sciatic nerve of the left hind limb. Denervated and nondenervated TA muscles were isolated at day 28 post-denervation, sectioned using a cryostat microtome and stained with haematoxylin and eosin dyes. Images were taken using an Axioskop microscope and Northn Eclipse software.

(**B**) The H&E stained sections, of TA muscle collected from C57BL/6 (n=3) and cIAP1-null (n=4) mice at day 28 post-denervation, were photographed using Zeiss Axiophot microscope equipped with a digital camera and Northern Eclipse image analysis software. For each muscle, fiber cross-sectional areas (CSA) were traced and measured in μm^2 using ImageJ software. Data was transferred into a Microsoft Excel sheet, mean fiber CSA was calculated using standard formula and the results were reported as means ± standard errors. * indicates significant difference, with $p < 0.01$.

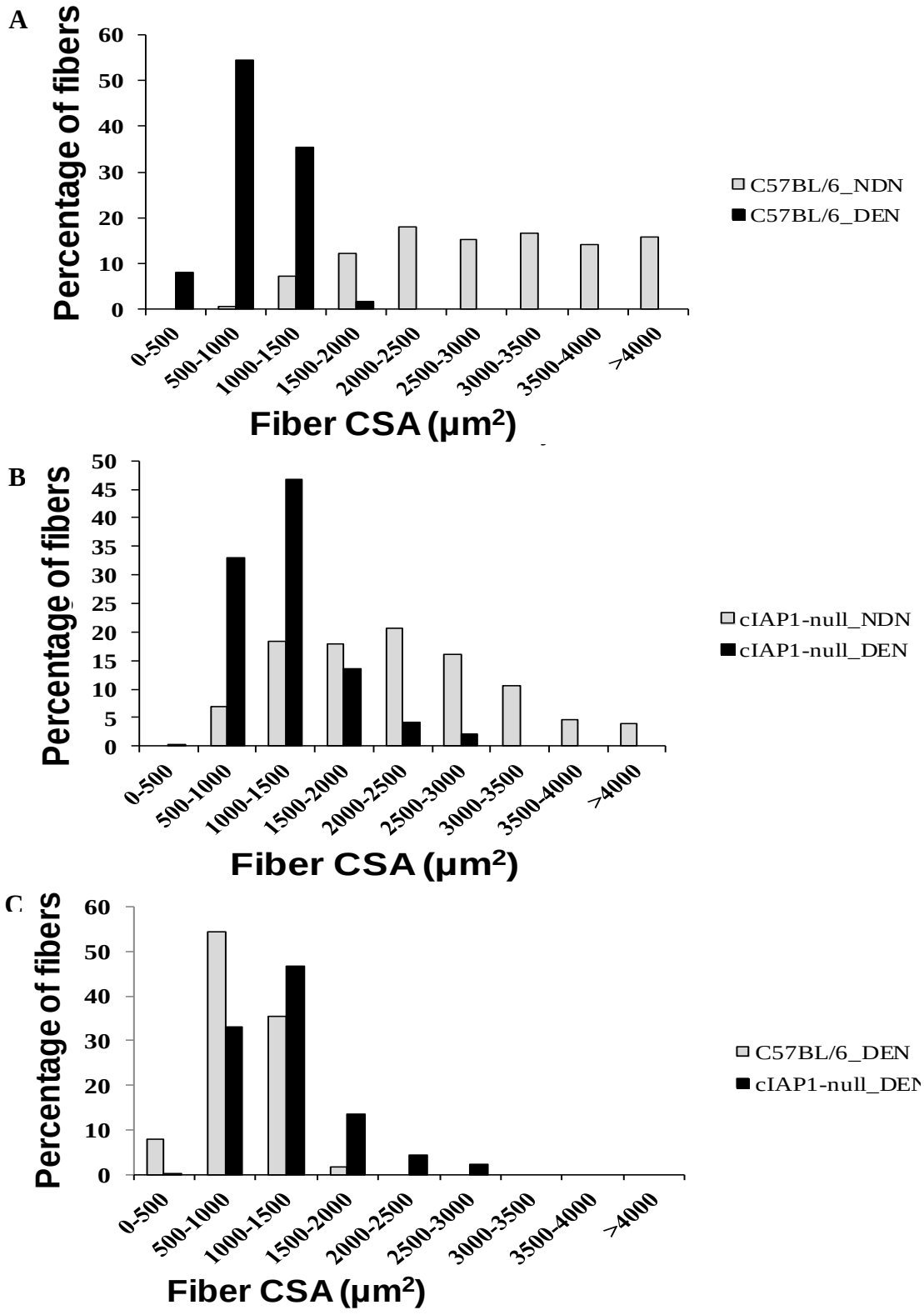
A
Percentage of fibers
60
50
40
30
20
10
0
0-500
500-1000
1000-1500
1500-2000
2000-2500
2500-3000
3000-3500
3500-4000
>4000
Fiber CSA (µm²)
C57BL/6_NDN
C57BL/6_DEN
B
Percentage of fibers
50
45
40
35
30
25
20
15
10
5
0
0-500
500-1000
1000-1500
1500-2000
2000-2500
2500-3000
3000-3500
3500-4000
>4000
Fiber CSA (µm²)
cIAP1-null_NDN
cIAP1-null_DEN
C
Percentage of fibers
60
50
40
30
20
10
0
0-500
500-1000
1000-1500
1500-2000
2000-2500
2500-3000
3000-3500
3500-4000
>4000
Fiber CSA (µm²)
C57BL/6_DEN
cIAP1-null_DEN

Figure 21. Atrophic shift of TA fiber cross-sectional area to smaller size is minimal in the absence of cIAP1 after 28 days of denervation

(**A**) Frequency distribution of fiber CSA of C57BL/6 TA muscle after 28 days of denervation. (**B**) Frequency distribution of fiber CSA of cIAP1-null TA muscle after 28 days of denervation. (**C**) Frequency distribution of fiber CSA of denervated C57BL/6 and cIAP1-nll TA muscle after 28 days of denervation. The H&E stained sections, of TA muscle collected from C57BL/6 (n=3) and cIAP1-null (n=4) mice at day 28 post-denervation, were photographed using Zeiss Axiophot microscope equipped with a digital camera and Northern Eclipse image analysis software. For each muscle, fiber cross-sectional areas (CSA) were traced and measured in μm^2 using ImageJ software. Data was transferred into a Microsoft Excel sheet, and the frequency distribution of nondenervated and denervated sections from each animal in both C57BL/6 and cIAP1-null mice were calculated by determining the number of fibers that fell within the given area ranges.

3.2.2 The protection against denervation-induced skeletal muscle atrophy is due to the absence of cIAP1 and not to strain differences

To verify that the protection against denervation-induced muscle atrophy seen in cIAP1-null compared to C57BL/6 is due to the loss of cIAP1 and not strain differences, cIAP1-null mice were backcrossed to a C57BL/6 inbred background for several generations to produce cIAP1-null and wild type littermates. Littermate offspring were genotyped by Polymerase Chain Reaction (PCR) analysis from ear or tail DNA to identify their genotypes. Four to six-week-old cIAP1-null and WT littermate mice were denervated as previously described. Fourteen days later, TA and soleus muscles were collected, cross-sectioned, and stained with H&E dyes. Fiber CSA were measured in each muscle, the average was calculated in denervated and nondenervated muscles of cIAP1-null and wild type littermate mice.

By 14 days, the denervated TA in wild type animals showed a significant reduction in the mean fiber CSA of about 54% compared to only 31% in cIAP1-null littermates (Figure 22A).

Moreover, cIAP1-null soleus fiber CSA only decreased by 34% after 14 days of denervation, compared to a more dramatic 62% decrease in WT littermates (Figure 22B).

In conclusion, these results reveal that the protection against denervation-induced skeletal muscle atrophy seen in cIAP1-null is significant and profound in comparison to WT littermates. In addition, these findings further confirm the protective phenotype seen in cIAP1-null when compared to C57BL/6 and indicate that this protection is likely due to the absence of cIAP1 and not strain differences.

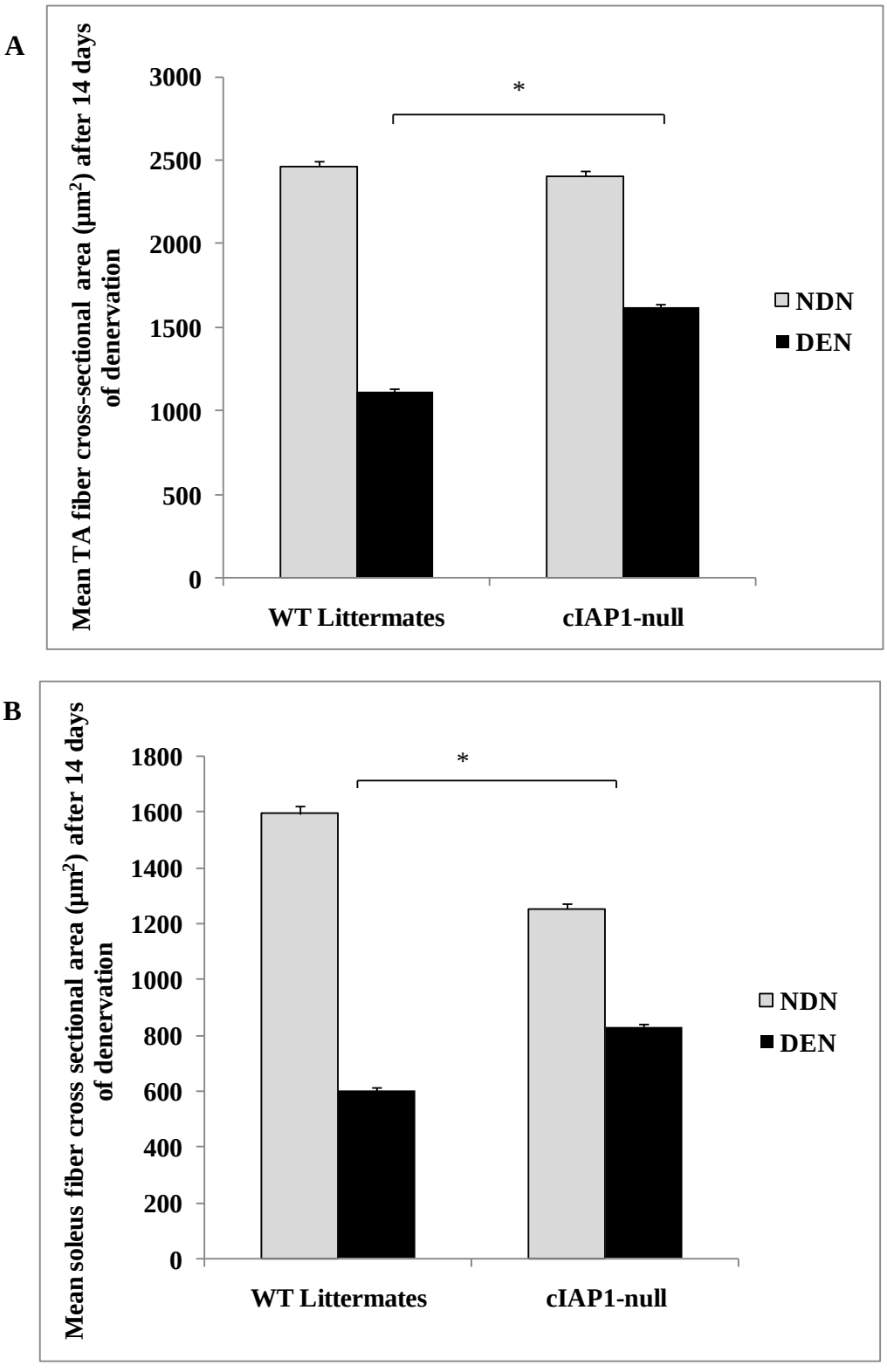

Figure 22. Reduction of fiber cross-sectional area is less in cIAP1-null TA compare to wild type littermates after 14 days of denervation

(**A**) H&E-stained TA sections of cIAP1-null and WT littermate (Lit) mice at 14 days post-denervation were photographed using Zeiss Axiophot microscope equipped with a digital camera and Northern Eclipse image analysis software. For each muscle, fiber cross-sectional areas (CSA) were traced and measured in μm^2 using ImageJ software. Data was transferred into a Microsoft Excel sheet, mean fiber CSA was calculated using standard formula and the results were reported as means ± standard errors. n=3 in each group. * indicates significant difference, with $p < 0.01$. (**B**) H&E-stained soleus sections of cIAP1-null and WT littermate mice at 14 days post-denervation were photographed using Zeiss Axiophot microscope equipped with a digital camera and Northern Eclipse image analysis software. For each muscle, fiber cross-sectional areas (CSA) were traced and measured in μm^2 using ImageJ software. Data was transferred into a Microsoft Excel sheet, mean fiber CSA was calculated using standard formula and the results were reported as means ± standard errors. n=3 in each group. * indicates significant difference, with $p < 0.01$.

3.2.3 Genetic ablation of cIAP1 blocks fiber type switch in response to denervation-induced skeletal muscle atrophy

In addition to the reduction in fiber CSA, disuse atrophy is also characterized by a switch of fiber type from slow (type I) to fast (type II) (Ohira et al., 1992; Midrio et al., 1992; Huey and Bodine, 1998; Mourkioti et al., 2006). To evaluate the role of cIAP1 in fiber type remodeling in response to denervation-induced skeletal muscle atrophy, I performed double immunostaining on cross-sections of denervated and nondenervated soleus muscles (which contain two types of fiber: slow and fast) of cIAP1-null and C57BL/6 mice with specific antibodies which recognize type I (slow) (Figure 23A and Figure 23B) or type II (fast) (Figure 23B) using anti-MHC along with anti-laminin antibody (which reveals the membrane surrounding each muscle fiber). Then, I quantified the percentage of fibers expressing each of these MHC isoforms in the denervated and nondenervated C57BL/6 and cIAP1-null muscles. Analysis of fiber-type distribution in C57BL/6 denervated soleus muscles revealed a significant decrease of about 17% in type I (slow) fibers compared to the contralateral muscle, which become type II (fast) fibers (Figure 23B). Interestingly, denervation-induced skeletal muscle atrophy did not alter the percentage of type I nor type II fibers in cIAP1-null soleus muscles (Figure 23B).

These data confirm previous findings that disuse atrophy causes a shift from slow to fast fibers in control animals and most importantly reveal a lack of this transition and maintenance of fiber-type distribution in cIAP1-null denervated soleus muscle. This finding further supports the protective phenotype seen in response to denervation-induced atrophy when cIAP1 is depleted.

A

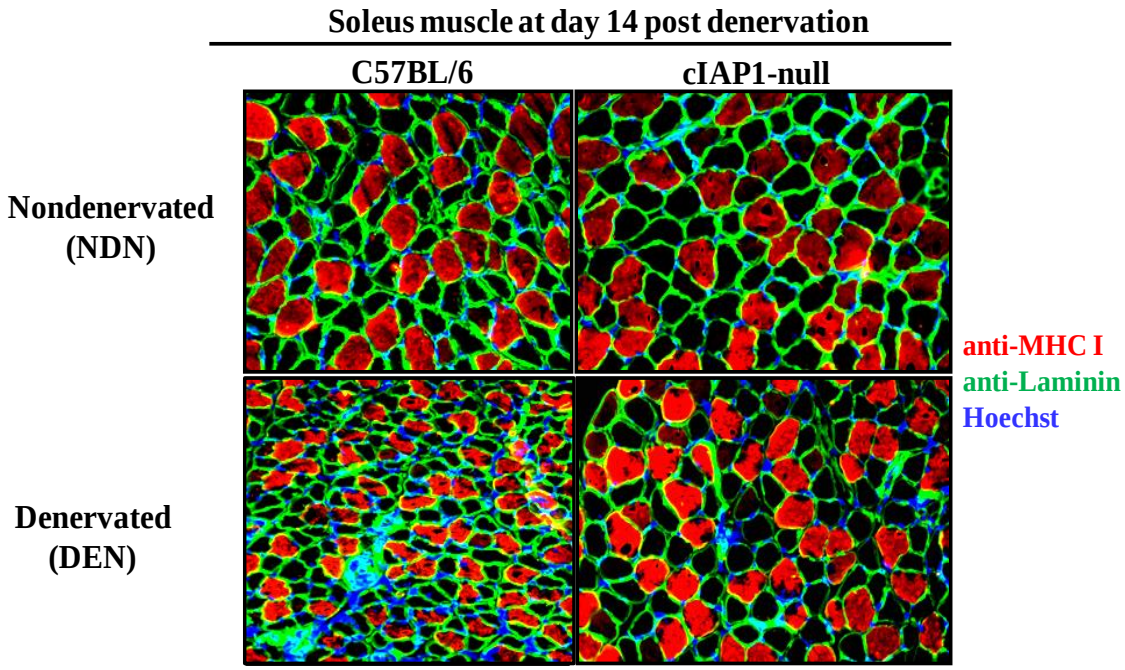

B

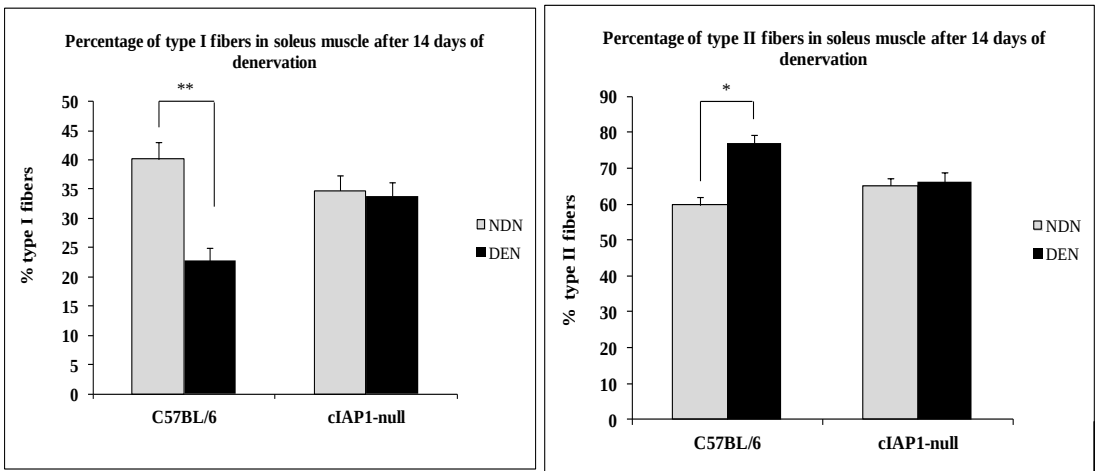

Figure 23. The absence of cIAP1 blocks fiber type switch in response to denervation-induced skeletal muscle atrophy

(**A**) Four to six-week-old C57BL/6 and cIAP1-null mice were denervated by transection of the sciatic nerve of the left hind limb. Denervated and nondenervated soleus muscles were isolated at day 14 post-denervation, sectioned using a cryostat microtome and

immunostaining with anti-type I MHC, anti-laminin and Hoechst. Images were taken using Axioskop microscope and Northern Eclipse software. (**B**) Fiber-type distribution in denervated soleus muscles from cIAP1-null and C57BL/6 after 14 days post-denervation. Note the significant decrease in slow (MHC I) fibers in control denervated muscles, which become fast (MHC II) and the maintenance of fiber-type distribution in cIAP1-null muscle. Error bars represent standard error. n=4 for each group. ** indicates $p < 0.001$ and * indicates $p < 0.01$.

3.2.4 Pharmacologic inhibition of cIAP1 using the SMC- LCL161 alleviates skeletal muscle atrophy in response to denervation

In addition to the genetic depletion, I used a pharmacological inhibitor of cIAP1 known as Smac Mimetic compound (SMC) to study the role of cIAP1 in denervation-induced skeletal muscle atrophy. I took advantage of a small-molecule antagonist of the IAPs that mimics their interaction with the endogenous inhibitor, Smac (Wu et al., 2000; Li et al., 2004; Sun et al., 2008; Cheung et al., 2009). These "Smac-mimetic" compounds (SMC) cause the rapid inhibition and proteasomal degradation of cIAP1 and its paralogue cIAP2 (which is absent in skeletal muscle (Mahoney et al., 2008)).

Remarkably, histological analysis of H&E-stained sections of soleus muscle treated with SMC revealed that the drug treatment protected against muscle atrophy after 14 days post-denervation (Figure 24A). Furthermore, measurements of the soleus fiber CSA revealed a dramatic decrease of 61% in control mice compare to only 23% decrease in SMC-treated mice after 14 days of denervation (Figure 24B).

This current study provides the first *in vivo* evidence that the inhibition of cIAP1 can block atrophy.

A

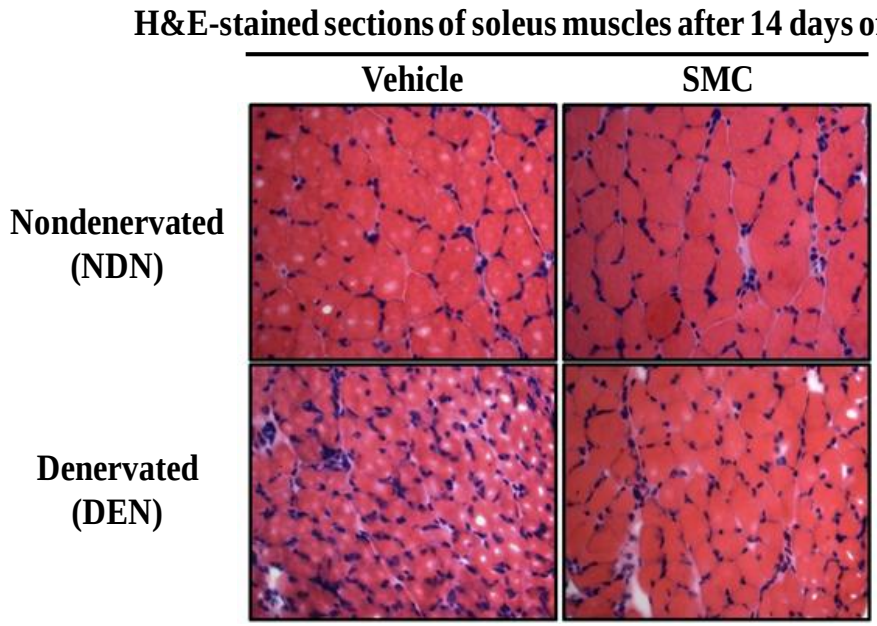

B

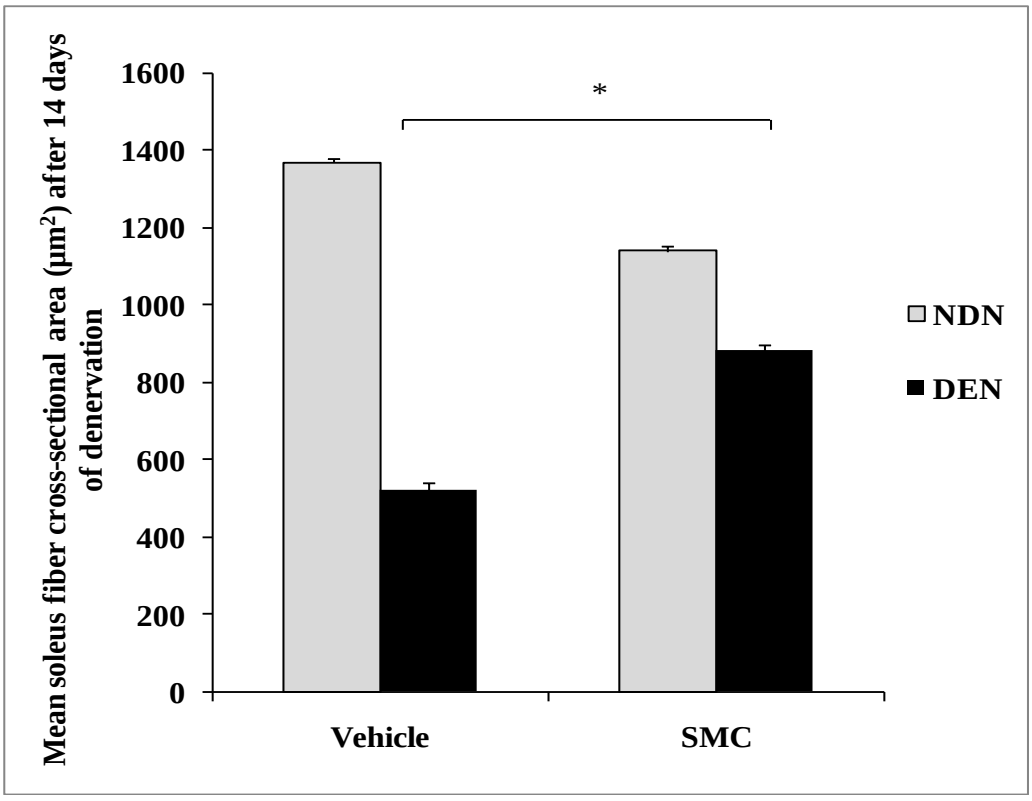

Figure 24. SMC treatment alleviates skeletal muscle atrophy in response to denervation

(**A**) Four to six-week-old C57BL/6 mice were randomly assigned to control (vehicle) or SMC-treatment, which was delivered once a week via oral gavage. Four days later, these mice were denervated as previously described. Fourteen days post-denervation, mice were sacrificed and denervated and nondenervated soleus muscles were collected. Muscles were then sectioned using a cryostat microtome and stained with haematoxylin and eosin dyes. Images were taken using an Axioskop microscope and Northern Eclipse software. (**B**) H&E-stained soleus sections of C57BL/6 mice, which were treated with either vehicle or SMC then denervated for 14 days, were photographed using Zeiss Axiophot microscope equipped with a digital camera and Northern Eclipse image analysis software. For each muscle, fiber cross-sectional areas (CSA) were traced and measured in μm^2 using ImageJ software. Data was transferred into a Microsoft Excel sheet, mean fiber CSA was calculated using standard formula and the results were reported as means ± standard errors. n=3 in each group. * indicates significant difference, with $p < 0.01$.

3.3 Molecular mechanism by which loss of cIAP1 confers protection in response to denervation-induced skeletal muscle atrophy

3.3.1 Expression of cIAP1 is increased in atrophied skeletal muscle

Although, cIAP1 is known to be expressed in skeletal muscle (Mahoney et al., 2008), it remains unknown how the expression of cIAP1 is affected in skeletal muscle in response to denervation. To address this issue, I prepared muscle extracts from NDN and DEN cIAP1-null and C57BL/6 gastrocnemius and TA muscles to measure the level of cIAP1 by Western blotting, using our RIAP1 antibody. This antibody reliably detects both cIAP1 and cIAP2 simultaneously, although it is difficult to visualize the separation between the two bands since cIAP2 migrates only 2 kDa higher than cIAP1. As shown in figure 25, the protein levels of cIAP1 were found to be increased in DEN compared to NDN gastrocnemius and TA muscles from C57BL/6 mice, suggesting that the expression of cIAP1 is up-regulated in skeletal muscle in response to denervation.

Although cIAP2 has been previously shown not to be expressed in skeletal muscle tissue (Mahoney et al., 2008), surprisingly, I found that in response to denervation, cIAP2 is up-regulated in cIAP1-null mice (Figure 25). These observations suggest that in response to denervation, the induction of cIAP2 is likely not from muscle cells.

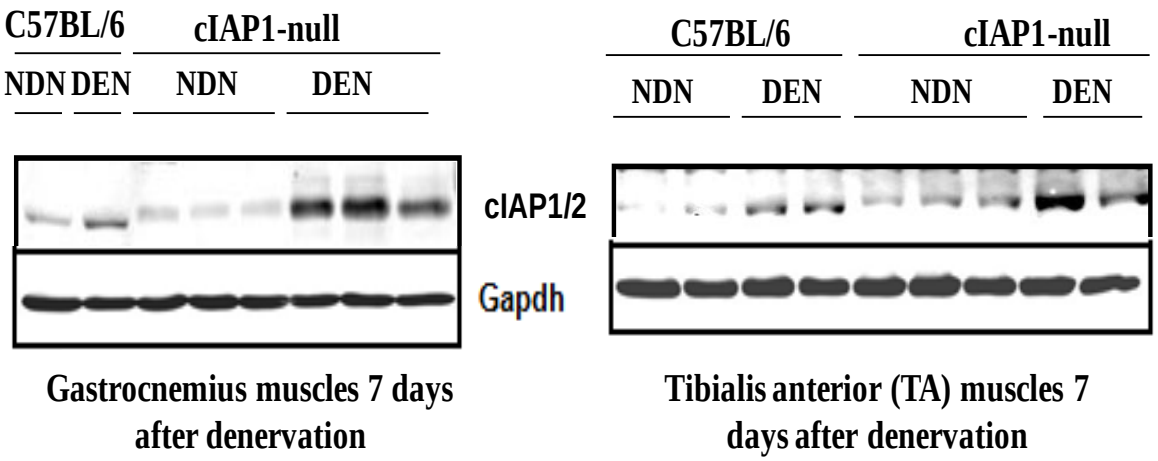

Figure 25. Expression of cIAP1 is increased in atrophied skeletal muscle

Representative Immunoblots show cIAP1 and cIAP2 protein levels, using our RIAP1 antibody which reliably detects both cIAP1 and cIAP2 simultaneously in denervated and nondenervated C57BL/6 and cIAP1-null gastrocnemius muscles after 7 days of denervation. Gapdh was used as loading control.

3.3.2 Genetic Depletion of cIAP1 blunts the induction of both MuRF1 and MAFbx in response to denervation-induced skeletal muscle atrophy

During different conditions of skeletal muscle atrophy, activation of a complex network of biochemical and transcriptional pathways occur, leading to the upregulation of two muscle -specific ubiquitin ligases, MuRF1 and MAFbx (Glass, 2003; Cao et al., 2005; Paul et al., 2010). To investigate the mechanism by which loss of cIAP1 protects against skeletal muscle atrophy, I first asked whether loss of cIAP1 affects the expression of these two ligases in response to denervation. To answer this question, I measured MuRF1 and MAFbx transcript levels in NDN and DEN skeletal muscle of cIAP1-null and C57BL/6 mice, using real-time PCR technique. As previously reported (Bodine et al., 2001; Gomes et al., 2001) the mRNA levels of both MAFbx and MuRF1 were up-regulated in denervated soleus muscle compared with the contralateral nondenervated muscle at day 7 post-denervation (Figure 26A and 26B). Interestingly, the mRNA levels of both MuRF1 and MAFbx were significantly down-regulated in denervated soleus muscle from cIAP1-null mice compared with C57BL/6 muscle (Figure 26A and 26B). Western blotting, using muscle extracts also validated that the expression of MuRF1 is blunted in denervated skeletal muscle of cIAP1-null compared to C57BL/6 mice (Figure 26C). Take together these results suggest that cIAP1 in muscle cells is required for denervation-induced expression of these ligases, MuRf1 and MAFbx.

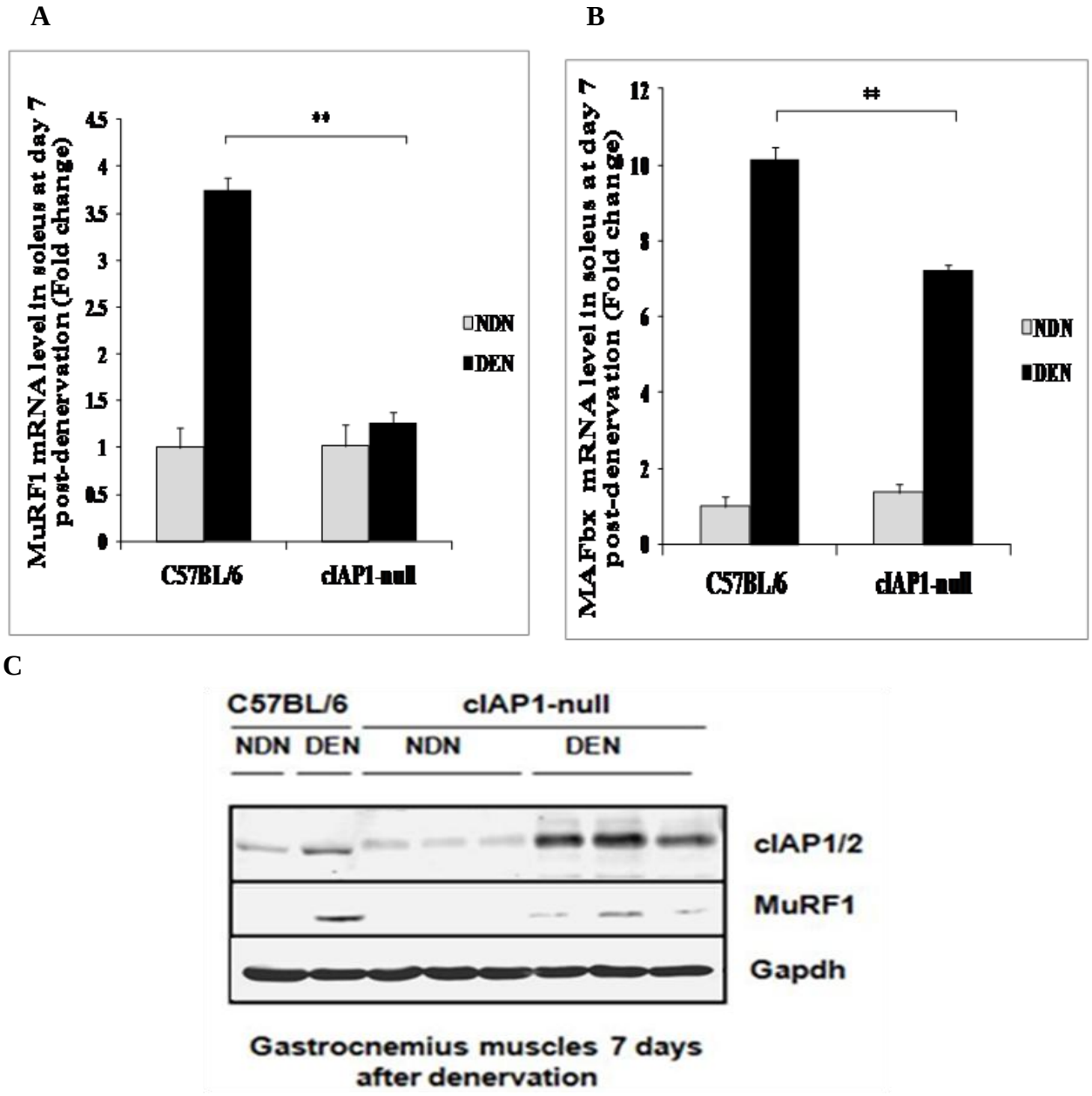

Figure 26. MuRF1and MAFbX mRNA induction is blunted in cIAP1-null soleus muscle after 7 days of denervation

(**A**) Relative mRNA levels of MuRF1, in denervated and nondenervated soleus muscle of cIAP1-null and C57BL/6 mice after 7 days post-denervation, was measured by

quantitative real-time RT-PCR method (n=4 in each group). Error bars represent the standard error of the mean (SEM). ** indicates $p < 0.001$. (**B**) Relative mRNA levels of MAFbx, in denervated and nondenervated soleus muscle of cIAP1-null and C57BL/6 mice after 14 days post-denervation, measured by quantitative real-time RT-PCR method (n=4 in each group). Error bars represent the SEM. ** indicates $p < 0.001$. (**C**) Representative immunoblots show cIAP1/2 and MuRF1 protein levels, using our RIAP1 (to reliably detect both cIAP1 and cIAP2 simultaneously) and MuRF1 antibodies, in denervated and nondenervated C57B/6 and cIAP1-null gastrocnemius muscles after 7 days of denervation. Gapdh was used as loading control.

3.3.3 SMC treatment downregulates cIAP1 and/or cIAP2 and attenuates MuRF1 induction in denervated skeletal muscle *in vivo*

The novel SMC used for the *in vivo* study, LCL161, is an orally-available monomeric SMC that binds to cIAP1 and 2 with high affinities, targeting them for rapid proteasomal degradation. LCL161 is currently in phase I testing in humans for cancer (Infante et al., 2010). In this thesis, I showed that cIAP1 inhibition by a pharmacological approach, such as using SMC, recapitulates the effects of genetic ablation of cIAP1 on denervation-induced skeletal muscle atrophy. In this study, I investigate the ability of SMC to induce the loss of cIAP1 protein expression in muscle during different time points. For this, age-matched C57BL/6 mice were orally treated once a week with either vehicle or SMC at 100 mg/kg, a dose proven safe and effective in mouse cancer models (Weisberg et al., 2010), then the mice were denervated four days after the first SMC administration and tissues were collected at various time points. Oral gavage of SMC has only a transient effect on cIAP1/2 downregulation in highly proliferative tissues such as the spleen (Figure 27A), but maintains sustained knockdown of cIAP1 in skeletal muscle such as the gastrocnemius (Figure 27B). In addition, MuRF1 induction in response to denervation was blunted in denervated muscle pre-treated with SMC (Figure 28).

A

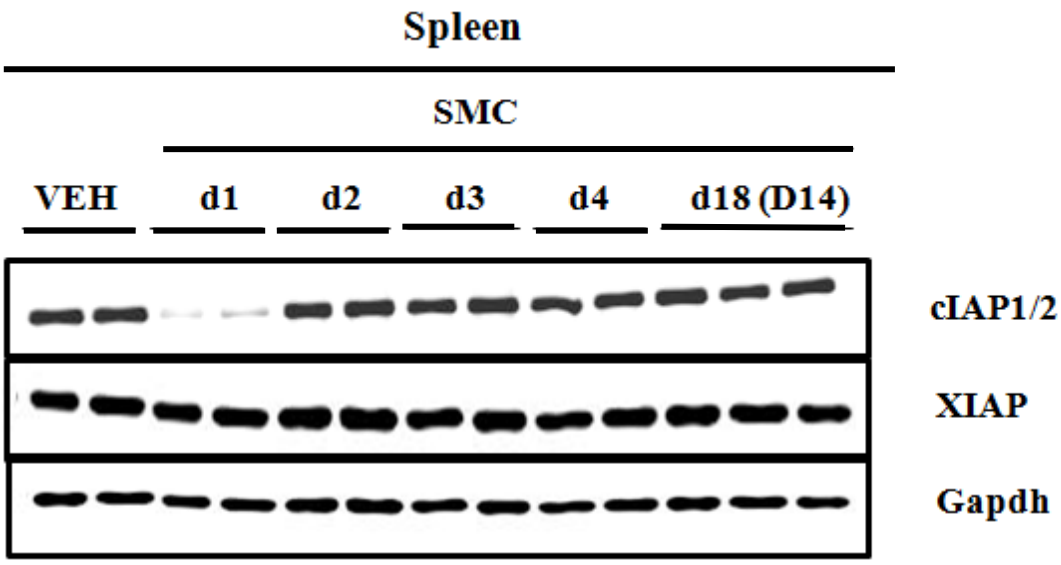

B

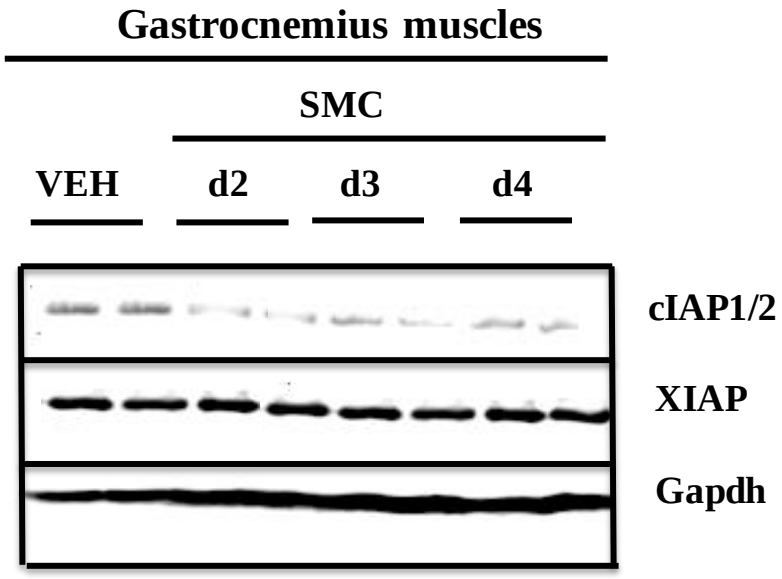

Figure 27. SMC treatment results in a quick knockdown of cIAP1 and cIAP2 in the spleen and sustained knockdown of cIAP1 and cIAP2 in muscle

(**A**) C57BL/6 mice were gavaged once a week with either vehicle or SMC (100 mg/kg). Mice were then sacrificed at multiple days post-dosing, and tissues were collected at the indicated time points to assess target knock-down (cIAP1/2, XIAP). SMC treatment results in a quick knockdown of cIAP1 and cIAP2 in the spleen. Equal amount of protein were analyzed by western blotting for levels of cIAP1/2 and XIAP. Gapdh was used as a loading control. Note that "d" means days post-SMC administration and "D" means days post-denervation. (**B**) SMC treatment results in sustained knockdown of cIAP1 and cIAP2 in Gastrocnemius muscle. Equal amount of protein were analyzed by western blotting for levels of cIAP1/2 and XIAP. Gapdh was used as a loading control. Note that "d" means days post-SMC administration and "d" means days post-treatment.

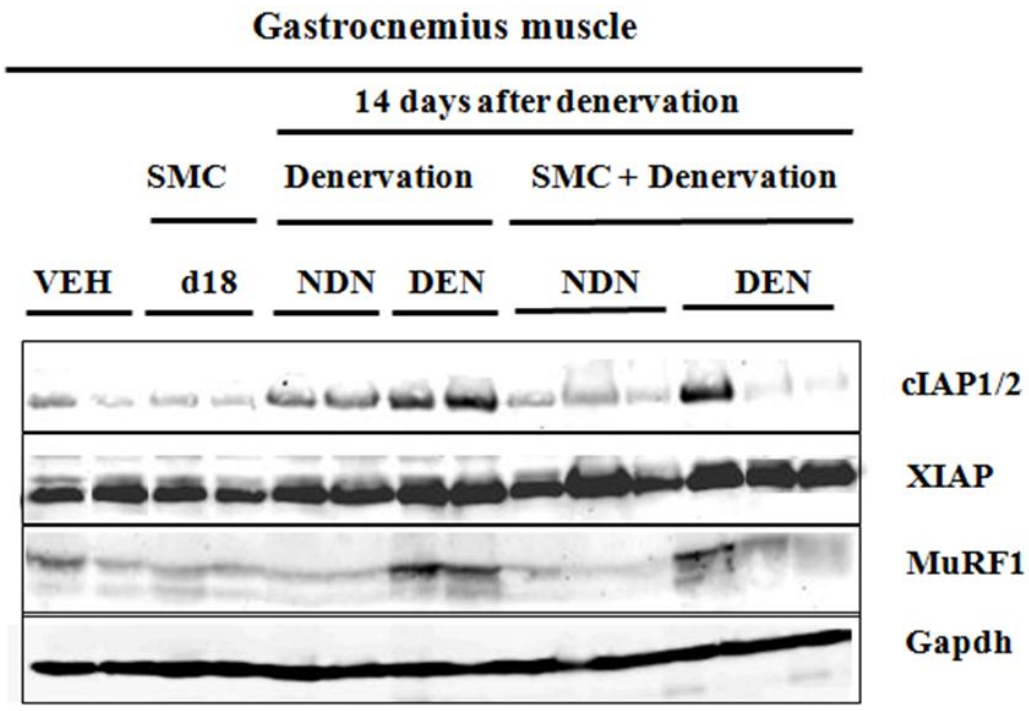

Figure 28. SMC successfully downregulate cIAP1 after 18 days of the initial drug administration and attenuates MuRF1 induction after 14 days of denervation in gastrocnemius muscle

C57BL/6 mice were treated once a week (gavage) either with vehicle or SMC then denervated four days later. Gastrocnemius muscles were collected at the indicated time points. Equal amount of protein were analyzed by western blotting and levels of cIAP1/2, XIAP and MuRF1. Gapdh was used as a loading control. Note that "d" means days post SMC administration and "D" days post denervation.

3.3.4 Ablation of cIAP1 inhibits Fn14 induction in response to denervation-induced skeletal muscle atrophy

To further investigate the mechanism by which cIAP1 confers protection against denervation-induced skeletal muscle atrophy, and because it has been recently shown that following denervation Fn14 but not TWEAK expression is upregulated (Mittal et al., 2010), I determined the expression of both TWEAK and Fn14 in C57BL/6 and cIAP1-null DEN and NDN muscles. Using qRT-PCR and western blot methods, I found that Fn14 expression increased dramatically in denervated C57BL/6, as anticipated. Remarkably, Fn14 was not induced to the same extent following denervation in cIAP1-null soleus muscle (see figure 29A and 29B). That is, upon denervation, Fn14 mRNA increases nearly seven-fold at day 7 and five-fold at day 14 post-denervation in C57BL/6 compare to only less than two-fold in cIAP1-null muscle at both time points (Figure 29A and 29B). Furthermore, and as expected, TWEAK mRNA is not significantly induced upon denervation in both strains after 7 as well as 14 days-post denervation (Figure 30A and 30B). These findings suggest that TWEAK receptor levels, and not the ligand itself, are the main determinants of TWEAK sensitivity in denervated muscle, and that Fn14 expression is influenced by the cIAP1 status of the cell.

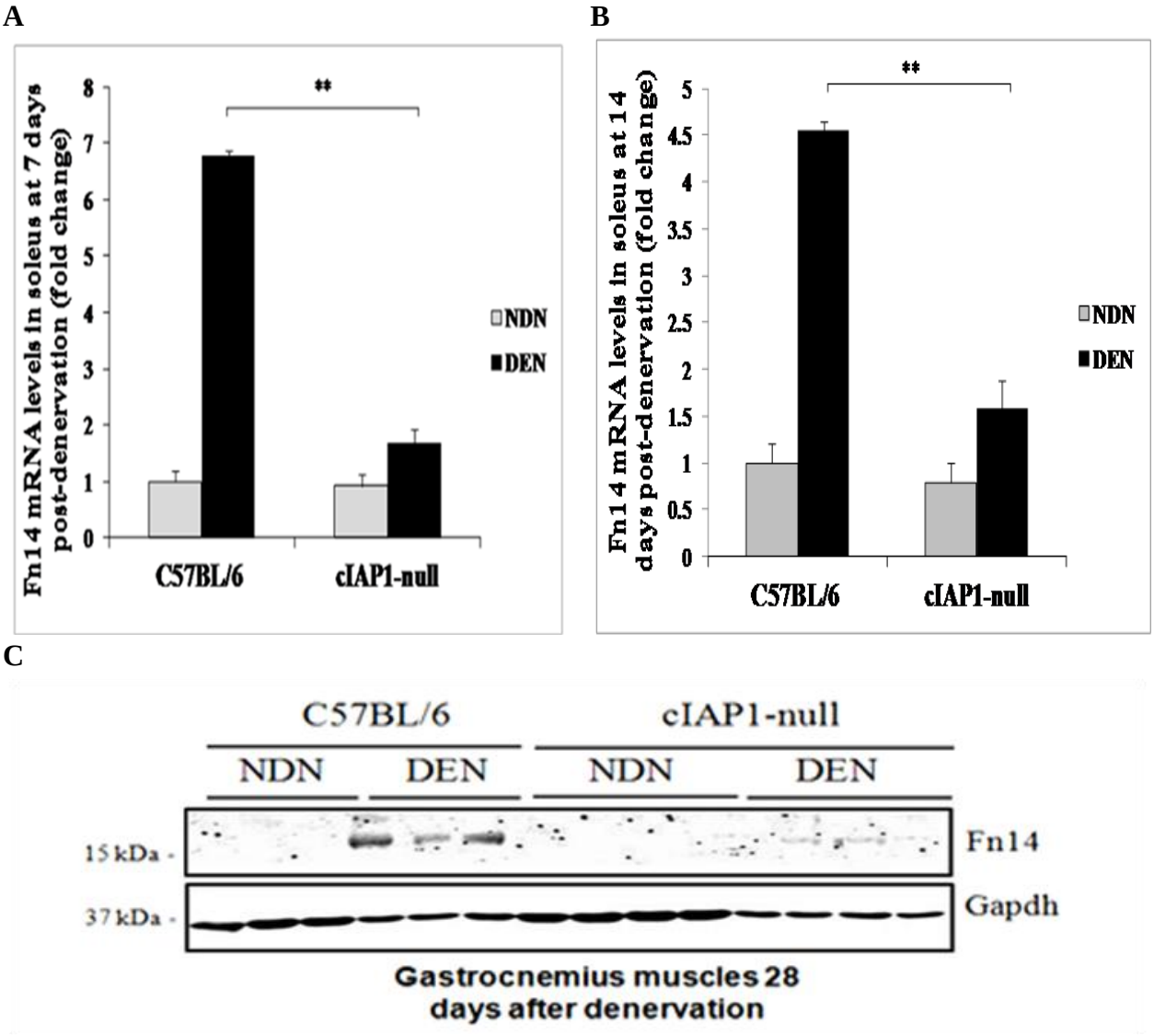

Figure 29. Fn14 mRNA upregulation is blunted in denervated cIAP1-null muscle

(**A**) Fn14 mRNA induction is inhibited in cIAP1-null soleus after 7 days of denervation. The expression of Fn14mRNA was measured in C57BL/6 and cIAP1-null denervated versus nondenervated soleus muscle (n=3) after 7 days of denervation, using quantitative real-time RT-PCR (qPCR). Error bars represent the SEM. ** indicates $p < 0.001$. **(B)**

Fn14 mRNA induction is inhibited in cIAP1-null soleus after 14 days of denervation. The expression of Fn14mRNA was measured in C57BL/6 and cIAP1-null denervated versus nondenervated soleus muscle (n=3) after 14 days of denervation using quantitative real-time RT-PCR (qPCR). Error bars represent the SEM. ** indicates $p < 0.001$. (**C**) Induction of Fn14 protein level is blunted in cIAP1-null gastrocnemius muscle after 28 days of denervation. The protein level of Fn14 was determined in C57BL/6 and cIAP1-null denervated versus nondenervated soleus muscle (n=3) using western blot methods. Error bars represent the SEM. ** indicates $p < 0.001$.

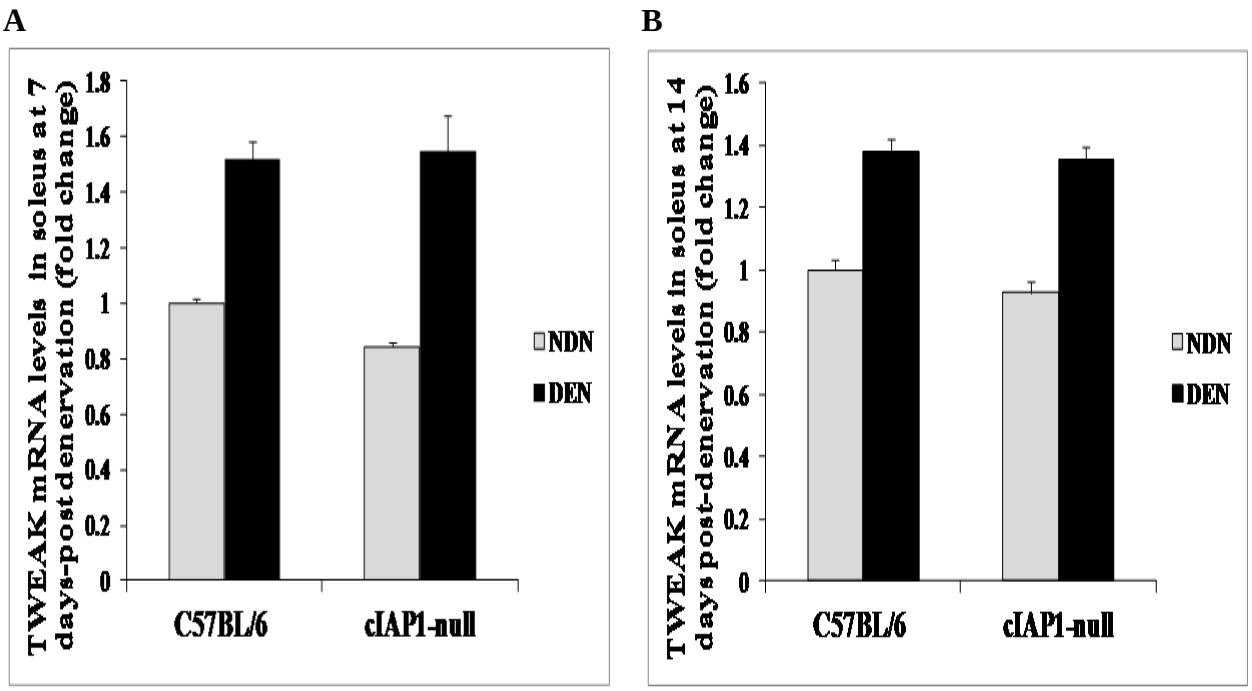

Figure 30. TWEAK mRNA level is unchanged in denervated cIAP1-null compared to C57BL/6 muscle

(**A**) TWEAK mRNA level is unchanged in denervated cIAP1-null compared to C57BL/6 soleus muscle following 7 days of denervation. The expression of TWEAK mRNA was measured in C57BL/6 and cIAP1-null denervated versus nondenervated soleus muscle (n=3) after 7 days of denervation using quantitative real-time RT-PCR (qPCR). Error bars represent the SEM. (**B**) TWEAK mRNA level is unaltered in cIAP1-null compare to C57BL/6 soleus muscle after 14 days of denervation. The expression of TWEAK mRNA was measured in C57BL/6 and cIAP1-null denervated versus nondenervated soleus muscle (n=3) after 14 days of denervation using quantitative real-time RT-PCR (qPCR). Error bars represent the SEM.

3.3.5 Genetic ablation of cIAP1 prevents TWEAK-induced myotube atrophy

As no direct correlate exists for testing denervation-induced atrophy *in vitro*, I sought to test the effects of cIAP1-deficiency in culture models of TWEAK-induced atrophy. Notably, this cytokine has recently been shown to be involved in denervation-induced atrophy *in vivo* (Mittal et al., 2010). Furthermore, the association of cIAP1 with the TWEAK receptor, Fn14, suggests that this is a logical mechanism of action to evaluate as a possible explanation for our *in vivo* results. To investigate the effect of the loss of cIAP1 on TWEAK-induced atrophy in myotube atrophy, C57Bl/6 and cIAP1-null primary myoblasts were differentiated into myotubes by incubation in reduced-serum differentiation medium for 48 hours. Differentiated primary myotubes formed from cIAP1-null myoblasts display larger diameter than their C57BL/6 counterpart (figure 31A). These myotubes were incubated with or without soluble TWEAK (100 ng/ml) for 24 hours. As shown in figure 31A and 31B, the addition of TWEAK to cultured C57BL/6 myotubes induces atrophy by significantly decreasing the mean myotube diameter, increasing MuRF1 expression and MHC degradation. These data are consistent with a previously published report from Dogra et al., 2007. In contrast, loss of cIAP1 in primary cultures protected against TWEAK-induced myotube atrophy and completely blocked TWEAK-induced MuRF1 upregulation and MHC degradation (Figure 31A, 31B and 31C).

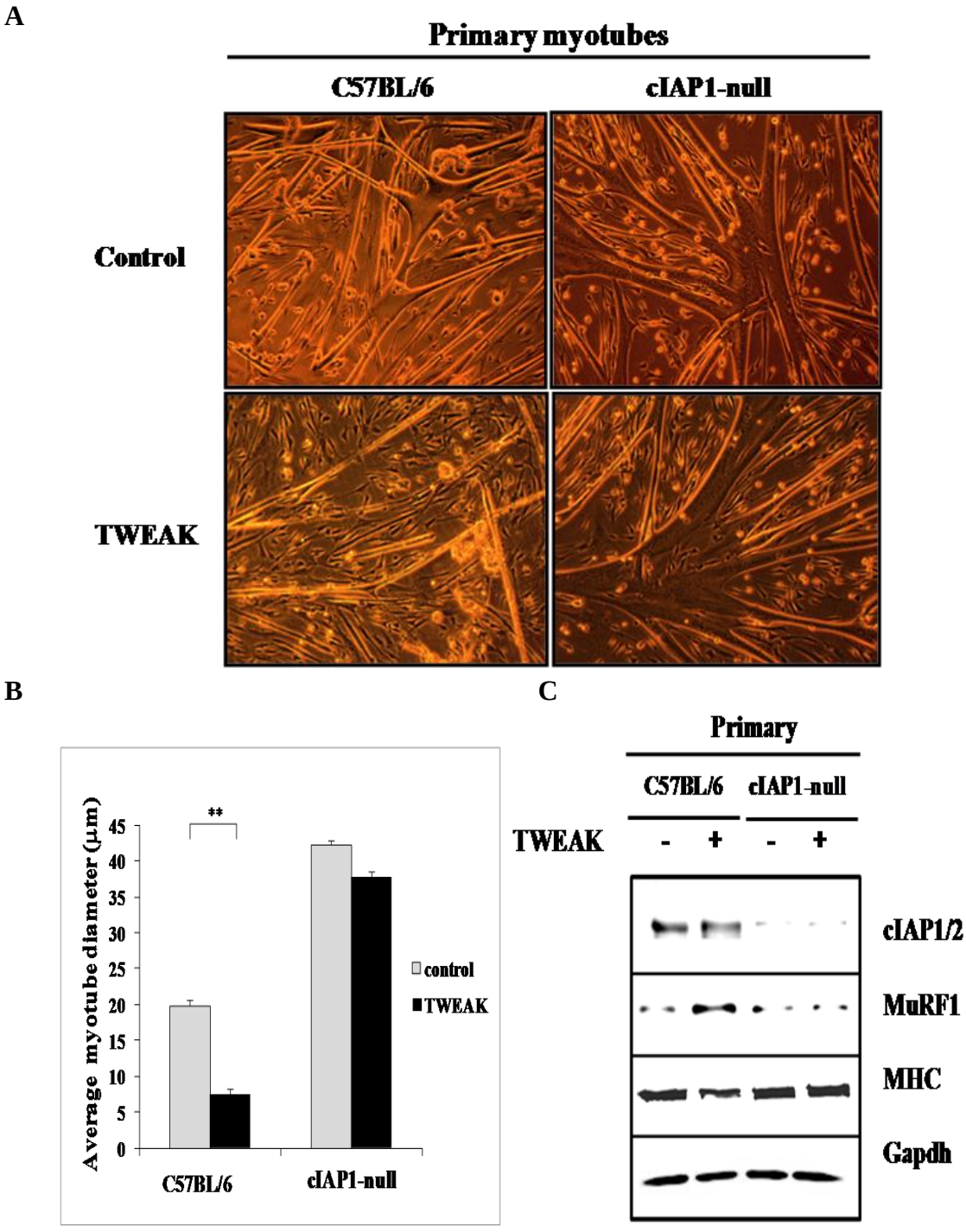

Figure 31. cIAP1-null primary myotubes resist TWEAK-induced myotube atrophy

(**A**) Loss of cIAP1 in primary culture blocks TWEAK-induced myotube atrophy. C57BL/6 and cIAP1-null primary myoblasts were differentiated into myotubes by incubation in reduced-serum differentiation medium for 48 hours. These myotubes were incubated with or without soluble TWEAK (100 ng/ml) for 24 hours. Shown are representative photomicrograph/phase contrast pictures. (**B**) Absence of cIAP1 inhibits TWEAK-mediated decrease in myotube diameter. C57BL/6 and cIAP1-null primary myoblasts were differentiated into myotubes by incubation in reduced-serum differentiation medium for 48 hours. These myotubes were incubated with or without soluble TWEAK (100 ng/ml) for 24 hours. Quantitative estimation of myotube diameter was determined using ImageJ software; diameters were measured between myotube branch points for greatest consistency. Data are mean ± standard error of three independent experiments. ** indicates significantly different with $p < 0.001$. (**C**) Loss of cIAP1 in primary culture blocks TWEAK-induced MuRF1 upregulation and MHC degradation. C57BL/6 and cIAP1-null primary myoblasts were differentiated into myotubes by incubation in reduced-serum differentiation medium for 48 hours. These myotubes were incubated with or without soluble TWEAK (100 ng/ml) for 24 hours. Equal amount of protein were analyzed by western blotting for levels of cIAP1/2, MuRF1, MHC. Gapdh was used as a loading control.

3.3.6 SMC downregulates cIAP1 and protects against TWEAK-induced myotube atrophy

To further confirm the effect of cIAP1 loss on TWEAK-induced myotube atrophy, I used the Smac mimetic compound (SMC), C57BL/6 myoblasts were differentiated in the presence of vehicle or 500 nM of SMC (a concentration that completely eliminated cIAP1 expression, see figure 32B) for 48 hours then either treated or not with 100 ng/ml of TWEAK for another 24 hours. The myotubes were washed, fixed and immunostained with MHC (red) and Hoechst (blue). The pharmacological inhibition of cIAP1 using SMC rendered myotubes larger than C57BL/6 ones, similar to the genetic knock-out of cIAP1, and made them resistant to TWEAK-induced atrophy (Figure 32A). Moreover, biochemical analyses revealed that elimination of cIAP1 using SMC blocks TWEAK-induced MuRF1 upregulation (Figure 32B). Taken together these data provide convincing evidence that the loss of cIAP1, using genetic and pharmacological means, blocks TWEAK-induced myotube atrophy *in vitro*.

3.3.7 cIAP1 overexpression in cIAP1-null myotubes restores atrophy following TWEAK treatment

To examine whether ectopic expression of cIAP1 was sufficient to overcome the resistance to TWEAK-induced myotube atrophy in the absence of cIAP1, cIAP1-null myoblasts were transfected for 24 hours with expression vectors encoding Green Fluorescent Protein GFP or 6 myc-tagged cIAP1. Differentiation was then induced by switching to low serum medium for 48 hours. Differentiated myotubes were then treated with vehicle or 100 ng/ml of soluble TWEAK for 24 hours. As expected, transfection

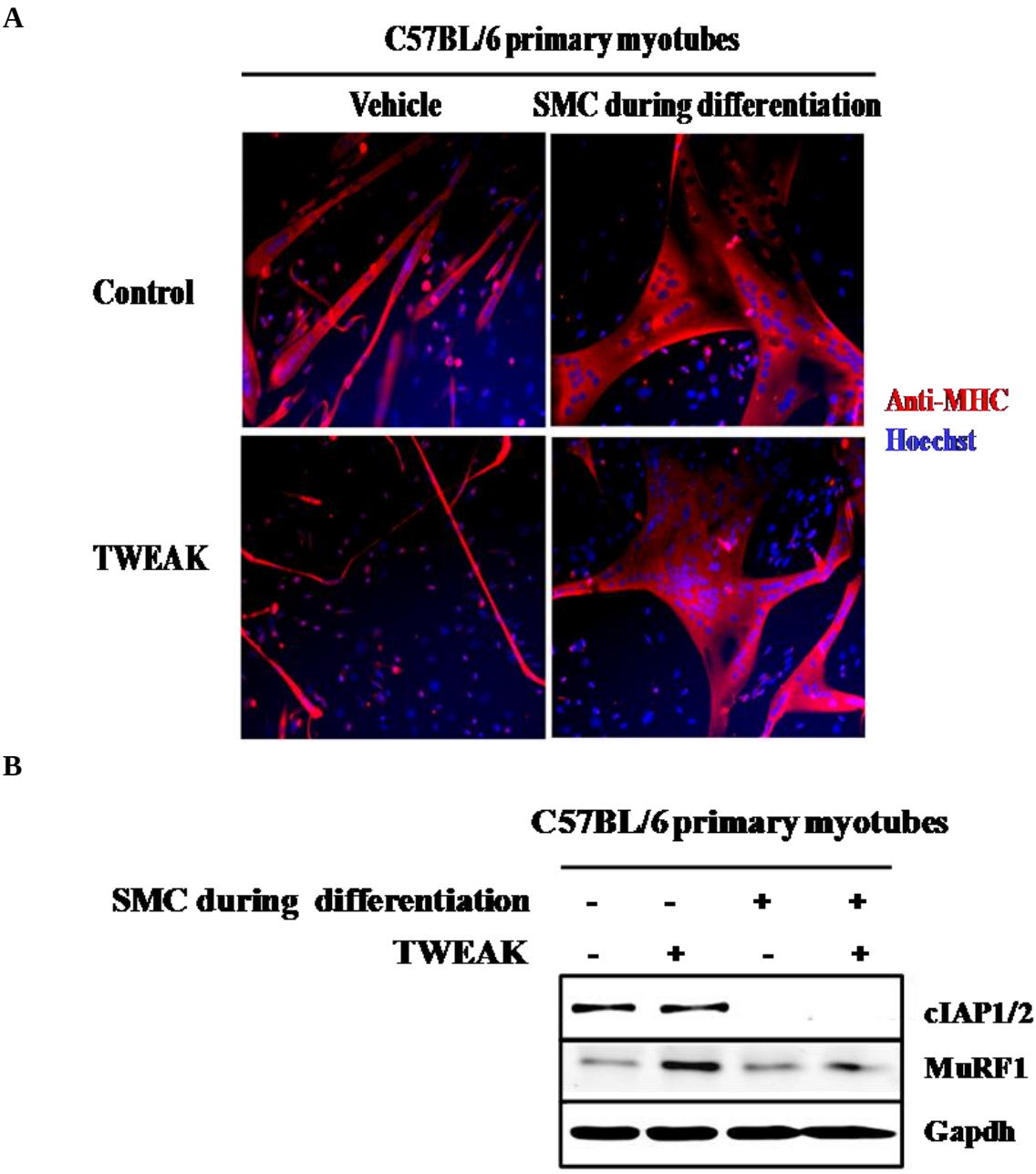

Figure 32. Pharmacologic inhibition of cIAP1 using SMC prevents TWEAK-induced myotube atrophy

(A) Downregulation of cIAP1 using SMC blocks TWEAK-induced myotube atrophy. C57BL/6 myoblasts were differentiated in the presence or not of 500 nM of SMC for 48

hours then treated with or without 100 ng/ml of TWEAK for another 24 hours. The resulting myotubes were washed, fixed, immunostained with MHC (red) and Hoechst (blue) and visualized under fluorescent microscope. (**B**) Downregulation of cIAP1 using SMC inhibits TWEAK-induced MuRF1 upregulation in primary muscle cells. C57BL/6 myoblasts were differentiated in the presence or not of 500 nM of SMC for 48 hours then treated with or without 100 ng/ml of TWEAK for another 24 hours. Protein lysates from myotubes differentiated with or without SMC then treated with or without TWEAK were analyzed by western blotting for expression of cIAP1/2, MuRF1, Gapdh was used as a loading control.

with the GFP vector in cIAP1-null muscle cells shows no effect on TWEAK-induced myotube atrophy. In contrast, cIAP1 overexpression induced myotube atrophy as well as MuRF1 induction following TWEAK treatment (Figure 33A and 33B). These data suggest that cIAP1 is a major regulator of the TWEAK-induced skeletal muscle atrophy *in vitro.*

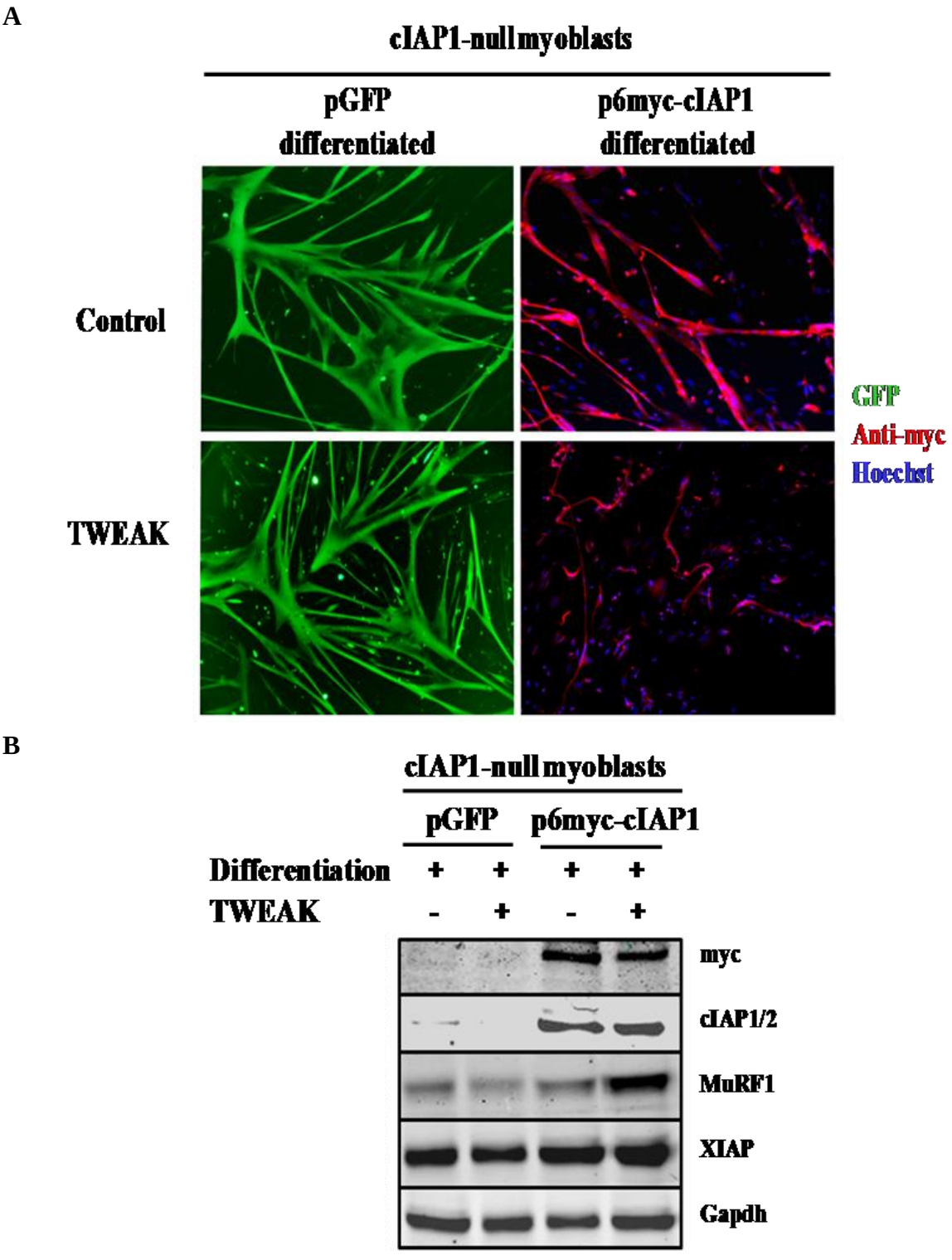

Figure 33. Ectopic expression of cIAP1 induced atrophy following TWEAK treatment in null muscle cells

(**A**) Overexpression of cIAP1 induced TWEAK-induced myotube atrophy in null muscle cells.

cIAP-null myoblasts were transfected for 24 hours with expression vectors encoding Green Fluorescent Protein GFP or 6 myc-tagged cIAP1. Differentiation was then induced by switching to low serum medium for 48 hours. Differentiated myotubes were then treated with or without 100 ng/ml of TWEAK for 24 hours. GFP-positive myotubes were visualized directly under fluorescent microscope. Cells transfected with 6 myc-tagged cIAP1 were washed, fixed and immunostained with myc (red) and Hoechst (blue) and visualized under fluorescent microscope.

(**B**) Overexpression of cIAP1 induced MuRF1 upregulation in TWEAK- treated null muscle cells. cIAP1-null myoblasts were transfected for 24 hours with expression vectors encoding Green Fluorescent Protein GFP or 6 myc-tagged cIAP1. Differentiation was then induced by switching to low serum medium for 48 hours. Differentiated myotubes were then treated with or without 100 ng/ml of TWEAK for 24 hours and protein lysates were prepared. Equal amount of protein were analyzed by western blotting for levels of myc, cIAP1/2, MuRF1, XIAP. Gapdh was used as a loading control.

Chapter 4: Discussion

Skeletal muscle atrophy is a significant clinical problem that affects nearly everyone at some point in his or her life. Atrophy is a phenomenon resulting from disuse, aging, acute and chronic diseases (Medina et al., 1995; Hornberger et al., 2001; Pereira et al., 2005; Cooper et al,, 2012). Generally, muscle atrophy is associated with increased morbidity, mortality, and poor quality of life resulting in significant increased health resource utilization and socio-economic costs (Celli 2010; IJzerman et al., 2012). With such a high prevalence in our society, a better understanding of its pathogenesis is greatly needed for the development of effective pharmacological treatments.

Although significant progress has been made to understand the molecular mechanism and/or signaling pathways leading to loss of skeletal muscle mass, upstream regulator events involved in the development of skeletal muscle atrophy remain poorly understood. Most importantly, there is still no approved drug for the treatment of skeletal muscle atrophy. Current therapies including anabolic steroids, resistance exercise, and electrical stimulation are inadequate to restore muscle mass and reverse muscle loss (Glass and Roubenoff, 2010; Smart et al., 2012; Toth et al., 2012).

Using cultured skeletal cells as experimental systems, the results presented in my thesis revealed a novel role for cIAPs in regulating NF-kB signal transduction. Given that the NF-kB pathway has been shown to be involved in several muscle diseases, including the pathogenesis of skeletal muscle atrophy (Cai et al., 2004; Hunter and Kandarian 2004; Mourkioti et al., 2006), I investigated the possibility that cIAPs have specific function in a validated model of denervation-induced skeletal muscle atrophy using novel

genetic and pharmacological means. I have focused on studying the role of cIAP1 in muscle biological or pathological context, since its paralog cIAP2 is not expressed in muscle (this result, presented in my thesis, was published in PNAS, 2008).

Interestingly, the result of my thesis demonstrate for the first time that cIAP1, an essential regulator of NF-kB signaling, is a critical mediator of skeletal muscle atrophy in response to denervation and represents a novel target for preventing atrophy. Thus, the work described in my thesis significantly advances our understanding of the molecular mechanisms involved in muscle atrophy, and opens up new avenues of investigation into the causes and treatment of muscle atrophy.

4.1 Loss of cIAP1 mediates differential expression of cIAP2

Typically, cIAP1 and cIAP2 are widely expressed, yet they are present in low abundance in the cell. Interestingly, Conze and co-workers have found that although cIAP1-null mice are both viable and fertile, they have increased cIAP2 expression. This phenomenon was observed at the protein levels and not at the mRNA levels, and has been attributed to the ability of cIAP1 to target cIAP2 for ubiquitin-mediated proteasomal degradation (Conze et al., 2005). Thus, in most cells, cIAP1 triggers the constitutive lysine-48 (K48)-ubiquitination and degradation of cIAP2 (Conze et al., 2005), which explains why cIAP2 expression is low in many cells.

Since the upregulation of cIAP2 expression was first observed in spleen and thymus isolated from cIAP1-null (Conze et al., 2005), I asked whether there might be some tissues in cIAP1-null mice in which cIAP2 expression is not increased as this would allow insight into possible tissue specific roles. In accordance to what was previously

reported (Conze et al., 2005), the result of my thesis demonstrates that in the cIAP1-null mouse, cIAP2 expression is dramatically induced in the spleen. However, cIAP2 is expressed to a much lesser extent in heart isolated from cIAP1-null mice. Thus, the induction of cIAP2 does not occur equally in all cIAP1-null tissues. Intriguingly, the result of my thesis reveals that there is very little cIAP2 expression in both soleus (slow twitch) and tibialis anterior (fast twitch) skeletal muscles, and none in the brain (also published in Mahoney et al., 2008), suggesting that cIAP1 might be critical in these tissues. In agreement with the tissue blots, my results show that cultured myoblast cells treated with siRNA targeting cIAP1 express little or no induction of cIAP2.

Collectively, these results reveal that skeletal muscle is a useful system to dissect cIAP1 functions individually, as the other highly similar cIAP (cIAP2) is not expressed in muscle and thus would not be able to compensate.

4.2 cIAP1 and cIAP2 redundantly regulate the classical NF-kB signaling upon TNFα treatment

Classical activation of NF-kB pathway is initiated by the phosphorylation-dependent ubiquitination and degradation of IkB, which in the resting state blocks a nuclear targeting sequence within NF-kB and retains it within the cytoplasm. IkB turnover allows nuclear translocation of NF-kB, whereupon target genes are transcriptionally induced. Accordingly, the result of my thesis shows a transient decline in IkB levels in wild type and cIAP1-null MEF cells treated with TNFα. Moreover, my results indicate that in wild type MEF cells treated with either cIAP1 or cIAP2 siRNA, substantial levels of the other cIAP are observed, and TNFα induces IkB degradation and

therefore mediates activation of the NF-kB. In contrast, siRNA-mediated knockdown of cIAP2 in cIAP1-null MEF cells or dual siRNA-mediated knockdown of cIAP1 and cIAP2 in MEF cells inhibits the degradation of IkB, indicating complete abrogation of the NF-kB signaling.

Phosphorylation of IkB is carried out by the IkB kinase complex (IKK), which is composed of two catalytic peptides (IKKα and IKKβ) and one regulatory subunit (IKKγ, or NEMO). In the classical NF-kB activation pathway, it is IKKβ that phosphorylates and promotes the degradation of IkB. I therefore assessed the phosphorylation of IkB and the activity of IKKβ (as evidenced by its phosphorylation), and found that, as expected, both were transiently induced after 5 minutes of TNFα treatment in wild type and cIAP1-null MEF cells. In cIAP1 and cIAP2 double null cells, no such activation was observed. Thus, in the absence of the cIAPs NF-kB activation is blocked upstream of the IKK complex.

In summary, I have used genetic knockout and siRNA-mediated knockdown methodologies to generate various versions of cIAP1 and cIAP2 double null cells and demonstrated that cIAP1 and cIAP2 are critical regulators of the classical NF-kB signal transduction and are functionally redundant in this role.

Mechanistically, upon TNFα occupancy the TNF receptor 1 (TNF-R1) recruits a signal transduction complex consisting of TNF-R1-associated DEATH domain (TRADD) as well as the receptor-interacting protein 1 (RIP1). TRADD binding in turn recruits TRAF2 and cIAP1 or cIAP2 (cIAP1/cIAP2) to form a large membrane complex. Either cIAP1 or cIAP2 can thus target RIP1 for K63-linked polyubiquitination (Dynek et al., 2010; Bertrand et al. 2008). The K63-linked chains on RIP1 serve as scaffolds for the assembly of an IKK complex consisting of TAB1, TAK1, NEMO, and IKKα,β (Wu et

al., 2006). Thus, IKKβ phosphorylates IκBα and triggers its polyubiquitination and degradation, which then enables the NF-kB dimers to translocate to the nucleus.

Interestingly, in addition to regulating TNFα-mediated classical NF-kB signaling, cIAP1 and cIAP2 have also been shown to modulate the activity of the alternative NF-kB pathway (Varfolomeev et al., 2007; Vince et al., 2007). cIAP1 and/or cIAP2 inhibit the NF-kB pathway through the alternative signaling arm that is mechanistically quite different from the classical arm. Upon induction of the alternative NF-kB signaling, NF-kB–inducing kinase (NIK), which is essential for activation of the alternative pathway, activates IKKα, and they both phosphorylate p100, leading to its partial degradation to form p52 (Senftleben et al., 2001). Subsequently, p52 forms a heterodimer with RelB, which translocates to the nucleus and activates the transcription of target genes. Interestingly, either cIAP1 or cIAP2 is capable of catalyzing the lysine 48–mediated ubiquitination of NIK, targeting it for proteasomal degradation and thus preventing the inducible processing of p100 (Zarnegar et al., 2008).

Collectively, the cIAP proteins have the capacity to either positively or negatively regulate NF-kB signaling.

4.3 Loss of cIAP1 blunts the classical NF-kB signaling pathway in muscle cells

Given the emerging role of the NF-kB signal transduction pathway in skeletal muscle biology (Mourkioti et al., 2008), and since the tissue blots have shown that cIAP2 is barely expressed in muscle, I investigated the role of cIAP1in regulating the classical NF-kB pathway in myoblasts. The result of my thesis demonstrates that unlike cIAP1-null MEFs, cIAP1-null myoblasts show greatly attenuated turnover of IkB (indicative of

NF-kB activation) in response to TNFα. In C2C12 myoblasts treated with cIAP1 targeting siRNA, IκB turnover was again attenuated and c-FLIP expression declined rapidly in response to TNFα. Loss of cIAP1 also inhibited NF-kB activation in C2C12 cells stably expressing an NF-kB responsive luciferase reporter construct

Taken together, the results of my thesis demonstrate that in skeletal myoblasts, where cIAP2 is not expressed at appreciable level, cIAP1 is required for an efficient NF-κB response to TNFα. Collectively, these data position cIAP1 as a potential candidate for therapeutic intervention for various muscle diseases that rely on NF-kB signaling, such as skeletal muscle atrophy.

4.4 Genetic ablation of cIAP1 protects skeletal muscle against fiber size reduction in response to denervation-induced skeletal muscle atrophy

To investigate the role of cIAP1 in denervation-induced muscle atrophy *in vivo*, I took advantage of our cIAP1 knockout mice and found that these mice exhibit a marked protection against denervation-induced skeletal muscle atrophy when compared to controls.

Interestingly, I found that the protection seen in the absence of cIAP1 occurred as early as seven days post denervation and was even more pronounced by fourteen and twenty height days post denervation. This varied temporal effect of cIAP1 may result from the engagement of different E3 ligases. The early protection seen in the absence of cIAP1 (at seven days post denervation) is similar to that seen in the absence MAFbx, and in contrast to MuRF1 deletion which demonstrates a delayed protective effect being evident at only fourteen days post denervation (Bodine et al., 2001). Whether the stronger

protection seen at a later stage of atrophy (day fourteen and twenty eight post denervation) is due to the loss of engagement of not only one but both if not several E3 ligases and/or other proteolytic system is still not clear.

In addition, the result of this thesis also demonstrates that fiber cross sectional area (CSA) is significantly preserved in both soleus (a predominantly slow twitch muscle) and TA (a predominantly fast twitch muscle) muscles of cIAP1-null mice compared to control mice, in response to denervation. Interestingly, the protection seen in the absence of cIAP1 is more pronounced in soleus compare to TA muscle, suggesting that the protection appear to be fiber type-specific. This could be explained by the fact that cIAP1 is differentially expressed in slow and fast muscle fibers. In fact the result of this thesis shows that basal cIAP1 expression is higher in soleus compare to TA muscle. This is not too surprising since soleus is more susceptible to atrophy than TA muscle, as seen in the result section of this study which is consistent with previously published study (Grossman et al., 1998). Taken together, my results suggest that differential cIAP1 expression may contribute to the differential level of atrophy seen in soleus and TA muscle.

In conclusion, using a novel and unique genetic tool, the cIAP1-null mouse, I have demonstrated that the whole-body loss of cIAP1 protects against denervation-induced skeletal muscle atrophy.

4.5 Genetic deletion of cIAP1 inhibits slow-to-fast fiber type transition following denervation-induced skeletal muscle atrophy

Muscle fibers of adult mouse are divided into four types: I, IIA, IIX and IIB based on the MHC isoform that is primary expressed in them (Ennion et al., 1995). Slow-twitch MHC is noted as type I, whereas fast-twitch MHC isoforms include type II fibers. Slow-twitch (MHC type I) fibers use oxidative metabolism, due to presence of a high number of mitochondria, and as a result are resistant to fatigue, are less pH sensitive, have a slower contraction/relaxation profile and are more suited for endurance-based activities. Fast-twitch (MHC type II) fibers use mainly glycolytic metabolism and demonstrate faster force-generating capacity than type I, making them more efficient for short bursts of speed but also more prone to fatigue (Pette et al., 2000; 2001). Types IIA and IIX fibers are called intermediate fibers as they have properties of slow and fast twitch fibers: they use oxidative metabolism and are rich in mitochondria (Sato et al., 2014).

Adult skeletal muscle has tremendous plasticity (Pette 2002). Protein composition in skeletal muscle changes overtime and muscle fibers have remarkable capacity to adjust their molecular, metabolic, and functional properties in response to altered functional demands, mechanical loading, or changes in neuromuscular activity (Schiaffino and Reggiani, 2011). For instance, denervation of skeletal muscle induces a fiber type switch from type I to type II fibers (Finkelstein et al., 1993; Grossman et al., 1998). The data presented in my thesis confirmed that upon denervation, a fiber type switch occurs which is characterized by a decrease in slow (type I) fiber number and a concomitant increase in fast (type II) fiber number in denervated C57BL/6 muscle, a fiber type switch as has been reported for rats (Ijkema-Paassen et al., 2005) and humans (D'Antona et al., 2003). In

contrast, in the absence of cIAP1 the transition of slow-type fibers into fast-type fibers was blunted in denervated cIAP1-null muscle, suggesting that cIAP1 favours the fast-type fiber phenotype in denervated skeletal muscle. This data is consistent with a study that was done by Mourkioti and coworkers where they used a similar model system to the one used in my thesis but with mice in which the classical NF-kB pathway was ablated in muscles. The investigators found that the suppression of classical NF-kB signaling inhibits the transition of fibers from slow-to-fast in denervated muscles (Mourkioti et al., 2006).

Interestingly, it has been reported that the peroxisome proliferator-activated receptor-gamma (PPAR-γ) coactivator 1α (PGC-1α) is a key player in preserving muscle mass and regulating skeletal muscle fiber composition, mitochondrial content, and oxidative metabolism in various catabolic conditions including denervation (Tajrishi et al., 2014; Sandri et al., 2006; Hindi et al., 2014; Sato et al., 2013). Muscle-specific PGC-1α-null mice showed a shift from slow (MHC I and IIA) fiber types to fast (IIX and IIB) muscle fibers (Handschin et al., 2007; Sato et al., 2014), whereas transgenic mice overexpressing PGC-1α in skeletal muscle have increased proportion of slow fibers expressing MHC I and IIA (Lin et al., 2002). Since PGC-1α has been shown to preserve skeletal muscle mass and regulate muscle fiber composition in response to denervation, it is thus tempting to speculate that one of the mechanisms by which cIAP1 blocks slow-to-fast fiber type transition following denervation-induced skeletal muscle atrophy is by upregulating PGC-1α.

4.6 Genetic inhibition of cIAP1 blunts the activation of the ubiquitin-proteasome system following denervation

The ubiquitin-proteasome mediated proteolysis appears to be the predominant mechanism leading to the development of skeletal muscle atrophy (Caron et al., 2011; Wang et al., 2006). In skeletal muscle undergoing atrophy, two specific E3 ubiquitin ligases, MuRF1 and MAFbx, which were identified more than a decade ago, label muscle target proteins for proteasomal degradation (Bodine et al., 2001; Gomes et al., 2001). These two ligases have been found to be highly expressed in several models of skeletal muscle atrophy including denervation (Bodine et al., 2001; Gomes et al., 2001). Furthermore, under atrophic conditions, mice null for either MuRF1 or MAFbx exhibit less atrophic phenotype as compared to control animals (Bodine et al., 2001; Gomes et al., 2001).

Consistent with a previously published study (Bodine et al, 2001; Gomes et al., 2001), the data presented in my thesis shows that the expression of both MuRF1 and MAFbx, which target muscle protein for proteasomal degradation, is stimulated in denervated skeletal muscle compared with control muscle. Moreover, my results demonstrate that in the absence of cIAP1, both MuRF1 and MAFbx fail to be upregulated in denervated muscle, suggesting that one of the mechanisms by which loss cIAP1 inhibits the degradation of muscle protein and thus confers protection against denervation-induced skeletal muscle atrophy is though blocking the upregulation of these two E3 ligases in denervated skeletal muscle.

Although the underpinning mechanisms by which depletion of cIAP1 blunts the increased expression of MuRF1 and MAFbx in denervated skeletal muscle remain

unknown, it is likely possible that cIAP1 functions through the activation of specific signaling pathways to augments the expression of muscle ligases. Because it has been consistently observed that activation of the classical NF-kB pathway leads to the upregulation of MuRF1 (but not MAFbx) expression in response to many conditions of atrophy, including denervation (Cai et al., 2004; Mourkioti et al., 2006, Li et al., 2008; Mittal et al., 2010; Paul et al., 2010; Tajrishi et al., 2014) and that p38 MAPK has been found to stimulate skeletal muscle atrophy by inducing the expression of MAFbx (Li et al., 2005), one can speculate that depletion of cIAP1 blunts the increased expression of MuRF1 and MAFbx in denervated skeletal muscle through the activation of the classical NF-kB and p38 MAPK signaling pathways, respectively.

Taken together, the present study suggests that one of the mechanisms by which depletion of cIAP1 confers protection against denervation-induced skeletal muscle atrophy is by upregulating the expression of both MuRF1 and MAFbx.

4.7 The absence of cIAP1 attenuates the expression of Fn14 under denervation conditions

The current study clearly demonstrates a previously undiscovered role of cIAP1 in skeletal muscle atrophy and indicates that mice lacking cIAP1 are greatly protected against atrophy that occurs as a consequence of denervation. However, the underpinning mechanisms behind this protection are still enigmatic. Previous reports indicate that denervation atrophy is mediated through NF-kB by TWEAK-Fn14 signaling. Given that cIAP1 regulates NF-kB signaling, I investigated the intriguing involvement of TWEAK-Fn14 into the mechanism behind this aforementioned protection.

TWEAK and its receptor Fn14, members of the TNF/TNFR superfamily, have emerged as a prominent molecular axis regulating denervation-induced skeletal muscle atrophy (Mittal et al., 2010). However, it has been demonstrated that the expression of the TWEAK receptor Fn14 is upregulated in denervated muscle (Mittal et al., 2010). In agreement with these results, the data presented in my thesis shows an increased expression of Fn14 in denervated muscle of control animal. Interestingly, in mice lacking cIAP1 the FN14 upregulation is blunted in response to denervation, suggesting that Fn14 expression is influenced by cIAP1 and that failure to upregulate Fn14 in the absence of cIAP1 may underlie the observed protective effects.

I further examined these phenomena *in vitro*, using differentiated cIAP1-null and wild type myoblasts. Treatment of myotubes with 100 ng/ml of TWEAK recapitulates many of the effects of denervation *in vivo*, including loss of muscle mass and upregulation of MuRF1 (Mittal et al., 2010). Remarkably, TWEAK fails to induce MuRF1 or reduce myotube size in cIAP1-null cells, whereas it causes the expected loss of myotube diameter in wild type cells.

Furthermore, the current study shows that TWEAK induced the upregulation of the atrophy-inducing muscle specific ubiquitin E3 ligase, MuRF1, and MHC. This result is in agreement with recent reports which indicate that MuRF1 targets thick filament proteins including MHC in skeletal muscle (Clarke et al., 2007; Cohen et al., 2009). In contrast, my data shows that in the absence of cIAP1, TWEAK fails to induce the upregulation of atrophy-inducing muscle-specific ubiquitin E3 ligase, MuRF1, resulting in the suppression of MHC degradation in cIAP1-null myotubes. Furthermore, I have found that overexpression of cIAP1 in cIAP1-null myotubes restored both MuRF1

upregulation and myotube atrophy in response to TWEAK. Taken together, these results identify cIAP1 as a critical regulator of muscle atrophy. In addition, pre-treatment of control myotubes with the SMC was able to prevent TWEAK from inducing loss of myotube diameter and MuRF1 upregulation. Collectively, the results of my thesis provide convincing evidence that loss of cIAP1, using genetic and pharmacological means, blocks TWEAK-induced myotube atrophy.

Although the result of my thesis reveals that cIAP1 upregulates the expression of the TWEAK receptor Fn14 in denervated skeletal muscle, investigating the mechanism(s) by which cIAP1 increases Fn14 expression in denervated skeletal muscle remains enigmatic. Some studies indicate that Fn14 itself may be an NF-kB target gene (Hosokawa et al., 2006; Tran et al., 2006), suggesting that a two-step feed-forward loop exists, whereby induction of atrophy using TWEAK first requires NF-kB-mediated upregulation of Fn14, and second involves Fn14-mediated upregulation of MuRF1. More recently, it has been shown that the upregulation of Fn14 expression in denervated skeletal muscle could be attributed to epigenetic mechanisms such as changes in promoter DNA methylation status (Tajrishi et al., 2015). In fact, denervation decreases DNA methylation at specific CpG sites in Fn14 promoter leading to an increased expression of Fn14 in skeletal muscle (Tajrishi et al., 2015**).** Furthermore, MAPK signaling has also been reported to regulate the levels of Fn14 in skeletal muscle on denervation (Tajrishi et al., 2015). Taken together, it is important to investigate whether cIAP1 activity increases Fn14 expression through NF-kB and MAPK signaling or through DNA hypomethylation in the Fn14 promoter.

It is interesting also to ask if cIAP1 regulates Fn14 induction of MuRF1 through NF-kB. This is important because other signaling axes may also regulate MuRF1 (Gonnella et al., 2011; Sandri et al., 2006). In fact, in addition to activating NF-kB signaling pathway, TWEAK-Fn14 system activates several other signaling pathways, such as the ERK/JNK/p38 MAP kinase axis (Vincent et al., 2009; Li et al., 2009). Since cIAP1 regulates all these modalities (Varfolomeev et al., 2012), it is essential to confirm that TWEAK upregulation of Fn14 is through the NF-kB signaling pathway.

4.8 Pharmacological inhibition of cIAP1 attenuates skeletal muscle atrophy upon denervation *in vivo*

Using an orally administered SMC, LCL161, I asked whether the systemic downregulation of cIAP1/2 can recapitulate the protection seen in the knockout animal. LCL161 is only transiently effective at cIAP1/2 downregulation in highly proliferative tissues such as the spleen, but maintains sustained knockdown of cIAP1 in skeletal muscle such as the gastrocnemius. I found that the biweekly delivery of this SMC also accorded significant protection from denervation-induced skeletal muscle atrophy. Furthermore, these results demonstrate that MuRF1 induction was blunted in denervated muscle pre-treated with SMC.

Interestingly, the data presented in my thesis shows that the protection against skeletal muscle atrophy in response to denervation seems to be more pronounced in SMC-treated animals compared with cIAP1-null mice. This led me to speculate that this effect could be due to the fact that SMC inhibit not only cIAP1, but also cIAP2. Although the result of my thesis shows that cIAP2 is not normally expressed in muscle, I have observed that

cIAP2 is upregulated in non-myogenic muscle cells during atrophy (data not shown). In order to understand whether cIAP2 plays a role in the protection against denervation-induced skeletal muscle atrophy, our lab investigated the role of cIAP2 in this process. The results showed that muscle atrophy in response to denervation is significantly attenuated in cIAP2-null mice, to an extent similar to that seen in cIAP1-null animals (unpublished data). Notably, the protection observed in wild type animals treated with an SMC may thus be mediated by multiple pathways involving muscle-extrinsic and-intrinsic cIAP activity.

4.9 Proposed mechanisms by which loss of cIAP1 confers protection against denervation-induced skeletal muscle atrophy

A consistent finding of this study was that, at multiple levels of analysis, loss of cIAP1 protects against denervation-induced skeletal muscle atrophy. I have summarized the possible mechanism of action of the role of cIAP1 in skeletal muscle atrophy in a graphical model (see figure 34). However, the protection against denervation-induced skeletal muscle atrophy observed in cIAP1-nul mice may be attributed to the convergence of several distinct and more complex mechanisms. First, the results of my thesis demonstrate that loss of cIAP1 inhibits activation of the classical NF-kB pathway in response to TNFα (published in PNAS, 2008). In addition, I have also found that depletion of cIAP1 blunts the expression of the MuRF1, and blocks the degradation of MHC in response to skeletal muscle atrophy. This is in agreement with previously published data which demonstrates that MuRF1 targets thick filament proteins including MHC in skeletal muscle (Clarke et al., 2007; Cohen et al., 2009). Furthermore, it has

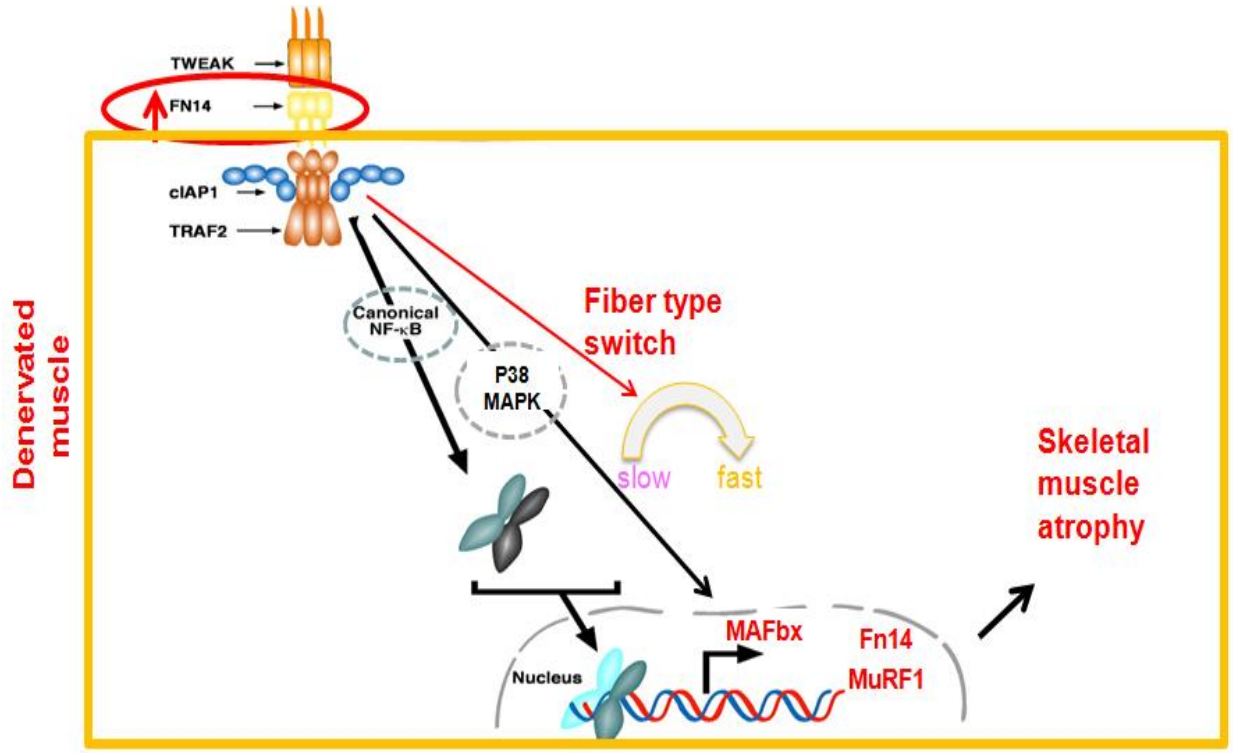

Figure 34. Graphical model illustrating the mechanisms of action of cIAP1 in skeletal muscle atrophy in response to denervation

Denervation-induced skeletal muscle atrophy augments the expression of Fn14 and cIAP1 in skeletal muscle tissues. In addition, following denervation, cIAP1 mediates the activation of NF-kB, p38MAPK signaling pathways, expression of muscle specific E3 ubiquitin ligase MuRF1 and MAFbx, and blunts the transition of slow-type fibers into fast-type fibers. The convergence of these distinct mechanisms eventually causes skeletal muscle atrophy.

been recently reported that the TWEAK receptor, Fn14,expression increases dramatically upon denervation; this allows TWEAK to activate the classical NF-kB pathway (Mittal et al., 2010). Therefore, I investigated whether cIAP1 regulates the expression of Fn14 in response to denervation-induced skeletal muscle atrophy and found that the absence of cIAP1 rescues Fn14 upregulation in denervated muscle. Collectively, these results suggest that the Fn14-cIAP1-NF-kB-MuRF1-MHC signaling cascade regulates skeletal muscle atrophy, and that depletion of cIAP1 confers a protective role against skeletal muscle atrophy by blunting this signaling cascade.

Second, our laboratory has recently found that loss of cIAP1 increases myoblast fusion, an essential step in the formation and regeneration of muscle fibers, by activating the alternative NF-kB signaling pathway (Enwere et al, 2012). These results suggest that cIAP1 depletion may also confer a protective role against denervation-induced skeletal muscle atrophy through the activation of the alternative NF-kB pathway which increases the number of myonuclei (this may outweigh any consequences of apoptosis-induced atrophy) and promotes larger muscle fibers. Interestingly, accumulating evidence also indicated that the alternative NF-kB pathway promotes the formation of oxidative muscle fibers (Bakkar et al., 2008; Bakkar et al., 2012), at least in part by the upregulation of the mitochondrial regulator PGC-1β (Arany et al., 2007; Bakkar et al., 2008; Bakkar et al., 2012, Enwere et al., 2012). It is, thus, tempting to speculate that loss of cIAP1 promotes an oxidative muscle fate which may also confer a protective role against denervation by increasing the number of slow fibers or limiting the transition from slow-to-fast fiber type, typically seen in response to denervation.

Third, in addition to the involvement of the NF-kB signaling in denervation-induced skeletal muscle atrophy, several other signaling pathways have been shown to play an important role in the atrophy, particularly MAPK which stimulates skeletal muscle atrophy by inducing the expression of MAFbx (Li et al., 2005). It has been reported that cIAP1 and cIAP2 play a key role in MAPK signaling (Bossen et al., 2006). Thus, depletion of cIAP1 seems to affect many signaling pathways to attenuate skeletal atrophy and preserve muscle size.

Fourth, it has been reported that in addition to an elevation in the rate of protein degradation by the ubiquitin proteasome pathway, denervation-induced muscle atrophy is also attributable to an increase in the incidence of programmed cell death (apoptosis). Apoptosis is an essential physiological process that maintains tissue homeostasis by eliminating damaged or dysfunctional cells. Unlike other forms of cell death in which groups of cells are eliminated, apoptosis is characterized by the targeted death of a single cell (Wyllie et al., 1980). However, skeletal muscle cells are one of three cell types in the body that contain multiple nuclei within a common cytoplasm (Allen et al., 1999). In mononucleated cells, the activation of apoptotic signaling cascades results in the fragmentation of nuclear DNA, and the death of the entire cell (Hengartner, 2000). In skeletal muscle, apoptosis does not result in the death of the cell, but rather leads to the elimination of a single myonuclei. The explanation for this phenomenon can be attributed, at least in part, to the myonuclear domain theory. This theory states that each myonuclei is responsible for a certain area of cytoplasm within a given muscle cell (Allen et al., 1999). When a myonuclei is eliminated, as a result of apoptosis, the overall volume of the cell decreases to a size that the remaining myonuclei can sustain (Allen et al.,

1999, Aravamudan et al., 2006). In response to denervation, atrophy was shown to be accompanied by a decrease in the number of muscle nuclei as a result of apoptosis (Rodrigues et al., 1995; Sui and Always, 2005). Interestingly, our laboratory has recently identified cIAP1 as a critical regulator of myoblast fusion (Enwere et al., 2012). In fact, we showed that loss of cIAP1 increases the number of myonuclei by activating the alternative NF-kB pathway (Enwere et al., 2012). These results may suggest that, following the loss of cIAP1, the pro-myogenic effects induced by the activation of the alternative NF-kB may outweigh any consequences of apoptosis-induced atrophy in response to denervation.

It has been recently reported that cIAP1-null mice were derived from ES cells of the 129 mouse strain also carry a caspase-11 mutation (Kenneth et al., 2012). Although cIAP1-null animals were extensively backcrossed into a C57BL/6 background, c-IAP1-null mice are also deficient in caspase 11 Kenneth et al., 2012; Enwere et al., 2012), as both caspase-11 and cIAP1 genes are in close proximity on chromosome 9 (Kenneth et al., 2012). Caspase 11, is usually undetectable in resting cells: once activated, it can induce a caspase-1 promoting inflammatory response (Wang et al., 1996; Kenneth et al., 2012). Inflammation plays a pivotal role in skeletal muscle wasting, especially in chronic disease states (Argilés et al., 2005). In contrast, disuse related skeletal muscle atrophy does not involve any systematic inflammatory response (Jackman and Kandarian, 2004; Mittal et al., 2010; Paul et al., 2010), suggesting that this caspase-11 mutation present in the cIAP1-null mice does not contribute to the protection observed in denervated soleus and TA muscles of these mice.

4.10 Future directions

The work presented in this thesis has impacted the skeletal muscle field and advanced our understanding of the molecular mechanisms involved in skeletal muscle atrophy. However, more work is needed to improve our understanding of the pathogenesis of muscle atrophy. Although the past few years have seen great contributions to the identification of intracellular signaling processes implicated in skeletal muscle atrophy, there is still much to be learned about this. An interesting and remaining task to be completed is to dissect the various signal transduction pathways that play a role in the atrophy process in the efforts to construct an integrated, unifying picture of the processes involved in muscle atrophy. This could allow us to generate pharmacological interventions to reverse atrophy.

In addition to mechanistic studies, investigating the role of cIAP1 in various models (i.e., cachexia, fasting and corticosteroid treatment) would be of interest to verify whether the loss of this gene protects against a broad spectrum of atrophies. Because denervation is an extreme model of muscle disuse that completely prevents contractile activity of skeletal muscle, it is possible that it is overwhelming the protective effects of the chronic contractile activity. Therefore, it is reasonable that a milder model of muscle disuse, such as hindlimb suspension, would provide more insight into the protective effects of chronic contractile activity.

Nevertheless, the present study provides strong evidence that cIAP1 is central regulator of skeletal muscle atrophy in response to denervation and open up new avenues to investigate potential therapeutic interventions for the treatment of muscle atrophy diseases in humans.

References

Allen DL, Roy RR and Edgerton VR. (1999). Myonuclear domains in muscle adaptation and disease. Muscle Nerve 22: 1350-1360.

Angione, A. R., Jiang, C., Pan, D., Wang, Y. X., & Kuang, S. (2011). PPARδ regulates satellite cell proliferation and skeletal muscle regeneration. Skeletal muscle, 1 (1), 33.

Annabelle, C., & Sonia, H. (2011). The proteasome inhibitor MG132 reduces immobilization-induced skeletal muscle atrophy in mice. Bmc Musculoskeletal Disorders, 12.

Arany, Z., Lebrasseur, N., Morris, C., Smith, E., Yang, W., Ma, Y., Chin, S. and Spiegelman, B.M. (2007). The transcriptional coactivator PGC-1beta drives the formation of oxidative type IIX fibers in skeletal muscle. Cell Metab., 5, 35-46.

Aravamudan B, Mantilla CB, Zhan WZ and Sieck GC. (2006). Denervation effects on myonuclear domain size o f rat diaphragm fibers. J Appl Physiol 100: 1617-1622.

Argilés, J.M., S. Busquets, and F.J. López-Soriano. (2005). The pivotal role of cytokines in muscle wasting during cancer. Int. J. Biochem. Cell Biol.37:2036-2046.

Ashkenazi, A. and V. M. Dixit (1998). Death receptors: signaling and modulation. Science 281(5381): 1305-1308.

Ashkenazi, A., Dixit, VM. (1999). Apoptosis control by death and decoy receptors.Current Opinion Cell Biology; 11:255-60.

Bai, L., & Wang, S. (2014). Targeting apoptosis pathways for new cancer therapeutics. Annu Rev Med 65 (20.21-20.17).

Bai, L., Smith D., Wang S. (2014). Small-molecule SMAC mimetics as new cancer therapeutics. Pharmacology & Therapeutics 144 (2014) 82-95.

Bakkar, N., Ladner, K., Canan, B.D., Liyanarachchi, S., Bal, N.C., Pant, M., Periasamy, M., Li, Q., Janssen, P.M. and Guttridge, D.C. (2012). IKKalpha and alternative NF-kappaB regulate PGC-1beta to promote oxidative muscle metabolism. J. Cell Biol., 196, 497-511.

Bakkar, N., Wang, J., Ladner, K.J., Wang, H., Dahlman, J.M., Carathers, M., Acharyya, S., Rudnicki, M.A., Hollenbach, A.D. and Guttridge, D.C. (2008). IKK/NF-kappaB regulates skeletal myogenesis via a signaling switch to inhibit differentiation and promote mitochondrial biogenesis. J. Cell Biol., 180, 787-802.

Bertrand M. J., S. Milutinovic, K. M. Dickson, W. C. Ho, A. Boudreault, J. Durkin, J. W. Gillard, J. B. Jaquith, S. J. Morris, P. A. Barker (2008). cIAP1 and cIAP2 facilitate cancer cell survival by functioning as E3 ligases that promote RIP1 ubiquitination. Mol. Cell 30, 689-700.

Bertrand MJ, Milutinovic S, Dickson KM, Ho WC, Boudreault A, Durkin J et al. (2008). cIAP1 and cIAP2 facilitate cancer cell survival by functioning as E3 ligases that promote RIP1 ubiquitination. Mol Cell 30: 689-700.

Bhatnagar S, Mittal A, Gupta SK, Kumar A. (2012) . TWEAK causes myotube atrophy through coordinated activation of ubiquitin-proteasome system, autophagy, and caspases. J Cell Physiol 227(3):1042-51.

Bhatnagar S. and Kumar A., (2012). The TWEAK-Fn14 System: Breaking the Silence of Cytokine-Induced Skeletal Muscle Wasting. Current Molecular Medicine, 12, 3-13.

Bigard AX, Boehm E, Veksler V, Mateo P, Anflous K, Ventura-Clapier R. (1998). Muscle unloading induces slow to fast transitions in myofibrillar but not mitochondrial properties. Relevance to skeletal muscle abnormalities in heart failure. J Physiol, 548: 649-661.

Blackwell, K., Zhang, L., Workman, L. M., Ting, A. T., Iwai, K., & Habelhah, H. (2013). Two coordinated mechanisms underlie tumor necrosis factor alpha-induced

immediate and delayed IkB kinase activation. Molecular and Cellular Biology, 33, 1901-1915.

Blankenship, J. W. et al. (2009). Ubiquitin binding modulates IAP antagonist-stimulated proteasomal degradation of c-IAP1 and c-IAP2. Biochem. J. 417, 149-160.

Bloomfield, S.A. (1997). Changes in musculoskeletal structure and function with prolonged bed rest. Med Sci Sports Exerc 29: 197-206.

Bodine S., Baehr L. (2014). Skeletal muscle atrophy and the E3 ubiquitin ligases MuRF1and MAFbx/atrogin-1. Am J Physiol Endocrinol Metab 307: E469-E484.

Bodine S.C., Latres E., Baumhueter S., Lai V.K., Nunez L., Clarke B.A., Poueymirou W.T., Panaro F.J., Na E., Dharmarajan K., Pan Z.Q., Valenzuela D.M., DeChiara T.M., Stitt T.N., Yancopoulos G.D., and Glass D.J. (2001). Identification of ubiquitin ligases required for skeletal muscle atrophy. Science. 294 (5547):1704-1708.

Bodine, S. C., Stitt, T. N., Gonzalez, M., Kline, W. O., Stover, G. L., & Bauerlein, R., et al. (2001). Akt/mTOR pathway is a crucial regulator of skeletal muscle hypertrophy and can prevent muscle atrophy in vivo. Nat Cell Biol, 3(11), 1014-1019.

Bonizzi, G., Bebien, M., Otero, D.C., Johnson-Vroom, K.E., Cao, Y., Vu, D., Jegga, A.G., Aronow, B.J., Ghosh, G., Rickert, R.C. et al. (2004). Activation of

IKKalpha target genes depends on recognition of specific kappaB binding sites by RelB:p52 dimers. EMBO J., 23, 4202-4210.

Bonizzi, G., Karin, M. (2004). The two NF-kB activation pathways and their role in innate and adaptive immunity. Trends Immunol 25: 280-288.

Boonyarom, O., and K. Inui. (2006). Atrophy and hypertrophy of skeletal muscles: structural and functional aspects. Acta Physiol (Oxf) 188: 77-89.

Bossen C, Ingold K, Tardivel A, Bodmer JL, Gaide O, Hertig S, et al. (2006). Interactions of tumor necrosis factor (TNF) and TNF receptor family members in the mouse and human. J Biol Chem 281(20):13964-71.

Bottinelli, R., M. Canepari, M.A. Pellegrino and C. Reggiani. (1996). Force-velocity properties of human skeletal muscle fibres: myosin heavy chain isoform and temperature dependence. J Physiol 495 (Pt 2): 573-586.

Brown SA, Richards CM, Hanscom HN et al. (2003). The Fn14 cytoplasmic tail binds tumour-necrosis-factor-receptor-associated factors 1, 2, 3 and 5 and mediates nuclear factor-kappaB activation. Biochem J, 371: 395-403.

Burkly LC, Dohi T. (2011). The TWEAK/Fn14 pathway in tissue remodeling: for better or for worse. Adv Exp Med Biol, 691: 305-322.

Cao, P. R., Kim, H. J., & Lecker, S. H. (2005). Ubiquitin–protein ligases in muscle wasting. Int J Biochem Cell Biol, 37(10), 2088-2097.

Cai, D., Frantz, J. D., Tawa, N. E., Jr., Melendez, P. A., Oh, B. C., Lidov, H. G., Hasselgren, P. O., Frontera, W. R., Lee, J., Glass, D. J., and Shoelson, S. E. (2004). IKKbeta/NF-kappaB activation causes severe muscle wasting in mice. Cell 119(2), 285-298.

Caron, A. Z., Haroun, S., Leblanc, E., Trensz, F., Guindi, C., & Amrani, A., et al. (2011). The proteasome inhibitor MG132 reduces immobilization-induced skeletal muscle atrophy in mice. BMC Musculoskelet Disord, 12, 185.

Celli, B. R. (2010). Predictors of mortality in COPD. Respir Med, 104(6), 773-779.

Centner T, Yano J, Kimura E, McElhinny AS, Pelin K, Witt CC, et al. (2001). Identification of muscle specific ring finger proteins as potential regulators of the titin kinase domain. J Mol Biol.;306:717-26.

Chai J, Du C, Wu JW, Kyin S, Wang X, Shi Y (2000). Structural and biochemical basis of apoptotic activation by Smac/DIABLO. Nature 406:855-862.

Chang, L., Kamata, H., Solinas, G., Luo, J. L., Maeda, S., Venuprasad, K., Liu, Y. C., and Karin, M. (2006). The E3 ubiquitin ligase itch couples JNK activation to TNFalpha-induced cell death by inducing c-FLIP(L) turnover Cell 124:601-613.

Chen D., Huerta S., Smac mimetics as new cancer therapeutics. (2009). Anti-Cancer Drugs, 20: 646-658.

Cheung, H., Mahoney, D., LaCasse, E., Korneluk, R. (2009). Down-regulation of c-FLIP Enhances Death of Cancer Cells by Smac Mimetic Compound. Cancer Res, 69, 7729-38.

Chicheportiche, Y., Bourdon, P.R., Xu, H., Hsu, Y.M., Scott, H., Hession, C., Garcia, I. and Browning, J.L. (1997). TWEAK, a new secreted ligand in the tumor necrosis factor family that weakly induces apoptosis. J Biol Chem, 272, 32401-32410.

Choi, Y. E. et al. (2009). The E3 ubiquitin ligase cIAP1 binds and ubiquitinates caspase-3 and -7 via unique mechanisms at distinct steps in their processing. J. Biol. Chem. 284, 12772-12782.

Chopard A, Hillock S, Jasmin B, (2009). Molecular events and signaling pathways involved in skeletal muscle disuse-induced atrophy and the impact of countermeasures. J. Cell. Mol. Vol 13, No. 9B, 3032-3050.

Clarke, B. A., Drujan, D., Willis, M. S., Murphy, L. O., Corpina, R. A., Burova, E., Rakhilin, S. V., Stitt, T. N., Patterson, C., Latres, E. et al. (2007). The E3 Ligase MuRF1 degrades myosin heavy chain protein in dexamethasone-treated skeletal muscle. Cell Metab. 6, 376-385.

Cohen S ,Braul JJ, Gygi SP, Glass DJ, Valenzuela DM, Gartner C, et al. (2009). During muscle atrophy, thick, but not thin ,filament components are degraded by MuRF1-dependen tubiquitylation. J CellBiol 185(6):1083-95.

Cohen, S., Brault, J. J., Gygi, S. P., Glass, D. J., Valenzuela, D. M., Gartner, C., Latres, E. and Goldberg, A. L. (2009). During muscle atrophy, thick, but not thin, filament components are degraded by MuRF1-dependent ubiquitylation. J. Cell Biol. 185, 1083-1095.

Conze, D. B., Albert, L., Ferrick, D. A., Goeddel, D. V., Yeh, W. C., Mak, T., and Ashwell, J. D. (2005). Mol. Cell. Biol. 25(8), 3348-3356.

Cooper, C., Dere, W., Evans, W., Kanis, J. A., Rizzoli, R., & Sayer, A. A., et al. (2012). Frailty and sarcopenia: definitions and outcome parameters. Osteoporos Int, 23(7): 1839-48.

Csibi, A., Cornille, K., Leibovitch, M. P., Poupon, A., Tintignac, L. A., Sanchez, A. M. and Leibovitch, S. A. (2010). The translation regulatory subunit eIF3f controls the

kinase-dependent mTOR signaling required for muscle differentiation and hypertrophy in mouse. PLoS ONE 5, e8994.

D'Antona, G., et al. (2003). The effect of ageing and immobilization on structure and function of human skeletal muscle fibres. J. Physiol. 552:499-511.

De Almagro MC, Vucic D. (2012). The inhibitor of apoptosis (IAP) proteins are critical regulators of signaling pathways and targets for anti-cancer therapy. Exp Oncol. Oct;34(3):200-11.

Deveraux, Q.L, Reed, J.C. (1999). IAP family proteins-suppressors of apoptosis. Genes and development. 13: 239-52.

Dogra C, Changotra H, Wedhas N, Qin X, Wergedal JE, Kumar A . (2007). TNF related weak inducer of apoptosis (TWEAK) is a potent skeletal muscle-wasting cytokine. FASEBJ 21(8):1857-69.

Dogra C, Hall SL, Wedhas N, Linkhart TA, Kumar A. (2007). Fibroblast growth factor inducible 14 (Fn14) is required for the expression of myogenic regulatory factors and differentiation of myoblasts into myotubes. Evidence for TWEAK-independent functions of Fn14 during myogenesis. J Biol Chem; 282: 15000-10.

Du C, Fang M, Li Y, Li L, Wang X (2000). Smac, a mitochondrial protein that promotes cytochrome c-dependent caspase activation by eliminating IAP inhibition. Cell 102: 33-42.

Dynek JN, Goncharov T, Dueber EC, Fedorova AV, Izrael-Tomasevic A, Phu L, et al. (2010). c-IAP1 and UbcH5 promote K11-linked polyubiquitination of RIP1 in TNF signalling. EMBO J 29(24):4198-209.

Dynek, J. N. et al. (2010). c-IAP1 and UbcH5 promote K11-linked polyubiquitination of RIP1 in TNF signalling. EMBO J. 29, 4198-4209.

Dynek, J., & Vuvic, D. (2013). Antagonists of IAP proteins as cancer therapeutics. Cancer Lett; 332: 206-214.

Eckelman, B. P., Salvesen, G. S. (2006) The human anti-apoptotic proteins cIAP1 and cIAP2 bind but do not inhibit caspases, J. Biol. Chem., 281, 3254-60.

Edgerton, V.R., R.R. Roy, D.L. Allen and R.J. Monti. (2002). Adaptations in skeletal muscle disuse or decreased-use atrophy. American Journal of Physical Medicine and Rehabilitation 81: S127-147.

Egerman MA, Glass DJ. (2014). Signaling pathways controlling skeletal muscle mass. Crit Rev Biochem Mol Biol. 2014 Jan-Feb;49(1):59-68.

Ennion S, Sant'ana Pereira J, Sargeant A J,Young A, Goldspink G. (1995). Characterization of human skeletal muscle fibres according to the myosin heavy chains they express. J MuscleResCellMotil 16(1):35-43.

Enwere E K, Boudreault L, Holbrook J, Timusk K, Earl N, LaCasse E, Renaud J-M and Korneluk R G. (2012). Loss of cIAP1 attenuates soleus muscle pathology and improves diaphragm function in mdx mice. Human Molecular Genetics, 1-12.

Enwere E K, Lacasse E C, Adam N J, Korneluk R G. (2014). Role of the TWEAK-Fn14-cIAP1-NF-kappaB signaling axis in the regulation of myogenesis and muscle homeostasis. Front Immunol 5: 34.

EnwereEK, HolbrookJ, Lejmi-Mrad R, Vineham J, Timusk K, Sivaraj B, Isaac M, Uehling D, Al-awar R, LaCasseE, Korneluk R G. (2012). TWEAK and cIAP1 regulate myoblast fusion through the noncanonical NF-kappaB signaling pathway. Sci Signal 5: ra75.

Fadeel, B., B. Gleiss, K. Hogstrand, J. Chandra, T. Wiedmer, P. J. Sims, J. I. Henter, S. Orrenius and A. Samali (1999). Phosphatidylserine exposure during apoptosis is a cell-type-specific event and does not correlate with plasma membrane phospholipid scramblase expression. Biochem. Biophys. Res. Commun. 266(2): 504-511.

Falempin, M., T. Leclercq, D. Leterme and Y. Mounier. (1990). Time-course of soleus muscle change in and-recovery from disuse atrophy. Physiologist 33: S88-89.

Fielitz, J., Kim, M. S., Shelton, J. M., Latif, S., Spencer, J. A., Glass, D. J., Richardson, J. A., Bassel-Duby, R. and Olson, E. N. (2007). Myosin accumulation and striated muscle myopathy result from the loss of muscle RING finger 1 and 3. J. Clin. Invest. 117, 2486-2495.

Finkelstein, D. I., Dooley, P. C., & Luff, A. R. (1993). Recovery of muscle after different periods of denervation and treatments. Muscle Nerve, 16(7), 769-777.

Flygare, J., Fairbrother, W. (2010). Small-molecule Pan-Iap Antagonists: A Patent Review. Expert Opin Ther Pat, 20, 251-67.

Foletta VC, White LJ, Larsen AE, Léger B, Russell AP. (2011). The role and regulation of MAFbx/atrogin-1 and MuRF1in skeletal muscle atrophy. Eur J Physiol 461:325–335.

Fulda S. (2008). Targeting inhibitor of apoptosis proteins (IAPs) for cancer therapy,Anticancer Agents Med. Chem, 8, 533-9.

Fulda, S., & Vucic, D. (2012). Targeting IAP proteins for therapeutic intervention in cancer. Nat Rev Drug Discov 11(2), 109-124.

Gao, Z., Tian, Y., Wang, J., Yin, Q., Wu, H., Li, Y. M., et al. (2007). A dimeric Smac/Diablo peptide directly relieves caspase-3 inhibition by XIAP. Dynamic and cooperative regulation of XIAP by Smac/Diablo. The Journal of Biological Chemistry, 282, 30718-30727.

Geserick, P., Hupe, M., Moulin, M., Wong, W.W., Feoktistova, M., Kellert, B., Gollnick, H., Silke, J. and Leverkus, M. (2009). Cellular IAPs inhibit a cryptic CD95-induced cell death by limiting RIP1 kinase recruitment. J Cell Biol, 187, 1037-1054.

Glass, D. J. (2010). Signaling pathways perturbing muscle mass. Curr Opin Clin Nutr Metab Care, 13(3), 225-229.

Glass, D., & Roubenoff, R. (2010). Recent advances in the biology and therapy of muscle wasting. Ann N Y Acad Sci, 1211(1), 25-36.

Glickman MH, Ciechanover A. (2002). The ubiquitin-proteasome proteolytic pathway: destruction for the sake of construction. Physiol Rev.82:373-428.

Goldberg A.L. (1969). Protein Turnover in Skeletal Muscle: Effects of Denervation and Cortisone on Protein Catabolism in Skeletal Muscle. The Journal of Biological Chemistry. 244: 3223-3229.

Goldberg AL (1969). Protein turnover in skeletal muscle. II. Effects of denervation and cortisone on protein catabolism in skeletal muscle. J Biol Chem 244:3223-3229.

Goll, D. E., Neti, G., Mares, S. W., & Thompson, V. F. (2007). Myofibrillar protein turnover: The proteasome and the calpains. J Anim Sci, 86(No 14,Sup 2008), E19-E35.

Gomes MD, Lecker SH, Jagoe RT, Navon A, Goldberg AL. (2001). Atrogin-1, a muscle-specific F-box protein highly expressed during muscle atrophy. Proc Natl Acad Sci USA 98: 14440-45.

Gonnella P, Alamdari N, Tizio S, Aversa Z, Petkova V, Hasselgren PO. (2011). C/EBPbeta regulates dexamethasone-induced muscle cell atrophy and expression of atrogin-1 and MuRF1. J Cell Biochem Jul; 112(7): 1737-1748.

Grossman EJ, Roy RR, Talmadge RJ, Zhong H, Edgerton VR. (1998). Effects of inactivity on myosin heavy chain composition and size of rat soleus fibers. Muscle Nerve. 21:375-89.

Guttridge, D. C., Mayo, M. W., Madrid, L. V., Wang, C. Y., and Baldwin, A. S., Jr. (2000). Science 289(5488), 2363-2366.

Gyrd-Hansen, M., Meier, P. (2010). IAPs: from caspase inhibitors to modulators of NF-kB, inflammation and cancer. Nature Reviews: Cancer 16 , 561-574.

Hacker H. and Karin M., (2006). Regulation and function of IKK and IKK-related kinases. Sci STKE. (357):re13.

Han S, Yoon K, Lee K, et al. (2003). TNF-related weak inducer of apoptosis receptor, a TNF receptor superfamily member, activates NF-kappa B through TNF receptor-associated factors. Biochem Biophys Res Commun. 305: 789-96.

Hansen, M. J., Gualano, R. C., Bozinovski, S., Vlahos, R., & Anderson, G. P. (2006). Therapeutic prospects to treat skeletal muscle wasting in COPD (chronic obstructive lung disease). Pharmacol Ther, 109(1-2), 162-172.

Harridge, S.D., R. Bottinelli, M. Canepari, M.A. Pellegrino, C. Reggiani, M. Esbjornsson and B. Saltin. (1996). Whole-muscle and single-fibre contractile properties and myosin heavy chain isoforms in humans. Pflugers Arch 432: 913-920.

Hayden, M.S. and S. Ghosh, (2008). Shared principles in NF-kappaB signaling. Cell,

He JQ, Saha SK, Kang JR, et al. (2007). Specificity of TRAF3 in its negative regulation of the noncanonical NF-kappa B pathway. J Biol Chem 282: 3688-94.

Hengartner MO. The biochemistry of apoptosis. Nature 407: 770-776, (2000).

Hershko, A. and Ciechanover, A. The ubiquitin system. Annu Rev Biochem, 67: 425-479, 1998.

Holcik M, Lefebvre CA, Hicks K, KornelukRG (2002). Cloning and characterization of the rat homologues of the Inhibitor of Apoptosis protein 1, 2, and 3 genes. BMC Genomics 3:5.

Hornberger, T. A., Hunter, R. B., Kandarian, S. C., & Esser, K. A. (2001). Regulation of translation factors during hindlimb unloading and denervation of skeletal muscle in rats. Am J Physiol Cell Physiol, 281(1), C179-C187.

Hornberger, T. A., Hunter, R. B., Kandarian, S. C., & Esser, K. A. (2001). Regulation of translation factors during hindlimb unloading and denervation of skeletal muscle in rats. Am J Physiol Cell Physiol, 281(1), C179-C187.

Hosokawa Y, Hosokawa I, Ozaki K, Nakae H, Matsuo T. (2006). Proinflammatory effects of tumour necrosis factor-like weak inducer of apoptosis (TWEAK) on human gingival fibroblasts. Clin Exp Immunol Dec; 146(3): 540-549.

Hsu, H., J. Xiong and D. V. Goeddel (1995). The TNF receptor 1-associated protein TRADD signals cell death and NF-kappa B activation. Cell 81(4): 495-504.

Hunter RB, Kandarian SC. (2004). Disruption of either the Nfkb1 or the Bcl3 gene inhibits skeletal muscle atrophy. J Clin Invest. 114:1504-1511.

Hunter RB, Stevenson E, Koncarevic A, Mitchell-Felton H, Essig DA, Kandarian SC. (2002). Activation of an alternative NF-kappaB pathway in skeletal muscle during disuse atrophy. FASEB J. 16:529-538.

Hunter, A.M., LaCasse, E.C. and Korneluk, R.G. (2007). The inhibitors of apoptosis (IAPs) as cancer targets. Apoptosis, 12, 1543-1568.

Ijkema-Paassen, J., Meek, M.F., and Gramsbergen, A. (2005). Long-term reinnervation effects after sciatic nerve lesions in adult rats. Ann. Anat.187:113-120.

Ijzerman, T. H., Schaper, N. C., Melai, T., Meijer, K., Willems, P. J. B., & Savelberg, H. H. C. M., et al. (2012). Lower extremity muscle strength is reduced in people with type 2 diabetes, with and without polyneuropathy, and is associated with impaired mobility and reduced quality of life. Diabetes Res Clin Pract, 95(3), 345-351.

Ikeda, F., Crosetto, N. & Dikic, I. (2010). What determines the specificity and outcomes of ubiquitin signaling? Cell 143, 677-681.

Jackman, R.W. and Kandarian, S.C. (2004). The molecular basis of skeletal muscle atrophy. American journal of physiology. Cell physiology, 287, C834-843.

Johansen, K. L., Shubert, T., Doyle, J., Soher, B., Sakkas, G. K., & Kent-Braun, J. A., et al. (2003). Muscle atrophy in patients receiving hemodialysis: effects on muscle strength, muscle quality, and physical function. Kidney Int, 63(1), 291-297.

Judge AR, Koncarevic A, Hunter RB, Liou HC, Jackman RW, Kandarian SC. (2007). Role for IkappaBalpha, but not c-Rel, in skeletal muscle atrophy. Am J Physiol Cell Physiol. 292(1):C372-382.

Kandarian, S. C., & Jackman, R. W. (2006). Intracellular signaling during skeletal muscle atrophy. Muscle Nerve, 33(2), 155-165.

Kandarian, S.C., and E.J. Stevenson. (2002). Molecular events in skeletal muscle during disuse atrophy. Exerc Sport Sci Rev 30: 111-116.

Kasper, C.E., L.A. Talbot and J.M. Gaines. (2002). Skeletal muscle damage and recovery. AACN Clinical Issues 13: 237-247.

Kenneth N S, Younger J M, Hughes E D, Marcotte D, Barker P A, Saunders T L and Duckett C S. (2012). An inactivating caspase 11 passenger mutation originating from the 129 murine strain in mice targeted for c-IAP1. Biochem. J. 443, 355-359.

Kerr JF, Wyllie AH and Currie AR. (1972). Apoptosis: a basic biological phenomenon with wide-ranging implications in tissue kinetics. B r J Cancer 26: 239-257,

Kravtsova-Ivantsiv Y, Ciechanover A. (2012). Non-canonical ubiquitin-based signals for proteasomal degradation. J Cell Sci 125: 539-548.

Kumar, S. (1999). Mechanisms mediating caspase activation in cell death. Cell Death Differentiation. 6: 1060-1066.

LaCasse E, Mahoney D, Cheung H, Plenchette S, Baird S and Korneluk R (2008). IAP-targeted therapies for cancer Oncogene, 27, 6252-6275.

Li Y P, Chen Y, John J, Moylan J, Jin B, Mann D L, Reid M. (2005). TNF-α acts via p38 MAPK to stimulate expression of the ubiquitin ligase atrogin1/MAFbx in skeletal muscle. FASEB Journal 19: 362-370.

Li, J., and Yuan, J. (2008). Caspases in apoptosis and beyond, Oncogene, 27, 6194–206.

Li, L., Thomas, R. M., Suzuki, H., De Brabander, J. K., Wang, X., & Harran, P. G. (2004). A small molecule Smac mimic otentiates TRAIL- and TNFa-mediated cell death. Science, 305, 1471–1474.

Li, Y.P., Schwartz, R.J., Waddell, I.D., Holloway, B.R. and Reid, M.B. (1998). Skeletal muscle myocytes undergo protein loss and reactive oxygen-mediated NF-kappaB activation in response to tumor necrosis factor alpha. The FASEB journal : official publication of the Federation of American Societies for Experimental Biology, 12, 871-880.

Lin J, Wu H, Tarr PT, Zhang CY, Wu Z, Boss O, et al. (2002).Transcriptional co-activator PGC-1 alpha drives the formation of slow-twitch muscle fibres. Nature 418:797–801.

Liston P., Roy N., Tamai K., Lefebvre C., Baird S., Cherton-Horvat G., Farahani R., McLean M., Ikeda J. E., MacKenzie A., Korneluk R. G., (1996). Suppression of apoptosis in mammalian cells by NAIP and a related family of IAP genes. Nature 379, 349–353.

Liu, Z., Sun, C., Olejniczak, E. T., Meadows, R. P., Betz, S. F., Oost, T., et al. (2000). Structural basis for binding of Smac/DIABLO to the XIAP BIR3 domain. Nature 408(6815), 1004–1008.

Lopez, J. et al (2011). CARD-mediated autoinhibition of cIAP1's E3 ligase activity suppresses cell proliferation and migration. Mol. Cell 42, 569–583.

Lu M, Lin SC, Huang Y, Kang YJ, Rich R, Lo YC, Myszka D, Han J, and Wu H (2007). XIAP induces NF-kB activation via the BIR1/TAB1 interaction and BIR1 dimerization. Mol Cell 26:689–702.

Lynch GS, Schertzer JD, Ryall JG. (2007). Therapeutic approaches for muscle wasting disorders. Pharmacol Ther, 113: 461-487.

Mace, P. D., Shirley, S., and Day, C.L. (2010). Assembling the building blocks:structure and function of inhibitor of apoptosis proteins, Cell Death Differ. 17, 46–53.

Mahoney D. J., Cheung H. H., Lejmi Mrad R., Plenchette S., Simard C., Enwere E., Arora V., Mak T. W., Lacasse E. C., Waring J., Korneluk R. G., (2008). Both cIAP1 and cIAP2 regulate TNFa-mediated NF-kB activation. Proc. Natl. Acad. Sci. U.S.A. 105, 11778–11783.

Mannhold R, Fulda S. and Carosati E. (2010). IAP antagonists: promising candidates for cancer therapy. Drug Discovery Today. 15(5/6), 210-219.

Marmor MD, Yarden Y. (2004) Role of protein ubiquitylation in regulating endocytosis of receptor tyrosine kinases. Oncogene.23:2057–70.

McElhinny AS, Kakinuma K, Sorimachi H, Labeit S, Gregorio CC. (2002). Muscle-specific RING finger-1 interacts with titin to regulate sarcomeric M-line and thick filament structure and may have nuclear functions via its interaction with glucocorticoid modulatory element binding protein-1. J Cell Biol.157:125–36.

Meighan-Mantha RL, Hsu DK, Guo Y, Brown SA, Feng SL, Peifley KA et al. (1999). The mitogen-inducible Fn14 gene encodes a type I transmembrane protein that modulates fibroblast adhesion and migration. J Biol Chem 274: 33166–33176.

Metzger MB, Hristova VA, Weissman AM. (2012). HECT and RING finger families of E3 ubiquitin ligases at a glance. J Cell Sci 125: 531–537.

Micheau, O. & Tschopp, J. (2003). Induction of TNF receptor I-mediated apoptosis via two sequential signaling complexes. Cell 114, 181–190.

Miller LK (1999). An exegesis of IAPs: salvation and surprises from BIR motifs. Trends Cell Biol 9:323-328.

Minetti, G.C., Feige, J.N., Rosenstiel, A., Bombard, F., Meier, V., Werner, A., Bassilana, F., Sailer, A.W., Kahle, P., Lambert, C. et al. (2011). Galphai2 signaling promotes skeletal muscle hypertrophy, myoblast differentiation, and muscle regeneration. Science signaling, 4, ra80.

Mitch W.E., and Goldberg A.L. (1996). Mechanisms of Muscle Wasting - The Role of the Ubiquitin–Proteasome Pathway. NE JM. 335:1897-1905.

Mittal A, Bhatnagar S, Kumar A, et al. (2010). The TWEAK–Fn14 system is a critical regulator of denervation-induced skeletal muscle atrophy in mice. J Cell Biol, 188: 833-49.

Mourkioti F, Kratsios P, Luedde T, Song YH, Delafontaine P, Adami R, Parente V, Bottinelli R, Pasparakis M, Rosenthal N. (2006). Targeted ablation of IKK2 improves skeletal muscle strength, maintains mass, and promotes regeneration. J Clin Invest 116:2945–2954.

Mourkioti F, Rosenthal N (2008). NF-kappaB signaling in skeletal muscle: prospects for intervention in muscle diseases. J Mol Med 86: 747–759.

Mukhopadhyay, D. and Riezman, H. (2007). Proteasome-independent functions of ubiquitin in endocytosis and signaling. Science, 315: 201-205.

Nagata, S. (1997). "Apoptosis by death factor." Cell 88(3): 355-65.

Navon A, Ciechanover A. (2009).The 26 S proteasome: from basic mechanisms to drug targeting. J Biol Chem 284: 33713–33718.

Park YC, Ye H, Hsia C, et al. (2000) A novel mechanism of TRAF signaling revealed by structural and functional analyses of the TRADD-TRAF2 interaction. Cell, 101: 777–87.

Passmore LA, Barford D. (2004). Getting into position: the catalytic mechanisms of protein ubiquitylation. Biochem J 379: 513–525.

Penner CG, Gang G, Wray C, Fischer JE, Hasselgren PO (2001). The transcription factors NF-kappab and AP-1 are differentially regulated in skeletal muscle during sepsis. Biochem Biophys Res Commun 281: 1331-1336.

Pereira, C., Murphy, K., Jeschke, M., & Herndon, D. N. (2005). Post burn muscle wasting and the effects of treatments. Int J Biochem Cell Biol, 37(10), 1948-1961.

Perkins, N. D. (2006). Post-translational modifications regulating the activity and function of the nuclear factor kappa B pathway. Oncogene 25, 6717–6730.

Peter, M. E. and P. H. Krammer (1998). "Mechanisms of CD95 (APO-1/Fas)-mediated apoptosis." Curr. Opin. Immunol. 10(5): 545-551.

Peterson JM, Bakkar N, and Guttridge DC. (2011). NF-kB Signaling in Skeletal Muscle Health and Disease. Current Topics in Developmental Biology, 96: 85 - 119.

Pette, D., & Staron, R. (2001). Transitions of muscle fiber phenotypic profiles. Histochemistry and Cell Biology, 115(5), 359-372.

Pette, D., & Staron, R. S. (2000). Myosin isoforms, muscle fiber types, and transitions. Microscopy Research and Technique, 50(6), 500-509.

Plati, J., Bucur, O., Khosravi-Far, R. (2011). Apoptotic cell signaling in cancer progression and therapy. Integrative Biology. 3, 279-96.

Polek TC, Talpaz M, Darnay BG, Spivak-Kroizman T. (2003). TWEAK mediates signal transduction and differentiation of RAW264.7 cells in the absence of Fn14/TweakR. Evidence for a second TWEAK receptor. J Biol Chem, 278: 32317-23.

Price S.R., Bailey J.L., Wang X., Jurkovitz C., England B.K., Ding X., Phillips L.S. and Mitch W.E. (1996). Muscle wasting in insulinopenic rats results from activation of the ATP-dependent, ubiquitin-proteasome proteolytic pathway by a mechanism including gene transcription. J. Clin.Invest. 98: 1703-1708.

Primeau AJ, Adhihetty PJ and Hood DA. (2002). Apoptosis in heart and skeletal muscle. Can JA ppl Physiol 27: 349-395.

Reed SA, Senf SM, Cornwell EW, Kandarian SC, Judge AR. (2011). Inhibition of IkappaB kinase alpha (IKKalpha) or IKKbeta IKKbeta) plus forkhead box O (Foxo) abolishes skeletal muscle atrophy. Biochem Biophys Res Commun., 405(3):491–496.

Rhoads, M. G., Kandarian, S. C., Pacelli, F., Doglietto, G. B., & Bossola, M. (2010). Expression of NF-kappaB and IkappaB proteins in skeletal muscle of gastric cancer patients.

Roos, C., Wicovsky, A., Muller, N., Salzmann, S., Rosenthal, T., Kalthoff, H., Trauzold, A., Seher, A., Henkler, F., Kneitz, C., and Wajant, H. (2010). J Immunol 185, 1593-1605.

Saitoh, T., Nakayama, M., Nakano, H., Yagita, H., Yamamoto, N., and Yamaoka, S. (2003). J Biol Chem 278, 36005-36012.

Sandri M, Lin J, Handschin C, Yang W, Arany ZP, Lecker SH, et al. (2006). PGC-1alpha protects skeletal muscle from atrophy by suppressing FoxO3 action and atrophy-specific gene transcription. Proc Natl Acad Sci U S A Oct 31; 103(44): 16260-16265.

Varfolomeev E, Goncharov T, Maecker H, Zobel K, Komuves LG, Deshayes K, et al. (2012). Cellular Inhibitors of Apoptosis Are Global Regulators of NF-kappaB and MAPK Activation by Members of the TNF Family of Receptors. Science signaling, 5(216): ra22.

Sandri, M. (2010). Autophagy in skeletal muscle. FEBS Lett. 584:1411-1416.

Sato S, Ogura Y and Kumar A (2014). TWEAK/Fn14 signaling axis mediates skeletal muscle atrophy and metabolic dysfunction. Front. Immunol. 5:18.

Schiaffino, S., & Reggiani, C. (2011). Fiber types in mammalian skeletal muscles. Physiological Reviews, 91(4), 1447-1531.

Schmukle, A. C., & Walczak, H. (2012). No one can whistle a symphony alone—How different ubiquitin linkages cooperate to orchestrate NF-kB activity. Journal of Cell Science, 125, 549-559.

Scott, W., Stevens, J., & Binder-Macleod, S. A. (2001). Human skeletal muscle fiber type classifications. Phys Ther, 81(11), 1810-1816.

Senftleben U, Cao Y, Xiao G, Greten FR, Krahn G, Bonizzi G, Chen Y, Hu Y, Fong A, Sun SC, Karin M (2001). Activation by IKKalpha of a second, evolutionary conserved, NF-kappa B signaling pathway. Science 293:1495-1499.

Shi Y (2002). Mechanisms of caspase activation and inhibition during apoptosis. Mol Cell 9:459-470.

Silke J. and Vucic D. (2014). IAP Family of Cell Death and Signaling Regulators. Methods in Enzymology Chapter 2 - Volume 545: 35- 65.

Silke J., Meier P., (2013). Inhibitor of Apoptosis (IAP) Proteins–Modulators of Cell Death and Inflammation Cold Spring Harb Perspect Biol 5: 1-19.

Silke, J. (2011). The regulation of TNF signalling: What a tangled web we weave. Current Opinion in Immunology, 23, 620-626.

Smale, S.T. (2012). Dimer-specific regulatory mechanisms within the NF-kappaB family of transcription factors. Immunol. Rev., 246, 193-204.

Solomon V, Goldberg AL (1996). Importance of the ATP– ubiquitin–proteasome pathway in the degradation of soluble and myofibrillar proteins in rabbit muscle extracts. J Biol Chem 271:26690-26697.

Srivastava AK, Qin X, Wedhas N, et al. (2007). Tumor necrosis factor-alpha augments matrix metalloproteinase-9 production in skeletal muscle cells through the activation of transforming growth factor-beta-activated kinase 1 (TAK1)-dependent signaling pathway. J Biol Chem, 282: 35113-24.

Steffen, J.M., R.D. Fell, T.E. Geoghegan, L.C. Ringel and X.J. Musacchia. (1990). Age effects on rat hindlimb muscle atrophy during suspension unloading. J Appl Physiol 68: 927-931.

Stevenson EJ, Giresi PG, Koncarevic A, Kandarian SC. Global analysis of gene expression patterns during disuse atrophy in rat skeletal muscle. J Physiol, (2003). 551: 33-48.

Straub, C. (2011). Targeting IAPs as An Approach to Anti-Cancer Therapy. Current Topics in Medicinal Chemistry: 4, 1-26.

Straub, C. (2011). Targeting IAPs as An Approach to Anti-Cancer Therapy. Current Topics in Medicinal Chemistry: 4, 1-26.

Sun, Y. (2006). E3 ubiquitin ligases as cancer targets and biomarkers. Neoplasia, 8: 645-654.

Tajrishi M M, Zheng T S, Linda C. Burkly L C, Kumar A. (2014). The TWEAK-Fn14 Pathway: A Potent Regulator of Skeletal Muscle Biology in Health and Disease. Cytokine Growth Factor Rev. April ; 25(2): 215-225.

Tajrishi M M, Shin J, Hetman M, and Kumar A (2015). DNA Methyltransferase 3a and Mitogen-activated Protein Kinase Signaling Regulate the Expression of Fibroblast Growth Factor-inducible 14 (Fn14) during Denervation induced Skeletal Muscle Atrophy. The journal of biological chemistry, 289 (29), 19985-19999.

Testelmans, D., Crul, T., Maes, K., Agten, A., Crombach, M., & Decramer, M., et al. (2010). Atrophy and hypertrophy signalling in the diaphragm of patients with COPD. The European Respiratory Journal, 35(3), 549-556.

Thomason, D.B., R.E. Herrick, D. Surdyka and K.M. Baldwin. (1987). Time course of soleus muscle myosin expression during hindlimb suspension and recovery. J Appl Physiol 63: 130-137.

Thornberry NA, Lazebnik Y. Caspases: enemies within. Science (1998); 281: 1312-6.

Tintignac, L. A., Lagirand, J., Batonnet, S., Sirri, V., Leibovitch, M. P. and Leibovitch, S. A. (2005). Degradation of MyoD mediated by the SCF (MAFbx) ubiquitin ligase. J. Biol. Chem. 280, 2847-2856.

Tong, X., et al. (2004). The p50-p50 NF-kappaB complex as a stimulus-specific repressor of gene activation. Mol. Cell. Biochem. 265, 171-183.

Toth, M. J., Miller, M. S., Vanburen, P., Bedrin, N. G., Lewinter, M. M., & Ades, P. A., et al. (2012). Resistance training alters skeletal muscle structure and function in human heart failure: effects at the tissue, cellular and molecular levels. J Physiol, 590(Pt 5), 1243-1259.

Tran NL, McDonough WS, Savitch BA, Fortin SP, Winkles JA, Symons M, et al. (2006). Increased fibroblast growth factor-inducible 14 expression levels promote glioma cell invasion via Rac1 and nuclear factor-kappaB and correlate with poor patient outcome. Cancer Res Oct 1; 66(19): 9535-9542.

Tskhovrebova, L., & Trinick, J. (2012). Making Muscle Elastic: The Structural Basis of Myomesin Stretching. Plos Biology, 10(2), e1001264.

Vallabhapurapu S, Matsuzawa A, Zhang W, et al. (2008). Nonredundant and complementary functions of TRAF2 and TRAF3 in a ubiquitination cascade that activates NIK-dependent alternative NF-kappaB signaling. Nat Immunol 9: 1364-70.

Van Gammeren D, Damrauer JS, Jackman RW, Kandarian SC. (2009). The IkappaB kinases IKKalpha and IKKbeta are necessary and sufficient for skeletal muscle atrophy. Faseb J. 23(2):362-370.

Vandenabeele P., Bertrand M., (2012). The role of the IAP E3 ubiquitin ligases in regulating pattern-recognition receptor signaling. Nature Reviews Immunology 12, 833-844.

Varfolomeev E, Goncharov T, Maecker H, et al. (2012). Cellular Inhibitors of apoptosis are global regulators of NF-kappaB and MAPK activation by members of the TNF family of receptors. Sci Signal 2012; 5: ra22.

Varfolomeev E., J. W. Blankenship, S. M. Wayson, A. V. Fedorova, N. Kayagaki, P. Garg, K. Zobel, J. N. Dynek, L. O. Elliott, H. J. Wallweber, J. A. Flygare, W. J. Fairbrother, K. Deshayes, V. M. Dixit, D. Vucic, (2007). IAP antagonists induce autoubiquitination of c-IAPs, NF-kB activation, and TNFa-dependent apoptosis. Cell 131, 669-681.

Varfolomeev, E. et al. (2008). c-IAP1 and c-IAP2 are critical mediators of tumor necrosis factor α (TNFα)-induced NF-κB activation. J. Biol. Chem. 283, 2429-24299.

Varfolomeev, E. et al. (2007). IAP antagonists induce autoubiquitination of c-IAPs, NF-κB activation, and TNFα-dependent apoptosis. Cell 131, 669-681.

Varfolomeev, E., Alicke, B., Elliott, J. M., Zobel, K., West, K., Wong, H., et al. (2009). X chromosome-linked inhibitor of apoptosis regulates cell death induction by proapoptotic receptor agonists. The Journal of Biological Chemistry, 284, 34553-34560.

Vaux DL, Silke J. (2003). Mammalian mitochondrial IAP binding proteins. Biochem Biophys Res Commun, 304: 499-504.

Vaux, D. L. and Silke, J. (2005). IAPs, RINGs and ubiquitylation. Nat Rev Mol Cell Biol, 6: 287-297.

Ventadour, S., and D. Attaix. (2006). Mechanisms of skeletal muscle atrophy. Curr Opin Rheumatol 18: 631-635.

Verhagen, A.M., Ekert, P.G., Pakusch, M., Silke, J., Connolly, L.M., Reid, G.E., Moritz, R.L., Simpson, R.J., Vaux, D.L. (2000). Identification of DIABLO, a mammalian protein that promotes apoptosis by binding to and antagonizing IAP proteins. Cell 102: 43-53.

Vince J. E., W. W. Wong, N. Khan, R. Feltham, D. Chau, A. U. Ahmed, C. A. Benetatos, S. K. Chunduru, S. M. Condon, M. McKinlay, R. Brink, M. Leverkus, V. Tergaonkar, P. Schneider, B. A. Callus, F. Koentgen, D. L. Vaux, J. Silke, (2007). IAP antagonists target cIAP1 to induce TNFa-dependent apoptosis. Cell 131, 682-693.

Vucic D, Dixit VM and Wertz IE. (2011). Ubiquitylation in apoptosis: a post-translational modification at the edge of life and death. Nat Rev Mol Cell Biol. Jun 23; 12(7):439-52.

Wajant H. (2013) . The TWEAK-Fn14 system as a potential drug target. British Journal of Pharmacology 170 748-764.

Wang, C. Y., M. W. Mayo, R. G. Korneluk, D. V. Goeddel, and A. S. Baldwin, Jr. (1998). NF-kB antiapoptosis: induction of TRAF1 and TRAF2 and c-IAP1 and c-IAP2 to suppress caspase-8 activation. Science 281:1680-1683.

Wang, S., Miura, M., Jung, Y., Zhu, H., Gagliardini, V., Shi, L., Greenberg, A. H. and Yuan, J. (1996). Identification and characterization of Ich-3, a member of the interleukin-1β converting enzyme (ICE)/Ced-3 family and an upstream regulator of ICE. J. Biol. Chem. 271, 20580-20587.

Wang, X., Hu, Z., Hu, J., Du, J., & Mitch, W. E. (2006). Insulin resistance accelerates muscle protein degradation: Activation of the ubiquitin-proteasome pathway by defects in muscle cell signaling. Endocrinology, 147(9), 4160-4168.

Wiley SR, Cassiano L, Lofton T, Davis-Smith T, Winkles JA, Lindner V et al. (2001). A novel TNF receptor family member binds TWEAK and is implicated in angiogenesis. Immunity 15: 837-846.

Wing, S. S., Haas, A. L., & Goldberg, A. L. (1995). Increase in ubiquitin-protein conjugates concomitant with the increase in proteolysis in rat skeletal muscle during starvation and atrophy denervation. Biochem J, 307 (Pt 3), 639-645.

Winkles JA. (2008). The TWEAK-Fn14 cytokine-receptor axis: discovery, biology and therapeutic targeting. Nat Rev Drug Discov 7: 411-25.

Wu CJ, Conze DB, Li T, Srinivasula SM, Ashwell JD. (2006). Sensing of Lys 63-linked polyubiquitination by NEMO is a key event in NF-kappaB activation. Nat Cell Biol 8: 398-406.

Wu H, Rothermel B, Kanatous S, Rosenberg P, Naya FJ, Shelton JM, et al. (2001). Activation of MEF2 by muscle activity is mediated through a calcineurindependent pathway. EMBO J ;20:6414-23.

Wu, H., Tschopp, J., Lin, S. C. (2007). Smac mimetics and TNF!: a dangerous liaison? Cell, 131, 655-658.

Wyllie AH, K err J F and Currie AR. (1980). Cell death: the significance of apoptosis. Int Rev Cytol 68: 251-306.

X. Yang, W. C. Yeh, T. W. Mak, R. G. Korneluk, G. Cheng, (2008). Noncanonical NF-kB activation requires coordinated assembly of a regulatory complex of the adaptors cIAP1, cIAP2, TRAF2 and TRAF3 and the kinase NIK. Nat. Immunol. 9, 1371-1378.

Yamaki T, Wu CL ,Gustin M, Lim J, Jackman RW, Kandarian SC. (2012). RelA/p65 is required for cytokine-induced myotube atrophy. Am J Physiol Cell Physiol 303(2):C135-42.

Yang, Q. H., & Du, C. (2004). Smac/DIABLO selectively reduces the levels of c-IAP1 and c-IAP2 but not that of XIAP and livin in HeLa cells. J Biol Chem 279(17), 16963-16970.

Zarnegar, B.J., Wang, Y., Mahoney, D.J., Dempsey, P.W., Cheung, H.H., He, J., Shiba, T., Yang, X., Yeh, W.C., Mak, T.W. et al. (2008). Noncanonical NF-kappaB activation requires coordinated assembly of a regulatory complex of the adaptors cIAP1, cIAP2, TRAF2 and TRAF3 and the kinase NIK. Nat Immunol, 9, 1371-1378.

Zhang P., Chen X., Fan M., (2007). Signaling mechanisms involved in disuse muscle atrophy. Med Hypotheses, 69(2):310-21.

Zhao, J., Brault, J. J., Schild, A., Cao, P., Sandri, M., & Schiaffino, S., et al. (2007). FoxO3 coordinately activates protein degradation by the autophagic/lysosomal and proteasomal pathways in atrophying muscle cells. Cell Metab, 6(6), 472-483.